Section des Sciences de la Terre et de l'Environnement

Docteur Serge Stoll

Modeling the Surface Properties and Behavior of Nanoparticles in Aquatic Systems. Monte Carlo Investigations

THÈSE

présentée à la Faculté des Sciences de l'Université de Genève pour obtenir le grade de Docteur ès Sciences, mention Interdisciplinaire

par

Arnaud Clavier

de

Montbéliard (France)

Thèse N° 5226

GENÈVE Atelier d'impression ReproMail 2018



DOCTORAT ÈS SCIENCES, MENTION INTERDISCIPLINAIRE

Thèse de Monsieur Arnaud CLAVIER

intitulée :

«Modeling the Surface Properties and Behavior of Nanoparticles in Aquatic Systems. Monte Carlo Investigations»

La Faculté des sciences, sur le préavis de Monsieur S. STOLL, docteur et directeur de thèse (Département F.-A. Forel des sciences de l'environnement et de l'eau), Madame C. BONADONNA, professeure associée (Département des sciences de la Terre), Monsieur J. KASPARIAN, professeur associé (Groupe de physique appliquée), Monsieur J. LABILLE, professeur (Centre Européen de Recherche et d'Enseignement des Géosciences de l'Environnement, Aix-en-Provence, France) et Monsieur P. LE COUSTUMER, professeur (Département des Sciences et Technologies, Université de Bordeaux, Pessac, France), autorise l'impression de la présente thèse, sans exprimer d'opinion sur les propositions qui y sont énoncées.

Genève, le 1 juin 2018

Thèse - 5226 -

Le Décanat



Contents

	Rem	perciements	(vi		
	Rési	umé en français	xix		
	Abstract				
1	Intr	oduction and Thesis Objectives	1		
	1.1	Nanomaterials and Nanoparticles	2		
	1.2	Nanomaterials in/and the Environment	3		
	1.3	Importance of NP surface charge and heteroaggregation processes	4		
	1.4	Thesis objectives	5		
	1.5	List of papers	8		
	Bibl	iography	10		
2	Mod	del, Theory and Simulation Methods	15		
	2.1	Coarse-grained model	16		
	2.2	Force field model an interaction potentials	18		
		2.2.1 Hard sphere interactions	19		
		2.2.2 Van der Waals interactions	19		
		2.2.3 Electrostatic interactions	20		

CONTENTS

	2.3	Period	ic boundary condition	21
	2.4	Surfac	e charge properties	22
		2.4.1	Origin of the surface charge	22
		2.4.2	Point of Zero Charge versus IsoElectric Point	25
		2.4.3	Henderson-Hasselbach equation	25
		2.4.4	Surface titrating site and Tanford-Kirkwood model	26
		2.4.5	Electrical double layer models	28
	2.5	Statist	ical mechanics and Monte Carlo simulations	33
		2.5.1	Statistical mechanics	33
		2.5.2	Monte Carlo Metropolis simulation method and procedure	34
	2.6	Particl	e aggregation	38
		2.6.1	Smoluchowski theory	38
		2.6.2	Attachment efficiencies	40
	Bibl	iograph	y	43
3			arging Behavior of Nanoparticles. Effects of Site Distribution and electric Constant and pH Changes.	
		• /	arlo Approach.	51
	3.1	Introdu	uction	52
	3.2	Main r	results	53
		3.2.1	$1 - pK_a^0 \dots \dots$	53
		3.2.2	$2 - pK_a^0$	55
	3.3	Conclu	usions	60
	Don	on I		61

4			urface and Salt Properties on the Ion Distribution around Spherical les. Monte Carlo Simulations	71
	4.1	Introd	uction	72
	4.2	Main l	Results	73
		4.2.1	NP charge behavior in the presence of counterions only	73
		4.2.2	NP surface charge behavior in presence of salt	75
	4.3	Conclu	usions	80
	Bibl	iograph	y	81
	Pap	er II .		83
5	Rate	es in Pr	ion of Nanoparticle Attachment Efficiencies and Heteroaggregation resence of Natural Organic Matter for Contrasting Conditions using to Modelling	95
	5.1	Introd	uction	97
	5.2	Model	theory and description	101
		5.2.1	Aggregation theory	101
		5.2.2	Aggregation model	102
		5.2.3	Physical time versus Monte Carlo time	103
		5.2.4	Attachment efficiency	104
	5.3	Result	s	107
		5.3.1	Model validation	107
		5.3.2	Surface coating and heteroaggregation rates at constant natural organic matter concentration	108
		5.3.3	Heteroaggregation rates at variable NOM concentration	111
	5.4	Conclu	usions	118

CONTENTS

	5.5 Acknowledgements	118
	Bibliography	119
6	Conclusions and Perspectives	127
	6.1 General conclusions	128
	6.2 Perspectives	130
A	Supporting Informations of Paper II	133
В	Paper Published in Chimia	137
C	Paper Published in	
	Environmental Science: Nano	139
D	Paper Published in	
	Polymers	143

List of Figures

1.1	Application domains of nanoparticles from self-cleaning textiles to reinforced plastics	2
	plusties	_
1.2	Nanoparticle behaviors and processes in aquatic systems	4
1.3	Different models developed and found in Papers I to III	7
2.1	Full and coarse-grained representation of a DNA strand in a water solution with ions	17
2.2	Periodic boundary conditions and minimum image convention	22
2.3	Origin of surface charges	24
2.4	Representation of the Tanford and Kirkwood model	27
2.5	Spatial distributions of surface discrete charges	28
2.6	Model of Stern-Grahame of the electrical double layer	29
2.7	Monte Carlo scheme to evaluate the size of the Lake Geneva	35
2.8	Scheme of the general Metropolis procedure	36
2.9	Description of homo- and heteroaggregation processes and corresponding attachment efficiencies	41
2.10	Various homo- and heteroaggregate structures obtained from the Monte Carlo aggregation model	42
3.1	Monte-Carlo titration curves for a NP with 50 sites and with different surface distributions $(1 - pK_a^0 \text{ model}) \dots \dots \dots \dots \dots \dots \dots \dots \dots$	53

LIST OF FIGURES

3.2	Monte-Carlo titration curves for a heterogeneous surface with different charge densities (10, 50, 100, 200 and 300 sites)	54
3.3	Monte-Carlo titration curves for a heterogeneous surface with 50 sites (25mC/m^2) and with various dielectric constants	55
3.4	${ m pH}-pK_a^0$ as a function of NP degree of ionization and number of charge type as a function of ${ m pH}-pK_a^0$ for a heterogeneous surface NP with variable ΔpK_a^0 values $(2-pK_a^0\ { m model})$	56
3.5	Variation of the total surface charge for different $\Delta p K_a^0$ considering a heterogeneous surface and for different site distributions with $\Delta p K_a^0 = 3 \ (2 - p K_a^0 \ \text{model}) \ \dots \ \dots \ \dots \ \dots$	57
3.6	${ m pH}-pK_a^0$ as a function of NP degree of ionization and total energy as a function of ${ m pH}-pK_a^0$	58
4.1	NP effective charge as a function of total surface charge number and surface charge density for a heterogeneous surface distribution without salt ions	74
4.2	NP effective charge for different surface site distributions as a function of total surface charge number and surface charge density	75
4.3	NP effective charge in presence of mono-, di- and trivalent cations as a function of different cation concentrations	76
4.4	Fraction of reduced NP charge as a function of the total surface charge number and of surface charge density and at different ionic strengths	78
4.5	NP effective charge as a function of total surface charge number and surface charge density at two different cation salt concentrations $(1x10^{-3} \text{ and } 5x10^{-3} \text{ M})$	79
5.1	Description of homo- and heteroaggregation processes and corresponding attachment efficiencies	105
5.2	Homoaggregation process with $\alpha_{NOM-NOM}=1$	108
5.3	Heteroaggregation (Surface Coating) in presence of NOM and NPs	110
5.4	Evolution of the NP surface coating in presence of 1000 NOM units for 1, 25 and 100 NPs	111

LIST OF FIGURES

5.5	Variation of the inverse of the object concentration for the different water models with $\alpha_{NP-NOM}=1$ and for 1000 NOM particles	112
5.6	Evolution of the heteroaggregation rate constant for each water models as a function of the number of NOM	114
5.7	Variation of the heteroaggregation attachment efficiencies for each water model as a function of the NP/NOM ratios	115
5.8	Snapshots of heteroaggregates and homoaggregates at different NOM concentrations and in different water models	117

List of Tables

2.1	Resume of the different ensembles in statistical mechanics with their indepen-	
	dent variables and their partition or microscopic functions	34
2.2	Acid/base reactions at the NP surface and associated energy changes $\Delta E . . $	37
2.3	Aggregation kinetic rates as a function of the different transport models	39
5.1	Individual attachment efficiencies representative of ultra-pure water, marine and fresh (0.1 and 0.01) water models	106
5.2	Heteroaggregation rate constants, k_{hetero}^{agg} (10 ⁻¹⁸ m ³ s ⁻¹) for ultrapure, marine and fresh water models at different NOM concentrations. NPs = 10	113
5.3	Heteroaggregation attachment efficiencies for ultrapure and fresh water at different NOM concentrations.	115

Remerciements

Le doctorat est une course de longue haleine dans laquelle le moindre encouragement représente une bouffée d'oxygène pour aller encore plus loin. Pour cette raison et par ces quelques mots, je souhaiterais adresser une pensée et des remerciements à toutes les personnes qui ont contribué de près ou de loin à la réalisation et à la réussite de cette thèse. Cette liste est non-exhaustive et j'ai une pensée pour tous ceux que je pourrais omettre dans celle-ci.

En premier lieu, le docteur Serge Stoll qui m'a offert l'opportunité d'effectuer ce doctorat en m'accueillant dans son groupe de recherche. Je lui suis très reconnaissant pour m'avoir fait confiance et m'avoir accompagné pendant ces cinq années, à la fois lors des bons et des mauvais moments. Nonobstant tout ton travail sur ce manuscrit, tes conseils, tes connaissances scientifiques, ton expérience et ta bonne humeur m'ont beaucoup apporté et aidé à accomplir ce travail de thèse. Serge, un grand Merci à toi.

Je voudrais remercier particulièrement les membres de mon jury de thèse, les professeurs Costanza Bonadonna et Jérôme Kasparian de Genève, Philippe Le Coustumer de Bordeaux ainsi que Jérôme Labille d'Aix en Provence pour avoir accepté de faire partie de ce comité et pour le temps qu'ils ont pris pour évaluer mon travail de thèse.

Je souhaiterais également adresser mes remerciements à mes ex directeurs de Master, les professeurs Christophe Ramseyer et Claude Girardet ainsi que le docteur Fabien Picaud qui m'ont donné l'envie de me lancer dans la recherche scientifique, la physique des particules, le monde des nanomatériaux et la modélisation numérique.

Un grand Merci à mon groupe de recherche et toutes les personnes qui sont passées par celui-ci pendant ce doctorat, Marie-Caroline, Olena, Catia, Lina, Marianne, Léo, Alexis, Fabrice et Fred, qui par leurs bonnes humeurs, leurs gentillesses, les pauses scientifiques et les quelques bières partagées à Genève ou au bord du lac, ont rendu ce long marathon plus agréable. Sans oublier, les membres cachés de notre groupe, Venus, Eros et Dyonisos, sans qui ce travail n'aurait pas vu le jour.

Mes remerciements s'adressent également à tous les foréliens et foréliennes ainsi qu'à toutes les personnes que j'ai pu rencontrer lors de ces années, notamment à travers les travaux pratiques, et qui ont tous apporté leur pierre à l'édifice à leur manière. Je pense plus particulièrement à Carmen, Perrine, Séverine, Nadia, Giulia, Sonia, Armelle, Teofana, Alexandra, Sandro, La liste est longue et non-exhaustive.

Mes pensées vont également à mes amis de Besançon, Aude, Julie, Batiste, Jacques, Éric, Ludo, Clément, Antoine, qui m'ont supporté et soutenu tout au long de mes années d'études, de loin ou de près. Merci à Antoine pour nos discussions longues distances qui m'ont accompagné lors de mes journées de bureau et merci à Julie qui m'a accueilli et aidé à vivre dans le pays de Gex. Merci à vous tous.

Un grand et chaleureux merci à Elena qui m'a supporté (dans tous les sens du terme) pendant ces longues années de doctorat, merci pour ton sourire, ta bonhomie naturelle et ta chaleur espagnole. Marcel Proust a dit *Soyons reconnaissants aux personnes qui nous donnent du bonheur ; elles sont les charmants jardiniers par qui nos âmes sont fleuries.*, je pense que cette phrase te va parfaitement.

Enfin, mes derniers remerciements, et les plus profonds, sont pour ma famille, mes parents, Lucie et Jean Marie, ainsi que mon frère, Stéphane, pour tout l'amour qu'ils m'ont donné, leur soutien indéfectible depuis le début et le fait qu'il ait toujours cru en ma capacité à réussir. J'ai également une pensée émue pour ma grand-mère Ida qui nous a malheureusement quitté.

Merci à vous tous

Résumé en français

Les " nanos ", ces objets se trouvant entre l'échelle macroscopique et atomique (au moins une dimension comprise entre 1 et 100 nm) sont censés révolutionner notre quotidien ainsi que notre futur, des matériaux à la médecine, de l'environnement à l'électronique, en passant par l'énergie ou l'agriculture. Certains spécialistes parlant même de nouvelle révolution industrielle. À cette échelle, le milliardième de mètre, la matière manifeste des propriétés surprenantes et encore inimaginables il y a quelques années. Ces propriétés, fortement reliées aux importantes surfaces spécifiques des nanomatériaux et donc à la grande proportion d'atome en surface, ouvrent tout un nouveau champ de recherches et de possibilités. Pouvoir les exploiter et repousser les limites technologiques offre donc des challenges intéressants pour les chercheurs et le monde industriel. Cependant, tous les produits de ces découvertes technologiques apportent également des incertitudes en termes de risques potentiels pour l'environnement et la santé. La production et la présence de nanoparticules dans des produits du quotidien devient, par conséquent, de plus en plus importante tout comme leur dissémination dans les milieux environnementaux. Cependant, des questions restent en suspens concernant leurs comportements et leurs toxicités sur le court mais également sur le long terme dans l'environnement et les milieux aquatiques. Il semble donc primordial de mieux cerner et mieux comprendre les mécanismes qui entourent ces nanoparticules mais également d'estimer leurs réactivités et leurs diffusions à travers les systèmes aquatiques et les êtres vivant afin d'améliorer et rationaliser la fabrication et l'utilisation de ces particules. Les propriétés de surface de ces nanomatériaux, les propriétés physico-chimiques du milieu dans lequel elles se trouvent ainsi que la composition de l'écosystème vont donc jouer un rôle prépondérant dans l'évaluation des risques liés à l'usage des nanoparticules manufacturés.

Ce travail de thèse s'inscrit dans cette optique de mieux comprendre le comportement des nanoparticules manufacturées dans les milieux aquatiques et d'estimer l'importance de plusieurs paramètres physico-chimiques tels que le pH, la concentration et la valence des électrolytes, les charges de surface et leurs distributions ainsi que la teneur en matière organique. Pour cela, trois modèles numériques, basés sur des méthodes Monte Carlo, ont été développés afin de simuler différents mécanismes et situations représentatives des écosystèmes. Dans cette étude, les processus de chargement, de condensation et d'agrégation ont ainsi été pris en compte et modéliser pour divers scénarios et différents types de nanoparticules. Dans ces processus, les interactions électrostatiques sont connues pour jouer un rôle important.

Le premier modèle proposé dans ce travail de thèse concerne les mécanismes de chargement des nanoparticules. Les processus de simple et double protonations sont considérés pour une nanoparticule avec une surface discrétisée. L'influence des sites de titration via leurs propriétés intrinsèques (densité, distribution, propriétés acido-basique) est ainsi étudiée pour trois types de nanoparticules (dioxyde de titane, hématite et " soft nanoparticle ") en suivant l'effet de la variation du pH sur les propriétés de surface des nanoparticules. Dans ces processus, la densité surfacique de charge est amenée à fortement modifier des quantités telles que la charge totale des nanoparticules ou leurs degrés d'ionisation. Les interactions électrostatiques ayant lieu sur la surface, qui sont fortement dépendantes des distances intercharges et donc de la distribution et de la densité de surface, vont jouer un rôle clé dans le chargement des nanoparticules en altérant le comportement des courbes de titration. En outre, les propriétés acido-basique des sites de surface représentent également un paramètre important dans ces mécanismes de chargement, en particulier lors de doubles déprotonations. Des transitions de charges directes (modification de charges, de positive à négative) ainsi que progressives (étape par étape, extinction totale de la charge de surface puis rallumage de celle-ci) sont observées, donnant lieu à des points isoélectriques ou de charges nulles en fonction des propriétés acido-basiques de la nanoparticule.

L'influence des propriétés des sels électrolytes sur les processus de condensation a ensuite été explorée via le développement d'un second modèle en tenant compte la présence explicite de particules de sels dans nos boites de simulations (contre-ion, cation et anion). En plus des propriétés de surface des nanoparticules, la répercussion de paramètres de la solution tels que la valence et la concentration des ions ainsi que la force ionique a été étudiée en observant notamment leurs impacts sur la charge effective des nanoparticules. Nos investigations ont clairement démontré que, outre le fait que les particules de sel modifient la charge de surface d'une nanoparticule, la présence d'une charge dans un milieu aquatique réciproquement altère celui-ci en structurant la solution. La formation de couche d'ions autour des nanoparticules

est fortement contrôlée par les propriétés de surface de celle-ci, et plus spécifiquement de la densité surfacique de charge. Avec l'augmentation de la densité, la charge effective est progressivement réduite, surtout en présence de cations di- et trivalents, favorisant ainsi le processus de condensation ionique autour des nanoparticules. Cependant, aucune inversion de charge n'est observée, principalement en raison de limites stériques et de répulsions électrostatiques entre les cations dans la couche de condensation. Pour de fortes concentrations en cations trivalents, une neutralisation de la charge de surface des nanoparticules est obtenue et l'interface est structurée en plusieurs couches d'ions, une première composée de cations autour de la particule puis une seconde formée par des anions. Les mécanismes de condensation et de réduction de charge sont finalement le résultat d'une subtile compétition entre les interactions électrostatiques, attractions (surface-cation) et répulsions (cation-cation, surface-surface) ainsi que de la concentration en cations de la solution.

Finalement, une attention particulière est portée pour notre dernier modèle sur les phénomènes d'agrégation et plus spécifiquement d'hétéroagrégation. L'interaction des nanoparticules manufacturées dans l'environnement avec de la matière organique naturelle (MON), en particulier des monomères d'acide fulvique est plus spécifiquement étudiée via le développement et la validation d'un nouveau modèle numérique. Différents scénarios environnementaux sont pris en compte à travers divers modèles aquatiques et pour plusieurs rapports de concentration entre la MON et les nanoparticules. Avant de rentrer plus dans les détails, une définition claire des diverses étapes lors de l'agrégation est donnée ainsi que les différents coefficients d'efficacité de collisions (primaire, secondaire et global). Parmi les différents modèles d'eaux présentés, l'eau marine représente un cas intéressant dans lequel tous les contacts résultent en la formation d'agrégats, ce cas particulier permettant la détermination de coefficients de collision. Pour un système dans lequel juste l'hétéroagrégation est considérée (eau ultrapure), des effets de saturation peuvent se produire à long terme en fonction du ratio entre le nombre de MON et de nanoparticules. Après une rapide hétéroagrégation aux temps courts, la surface de la nanoparticule est totalement saturée, réduisant l'efficacité d'attachement des monomères de MON sur des temps plus longs. Enfin, comme démontré dans les modèles précédents, il est établi qu'un changement subtil des propriétés de surface des nanoparticules mais également de la solution peut profondément modifier le processus d'agrégation et les valeurs de coefficient d'efficacité de collision. Dans ces conditions, l'homoagrégation entre les particules de MON joue un rôle important en favorisant la formation d'agrégats de plus grande taille via des mécanismes de pontage.

Abstract

anos ", these objects between the macroscopic and the atomistic scales (at least one dimension between 1 and 100 nm) are supposed to revolutionize our daily life as well as our future, from materials to medicine, from environment to electronic, via energy or agriculture. Some experts even speaking of a new industrial revolution. At this scale, the billionths of a meter, the matter shows surprising properties that were totally unimaginable few years ago. These properties, strongly related to the large specific surface of the nanomaterials and so to the important proportion of atom situated on the surface, open a whole new area of researches and possibilities. Being able to exploit them and pushing back the technologic boundaries offer interesting challenging for researchers and for the industrial world. However, all the products coming from these discoveries provide also uncertainties around their potential risks for our environment and our health. The production and the presence of nanoparticles (NPs) in daily products becomes more and more important, as well as their dissemination in the environment. However, some questions remain unresolved about their behavior and toxicity at long and short terms, especially in aquatic environment. It seems therefore essential to identify and to better understand the mechanisms surrounding nanoparticles but also to estimate their reactivities and diffusions through aquatic systems and living being so as to improve and to rationalize the production and the use of these particles. The surface properties of these nanomaterials, the physico-chemical properties of the environment in which the nanoparticle is as well as the composition of the ecosystem will play a key role in risk assessment related to the use of manufactured particles.

This thesis work is in line with this perspective to better understand the behavior of manufactured nanoparticles in aquatic environments and to estimate the importance of several physicochemical parameters such as the pH, concentration and valence of electrolytes, surface charges and distributions as well as the organic matter content. For that purpose, three numerical mod-

els, based on Monte Carlo methods, have been developed in order to simulate different mechanisms and situations occurring in the environment. In this study, surface charging, condensation and aggregation processes have been taking into account and modelling for various scenarios and different types of nanoparticles. In these processes, the electrostatic interactions are known to play a significant role.

The first model proposed in this thesis work concern the surface charging mechanism of nanoparticles. Simple and double protonation processes are considered for a nanoparticle with discrete site on the surface. The influence of titrating sites *via* the intrinsic properties (density, distribution, acido-basic properties) are studied for three different types of particles (titanium dioxide, hematite and "soft nanoparticles") by following the effect of the pH variation on the NP surface properties. In these processes, the surface charge density will strongly modify quantities such as total NP surface charge or ionization degree. The electrostatic interactions occurring on the surface which are strongly dependent on the charge distances and thus on the distribution and surface density, will play a key role on the NP surface charging process by altering the behavior of titration curves. Moreover, the acido-basic properties of surface sites also represent an important parameter in the surface charging mechanism, in particular for double deprotonations. Both direct charge (charge modification, positive to negative) and progressive transitions (step by step process, NP switch off and switch on) are observed, giving rise to isoelectric point and point of zero charge as a function of the acido-basic properties of the nanoparticle.

The influence of salt properties on the condensation processes are then explored *via* the development of a second model which takes into account the explicit presence of salt particles in the simulation boxes (counterion, cation and anion). In addition to the NP surface properties, the influence of the solution parameters such as ionic strength, ion valence and concentration are studied by observing their impacts on the NP effective surface charge. Our investigations have clearly demonstrated, besides the fact that salt particles modify the NP surface charge, the presence of a charge in an aquatic system reciprocally alters this one by structuring the solution. The formation of ion layers around nanoparticles is strongly controlled by the NP surface properties, and more specifically the surface charge density. With the increase of the density, the effective charge is progressively reduced, especially in presence of di- and trivalent cations, promoting the ionic condensation process around nanoparticles. However, no charge reversal is observed, mainly due to steric limits and electrostatic repulsions between cations in the condensation layer. For high trivalent cation concentrations, a NP surface charge neutralization is

obtained and the interface is structured with multiple ion layers, a first one composed by cation around the particle and then a second formed by anions. The mechanisms of condensation and charge decrease are finally the result of a subtle competition between electrostatic interactions, attractions (surface-cation) and repulsions (cation-cation and surface-surface) as well as the cation concentration of the solution.

Finally, particular attention is paid to the last model on the aggregation phenomenon and more specifically on the heteroaggregation. The interaction between manufactured NP and natural organic matter (NOM), represented by fulvic acid monomers, are in particular studied via the development and the validation of an original numerical model. Several environmental scenarios are taken into account through various aquatic models and different concentration ratios between NOM and NPs. Before going into details, a clear definition of the diverse steps of aggregation is given as well as the corresponding attachment efficiencies (primary, secondary and global). Among the different water models presented in this study, marine water represents an interesting case in which all contacts result in the formation of aggregates, this specific case allows the possibility to determine attachment efficiency values. For a system where only heteroaggregation is considered (ultrapure water), saturation effects can occur at long time scale as a function of NP/NOM ratio. After a quick heteroaggregation at short scale, the NP surface is completely saturated, reducing the attachment efficiency of NOM monomer for longer time scales. Finally, as demonstrated in the previous models, a subtle change in the NP surface properties but also in the solution can deeply modify the aggregation processes and the attachment efficiency values. In these conditions, the homoaggregation between NOM particles plays a significant role by promoting the formation of larger aggregates via bridging mechanisms.

CHAPTER 1

Introduction and Thesis Objectives

1.1 Nanomaterials and Nanoparticles

here's Plenty of Room at the Bottom", with these words Richard Feynman has indirectly introduced in 1959 the concept of nanotechnology and encouraged scientists to take the possible benefits of the atomistic properties of matter. At this scale, the specific surface area and number of atoms located at the surface of nano-particles become predominant and give materials unique properties and high reactivity [1–3] which are generally different from the macroscopic ones. Since Feynman's famous lecture, the progress in nano-sciences has been significant and nowadays, as shown in **Figure 1.1** [4], engineered nanomaterials have tremendous potential to produce beneficial technological impact in many sectors in society such as medicine, cosmetic, electronics, textiles, etc [5–8]. It should be noted that from the European commission, nanomaterials are defined as *natural or manufactured material having at least 50% of the particles, for a number size distribution, with one of more external dimension in the range of 1 to 100 nm (1363/2013)*.

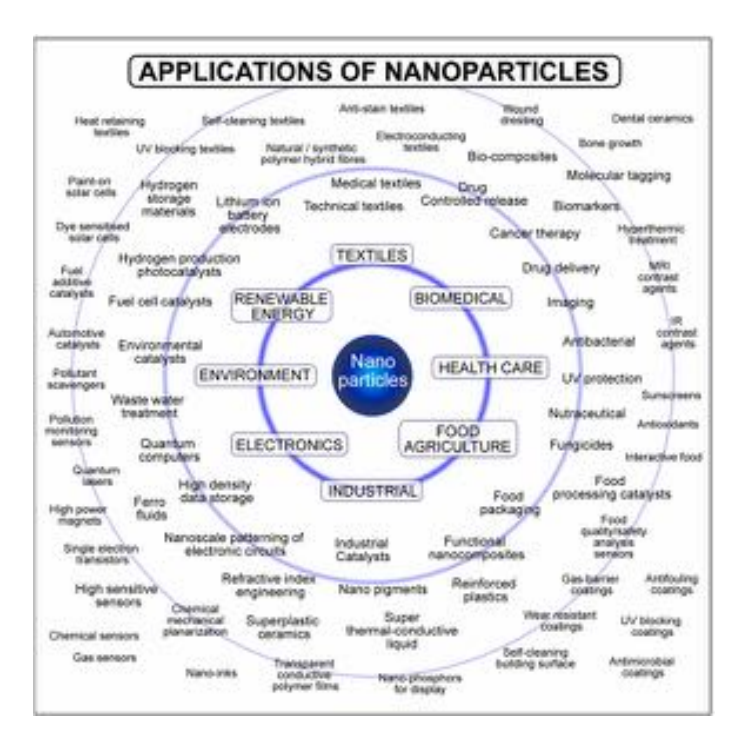


Figure 1.1: Application domains of nanoparticles from self-cleaning textiles to reinforced plastics [4].

From an industrial point of view, the main interest of nanomaterials is related in the numerous properties (optical, mechanical, chemical, physical, etc) allowing a wide variety of applications. [3, 8, 9] In particular, nanoparticles defined as engineered or manufactured nanoparticles (NPs), are specifically synthetized, functionalized and largely produced in order to respond to the industrial needs [10–12]. Consequently, their presence is becoming increasingly significant in our daily life and in our environment [13] [14]. For instance, silver NPs are widely used in textile, gold nanoparticles in medicine, cerium oxide in fuel, and titanium dioxide in cosmetic, and as food additive such as the E171 [7, 15–17].

1.2 Nanomaterials in/and the Environment

Unfortunately, the increasing use of nanomaterials in consumer and industrial applications has increased the likelihood of human and environmental exposure, giving rise to concerns regarding their safety [2, 3, 6, 8]. The large production of NPs inevitably leads to accidental, deliberate or unintentional release in environmental compartments (air, water, soil, sediments) [10–12] through industrial discharge, surface runoff or simply by consumer use [13,18]. Moreover, wastewater treatments are currently not adapted to deal with this type of materials and it remains difficult to remove nanoparticles from environmental compartments in particular in soils. In addition, limited data are available in this domain due to the difficulty of detecting and quantifying the NP concentrations in the environment [13, 19–21].

Once released in aquatic systems, manufactured nanoparticles NPs will be altered, transformed and transported, therefore introducing many uncertainties regarding risk assessment and risk management in the environment [21–27]. Behavior and stability are strongly related to their intrinsic properties (surface chemistry, charge, size, shape), physicochemical properties (pH, ionic strength, cation valency) as well as to the water composition (natural organic matter, polymers) [28–31]. The fate, behavior as well as the transport of nanoparticles in aquatic environment are principally driven by the NP surface charges, mainly resulting from the acid/base properties of surface sites. All these parameters will play a key role in the NP behavior and stability regarding aggregation, coating, dissolution processes and many possible scenarios are possible as shown in **Figure 1.2**. For example, when NPs are stable in a dispersing medium, they are more mobile and more bioavailable, whereas when NPs are destabilized via aggregation, they form large structures, which are eliminated from the aquatic systems by sedimentation [3,24]. **Therefore, understanding the transformation and transport of NPs, in particu-**

lar aggregation processes, remains an important issue to evaluate the environmental risks.

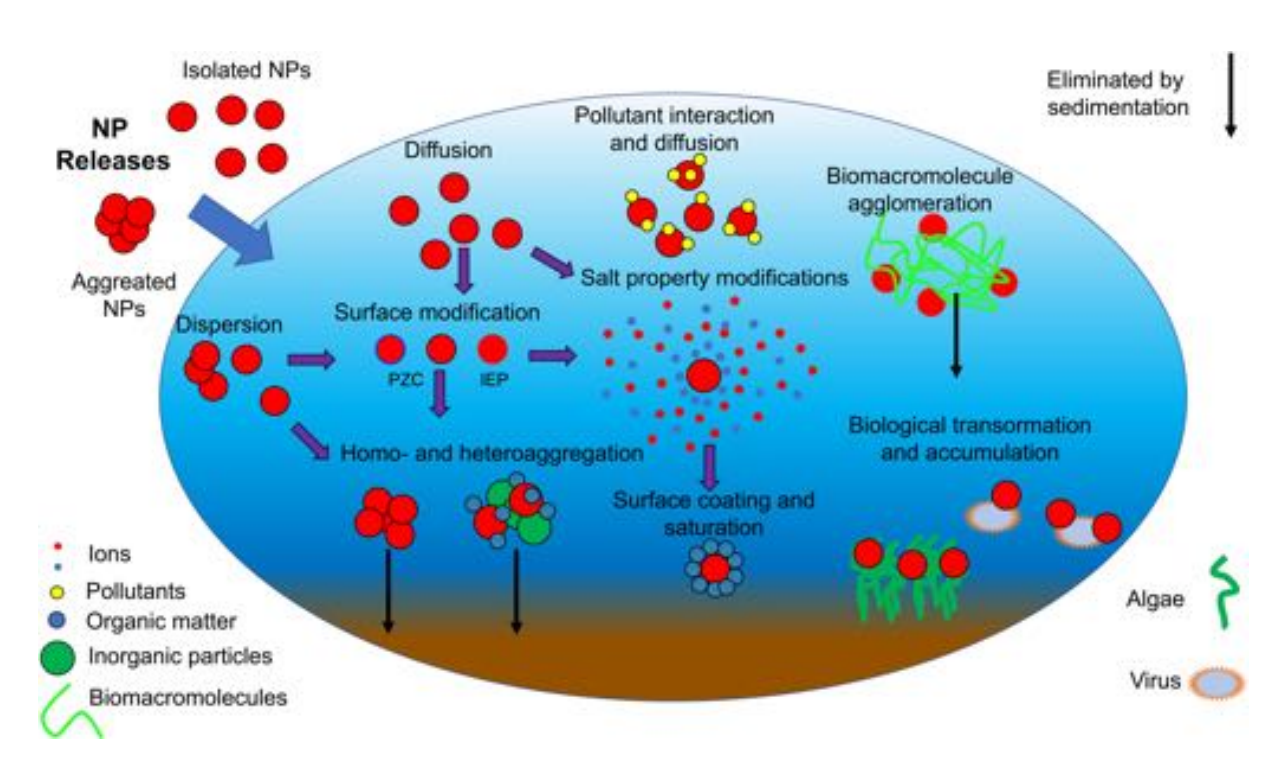


Figure 1.2: Nanoparticle behaviors and processes in aquatic systems.

1.3 Importance of NP surface charge and heteroaggregation processes

As mentioned previously, the NP surface charge is playing a key role on the environmental fate of nanoparticles [17, 32–34]. In contact with an aqueous media, most of the nanoparticles are charged, originating from different mechanisms such as surface ionization, isormorphous substitution, dissolution processes or adsorption of polyelectrolytes or ionic surfactants, which provide various distributions of surface charges (heterogeneous, homogeneous and patch) [35]. These charges are mainly resulting from the acid/base properties of the surface but also depend on the physicochemical dispersion media (temperature, pH, ion concentration). Moreover, these surface charges may evolve over time and conditions. At low and high pH, it is common to respectively have positive and negative surfaces for metal oxide particles (TiO₂, CeO₂). However, in very specific situations, an "effective" neutral surface may be observed corresponding to an extinction of all sites (Point of Zero Charge (PZC)) or to a coexistence of an equal number of opposite charges (IsoElectric Point (IEP)). In this context, the electrostatic interactions arising

from the surface charge is a key parameter in the NP behavior. A subtle competition between attraction and repulsions occurs which can be altered by the ion composition. Mono-, di- and trivalent cations may alter the nanoparticle behavior depending on the electrostatic screening effect [36]. From an experimental point of view, ζ potential measurements may be performed to obtain a surface charge description [28, 37, 38]. In aquatic media, the composition of the water column also plays a key role in the stability of nanoparticles. Natural organic matter (NOM) composed by humic and non-humic substances represents an important part of particles present in solution [39] and is expected to interact with nanoparticles via heteroaggregation or surface saturation (Figure 1.2). As shown by Loosli et al. [28], a low NOM concentration will lead to charge neutralization and the formation of large aggregates via bridging mechanisms while a high concentration promotes the disaggregation. Heteroaggregation as well as homoaggregation between nanoparticles is an important process in the fate of nanoparticles and especially in order to eliminate nanoparticles from the solution. In both mechanisms, the surface charges and electrostatic interactions are important parameters in order to understand their behavior. Due to the numerous possible scenarios and the large range of properties to take into account, understanding the nanoparticle behavior in aquatic remains a complex challenge. However, the scientific interest is growing due to the possible ecological and human health risks at short and long terms. Consequently, studying and understanding the influence of various physicochemical properties on such scenarios is then of main importance in order to improve the knowledge on these (possible) contaminants.

1.4 Thesis objectives

The main objective of this thesis work consists to develop original models, approaches and tools based on computer modelling to get an insight into i) the surface charge behavior of nanoparticles in aquatic systems as well as ii) heteroaggregation process between nanoparticles and an important aquagenic compounds i.e natural organic matter (NOM). Most actual models in this domain do not take into account a detailed description of the nanoparticle surface and solution chemistry including explicit counterions, salt particles and NOM. Physical and chemical investigations are performed here using Monte Carlo simulations, which is a powerful and rewarding method. In this context, the surface charging behavior of a nanoparticle is first investigated in **Chapter 3** by following the impact of site distribution, surface charge density, dielectric and acid/base properties (**Paper I**). Then, the ion condensation is studied by investigating the influence of surface and salt properties in **Chapter 4**. Surface distribution and density as well as salt concentrations and cation valencies are taking into account (Paper II). In **Chapter**

Introduction and Thesis objectives

5, a novel model of heteroaggregation is proposed and validated in order to calculate specific kinetic aggregation rate constants and attachment values (**paper III**). A case study composed of nanoparticles in presence of NOM units (fulvic acid) is considered and different environmental scenarios are investigated from ultrapure waters to marine and fresh waters. Then in the conclusion part (**Chapter 6**), a synthesis of the main results obtained during this thesis is presented with some future perspectives. The different models developed all along this thesis work are presented in **Figure 1.3**.

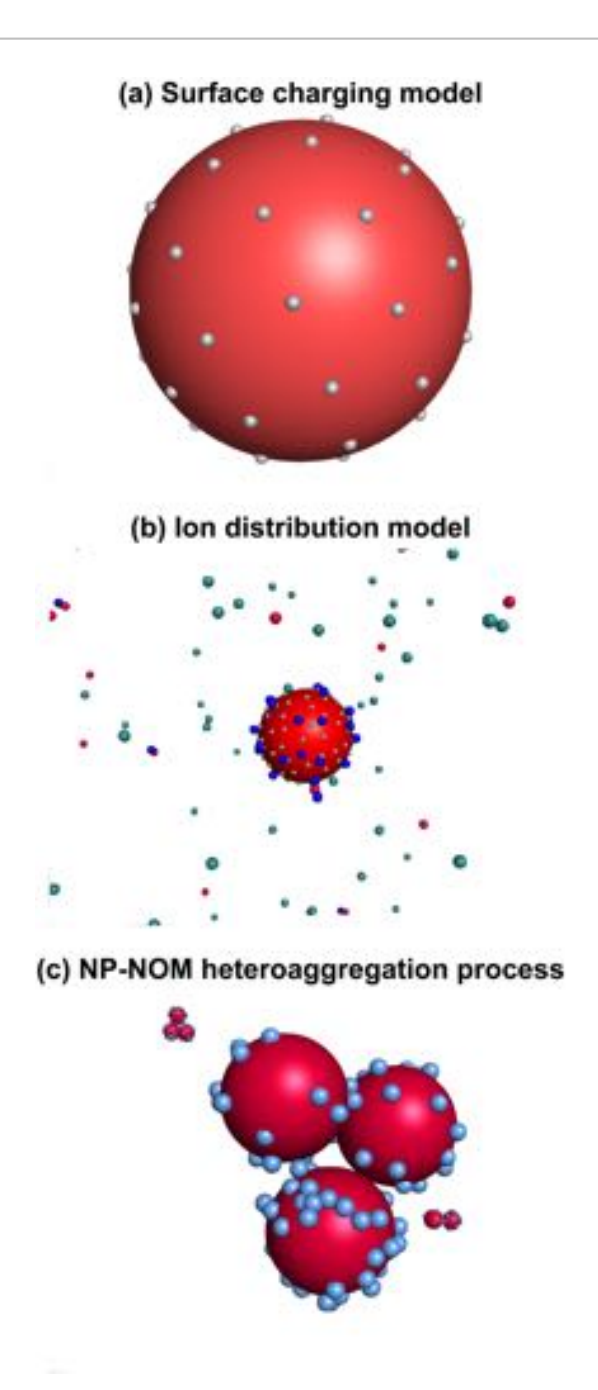


Figure 1.3: Different models developed and found in Papers I to III. (a) Surface charging process of a surface-detailed nanoparticles (b) Ion distribution around a spherical nanoparticles with explicit ions (c) Homoaggregation of nanoparticles and (d) heteroaggregation model of NPs with NOM units.

1.5 List of papers

Papers included in this Thesis

Published:

Paper I

Clavier, A., Seijo, M., Carnal, F., et Stoll, S., 2015, "Surface charging behavior of nanoparticles by considering site distribution and density, dielectric constant and pH changes – a Monte Carlo approach", *Physical Chemistry Chemical Physics*, v. 17, no. 6, p. 4346-4353.

Paper II

Clavier, A., Carnal, F., et Stoll, S., 2016, "Effect of Surface and Salt Properties on the Ion Distribution around Spherical Nanoparticles: Monte Carlo Simulations", *Journal of Physical Chemistry. B, Condensed Matter, Materials, Surfaces, Interfaces and Biophysical*, v. 120, no. 32, p. 7988-7997.

Submitted:

Paper III

Clavier, A., Praetorius, A., Stoll, S., "Determination of Nanoparticle Attachment Efficiencies and Heteroaggregation Rates in Presence of Natural Organic Matter for Contrasting Conditions using Monte Carlo Modelling", *Science of the TOtal Environment*.

Papers not included in this thesis

Published:

Loosli, F., Omar, F.M., Carnal, F., Oriekhova, O., Clavier, A., Chai, Z., et Stoll, S., 2014, "Manufactured Nanoparticle Behavior and Transformations in Aquatic Systems. Importance of Natural Organic Matter", *Chimia*, v. 68, no. 11, p. 783-787.

Carnal, F., Clavier, A., et Stoll, S., 2015, "Modelling the interaction processes between nanoparticles and biomacromolecules of variable hydrophobicity: Monte Carlo simulations", *Environmental Science: Nano*, v. 2, no. 4, p. 327-339.

Carnal, F., Clavier, A., et Stoll, S., 2016, "Polypeptide-Nanoparticle Interactions and Corona

Formation Investigated by Monte Carlo Simulations", *Polymers*, v. 8, no. 6, p. 203.

Submitted:

Praetorius A., Walch H., von der Kammer F., Tepe N., Brunelli A., Badetti E., Marcomini A., Gondikas A., Hassellöv M., Stoll S., Clavier A., Peijnenburg W., Quik J., "Review paper on suitable analytical methods to determine heteroaggregation attachment efficiencies between engineered nanoparticles and natural colloids/SPM", *Environmental Science Nano*.

Bibliography

- [1] Qianqian Cao and Michael Bachmann. Electrostatic complexation of linear polyelectrolytes with soft spherical nanoparticles. *Chemical Physics Letters*, 586:51–55, October 2013.
- [2] Konstantin Sobolev, Miguel Ferrada Gutiérrez, and The American Ceramic Society. How Nanotechnology Can Change the Concrete World. In *Progress in Nanotechnology*, pages 113–116. John Wiley & Sons, Inc., 2009.
- [3] Arturo A. Keller, Hongtao Wang, Dongxu Zhou, Hunter S. Lenihan, Gary Cherr, Bradley J. Cardinale, Robert Miller, and Zhaoxia Ji. Stability and Aggregation of Metal Oxide Nanoparticles in Natural Aqueous Matrices. *Environmental Science & Technology*, 44(6):1962–1967, March 2010.
- [4] Takuya Tsuzuki. Commercial scale production of inorganic nanoparticles. *International Journal of Nanotechnology*, 6(5/6):567, 2009.
- [5] Makio Naito, Masuo Hosokawa, Toyokazu Yokoyama, and Kiyoshi Nogi. *Nanoparticle Technology Handbook*. Elsevier, October 2007. Google-Books-ID: 6fvcH6SLSMIC.
- [6] Mélanie Auffan, Jérôme Rose, Jean-Yves Bottero, Gregory V. Lowry, Jean-Pierre Jolivet, and Mark R. Wiesner. Towards a definition of inorganic nanoparticles from an environmental, health and safety perspective. *Nature Nanotechnology*, 4(10):634–641, October 2009.
- [7] J. M. Wilkinson. Nanotechnology applications in medicine. *Medical device technology*, 14(5):29–31, June 2003.
- [8] W. J. Stark, P. R. Stoessel, W. Wohlleben, and A. Hafner. Industrial applications of nanoparticles. *Chemical Society Reviews*, 44(16):5793–5805, 2015.
- [9] K. Lance Kelly, Eduardo Coronado, Lin Lin Zhao, and George C. Schatz. The Optical Properties of Metal Nanoparticles: The Influence of Size, Shape, and Dielectric Environment. *The Journal of Physical Chemistry B*, 107(3):668–677, January 2003.
- [10] Christine Ogilvie Hendren, Xavier Mesnard, Jocelyn Dröge, and Mark R. Wiesner. Estimating Production Data for Five Engineered Nanomaterials As a Basis for Exposure Assessment. *Environmental Science & Technology*, 45(7):2562–2569, April 2011.

- [11] Fabiano Piccinno, Fadri Gottschalk, Stefan Seeger, and Bernd Nowack. Industrial production quantities and uses of ten engineered nanomaterials in Europe and the world. *Journal of Nanoparticle Research*, 14(9):1109, September 2012.
- [12] Kaspar Schmid and Michael Riediker. Use of Nanoparticles in Swiss Industry: A Targeted Survey. *Environmental Science & Technology*, 42(7):2253–2260, April 2008.
- [13] Bernd Nowack, James F. Ranville, Stephen Diamond, Julian A. Gallego-Urrea, Chris Metcalfe, Jerome Rose, Nina Horne, Albert A. Koelmans, and Stephen J. Klaine. Potential scenarios for nanomaterial release and subsequent alteration in the environment. *Environmental Toxicology and Chemistry*, 31(1):50–59, January 2012.
- [14] Vicki L. Colvin. The potential environmental impact of engineered nanomaterials. *Nature Biotechnology*, 21(10):1166–1170, October 2003.
- [15] Alex Weir, Paul Westerhoff, Lars Fabricius, Kiril Hristovski, and Natalie von Goetz. Titanium Dioxide Nanoparticles in Food and Personal Care Products. *Environmental Science & Technology*, 46(4):2242–2250, February 2012.
- [16] Fadri Gottschalk, Tobias Sonderer, Roland W. Scholz, and Bernd Nowack. Modeled Environmental Concentrations of Engineered Nanomaterials (TiO2, ZnO, Ag, CNT, Fullerenes) for Different Regions. *Environmental Science & Technology*, 43(24):9216–9222, December 2009.
- [17] Minghua Li, Suman Pokhrel, Xue Jin, Lutz Mädler, Robert Damoiseaux, and Eric M. V. Hoek. Stability, Bioavailability, and Bacterial Toxicity of ZnO and Iron-Doped ZnO Nanoparticles in Aquatic Media. *Environmental Science & Technology*, 45(2):755–761, January 2011.
- [18] Nicole C. Mueller and Bernd Nowack. Exposure Modeling of Engineered Nanoparticles in the Environment. *Environmental Science & Technology*, 42(12):4447–4453, June 2008.
- [19] Bernd Nowack and Thomas D. Bucheli. Occurrence, behavior and effects of nanoparticles in the environment. *Environmental Pollution*, 150(1):5–22, November 2007.
- [20] Paul Schulte, Charles Geraci, Ralph Zumwalde, Mark Hoover, and Eileen Kuempel. Occupational Risk Management of Engineered Nanoparticles. *Journal of Occupational and Environmental Hygiene*, 5(4):239–249, April 2008.

Introduction and Thesis objectives

- [21] Brian Carl Englert. Nanomaterials and the environment: uses, methods and measurement. *Journal of Environmental Monitoring*, 9(11):1154, 2007.
- [22] Stephen J. Klaine, Pedro J. J. Alvarez, Graeme E. Batley, Teresa F. Fernandes, Richard D. Handy, Delina Y. Lyon, Shaily Mahendra, Michael J. McLaughlin, and Jamie R. Lead. Nanomaterials in the environment: Behavior, fate, bioavailability, and effects. *Environmental Toxicology and Chemistry*, 27(9):1825–1851, September 2008.
- [23] Amy L. Dale, Elizabeth A. Casman, Gregory V. Lowry, Jamie R. Lead, Enrica Viparelli, and Mohammed Baalousha. Modeling Nanomaterial Environmental Fate in Aquatic Systems. *Environmental Science & Technology*, 49(5):2587–2593, March 2015.
- [24] Laura-Jayne A. Ellis, Eugenia Valsami-Jones, Jamie R. Lead, and Mohammed Baalousha. Impact of surface coating and environmental conditions on the fate and transport of silver nanoparticles in the aquatic environment. *Science of The Total Environment*, 568:95–106, October 2016.
- [25] Gregory V. Lowry, Kelvin B. Gregory, Simon C. Apte, and Jamie R. Lead. Transformations of Nanomaterials in the Environment. *Environmental Science & Technology*, 46(13):6893–6899, July 2012.
- [26] Julia Fabrega, Samuel N. Luoma, Charles R. Tyler, Tamara S. Galloway, and Jamie R. Lead. Silver nanoparticles: Behaviour and effects in the aquatic environment. *Environment International*, 37(2):517–531, February 2011.
- [27] M. N. Moore. Do nanoparticles present ecotoxicological risks for the health of the aquatic environment? *Environment International*, 32(8):967–976, December 2006.
- [28] Frédéric Loosli, Philippe Le Coustumer, and Serge Stoll. TiO2 nanoparticles aggregation and disaggregation in presence of alginate and Suwannee River humic acids. pH and concentration effects on nanoparticle stability. *Water Research*, 47(16):6052–6063, October 2013.
- [29] P. Christian, F. Von der Kammer, M. Baalousha, and Th Hofmann. Nanoparticles: structure, properties, preparation and behaviour in environmental media. *Ecotoxicology (London, England)*, 17(5):326–343, July 2008.
- [30] Fatehah Mohd Omar, Hamidi Abdul Aziz, and Serge Stoll. Aggregation and disaggregation of ZnO nanoparticles: Influence of pH and adsorption of Suwannee River humic acid. *Science of The Total Environment*, 468–469:195–201, January 2014.

- [31] Amro M. El Badawy, Todd P. Luxton, Rendahandi G. Silva, Kirk G. Scheckel, Makram T. Suidan, and Thabet M. Tolaymat. Impact of Environmental Conditions (pH, Ionic Strength, and Electrolyte Type) on the Surface Charge and Aggregation of Silver Nanoparticles Suspensions. *Environmental Science & Technology*, 44(4):1260–1266, February 2010.
- [32] Enrique Navarro, Anders Baun, Renata Behra, Nanna B. Hartmann, Juliane Filser, Ai-Jun Miao, Antonietta Quigg, Peter H. Santschi, and Laura Sigg. Environmental behavior and ecotoxicity of engineered nanoparticles to algae, plants, and fungi. *Ecotoxicology*, 17(5):372–386, July 2008.
- [33] Biplab Mukherjee and James W. Weaver. Aggregation and Charge Behavior of Metallic and Nonmetallic Nanoparticles in the Presence of Competing Similarly-Charged Inorganic Ions. *Environmental Science & Technology*, 44(9):3332–3338, May 2010.
- [34] Antonia Praetorius, Jérôme Labille, Martin Scheringer, Antoine Thill, Konrad Hungerbühler, and Jean-Yves Bottero. Heteroaggregation of Titanium Dioxide Nanoparticles with Model Natural Colloids under Environmentally Relevant Conditions. *Environmental Science & Technology*, 48(18):10690–10698, September 2014.
- [35] M. Elimelech, R. Williams, J. Gregory, and X. Jia. *Particle deposition and aggregation: Measurement, modelling and simulation*. Butterworth-Heinemann, 1998.
- [36] James A. Davis, Robert O. James, and James O. Leckie. Surface ionization and complexation at the oxide/water interface: I. Computation of electrical double layer properties in simple electrolytes. *Journal of Colloid and Interface Science*, 63(3):480–499, March 1978.
- [37] Etelka Tombácz and Márta Szekeres. Interfacial AcidBase Reactions of Aluminum Oxide Dispersed in Aqueous Electrolyte Solutions. 1. Potentiometric Study on the Effect of Impurity and Dissolution of Solid Phase. *Langmuir*, 17(5):1411–1419, March 2001.
- [38] Márta Szekeres and Etelka Tombácz. Surface charge characterization of metal oxides by potentiometric acid–base titration, revisited theory and experiment. *Colloids and Surfaces A: Physicochemical and Engineering Aspects*, 414:302–313, November 2012.
- [39] E. M. Thurman, R. L. Wershaw, R. L. Malcolm, and D. J. Pinckney. Molecular size of aquatic humic substances. *Organic Geochemistry*, 4(1):27–35, March 1982.

CHAPTER 2

Model, Theory and Simulation Methods

Whith the major progress achieved during the last decades in computer technologies, computational modelling is now a powerful and rewarding approach to have a better understanding of many processes in chemical, physical and environmental sciences. Computer modeling acts as a useful bridge between theory and experiments [1]. Theoretical or mathematical models provide general predictions on the behavior of a system while computer simulations allow to get a more detailed insight into complex systems [2,3]. On the other hand, the measurement of some parameters remains difficult to achieve in experiments and can be easily accessible *via* modelling and post data treatments [4]. However, despite the huge progress observed in computer modelling, the direct comparison of modelling made at the atomistic level with experimental studies remains very difficult even with the best supercomputers. Computer simulations might be adapted in space (numbers of particles vs. size of modelling box) or in time (different time scales) and some approximations are essential to achieve realistic calculation times.

The significant number of algorithms developed as well as the resulting infinite combinations offer interesting tools to investigate how nanoparticles will interact and react in environmental compartments and more especially in aquatic systems [5–9]. At small-scale, to understand NP behavior, the NP surface charge is expected to play a key role on the macroscopic properties of nanoparticles [10, 11] and related processes such as NP coating [12, 13] and aggregation [14–16]. The surface charge, often resulting from the acid/base properties of surface sites [17–19], as well as surface charge sign and density, depends not only on the physical-chemical properties of nanomaterials but also on the dispersing media (mainly pH and ion concentration) and on the presence of soluble species (polyelectrolytes, natural organic matters, etc). To have the most adapted and detailed description of what happen s at the nanoscale, the type of computer simulations as well as the corresponding physical laws to use remains an important choice in our models. In this chapter, all the different models, theories and computer simulations developed during this thesis work are presented.

2.1 Coarse-grained model

In soft matter, classical atomistic models are not adapted to study environmental systems. For instance, a colloidal suspension is generally composed of several millions of atoms and, at least, by an equivalent number of solvent molecules. An all atom representation of such a system at a large time scale is impossible. Therefore, to describe such a system in a proper way and to save computing time, some internal degrees of freedom have to be reduced and, for that purpose, coarse-grained models are commonly used [3, 20] (**Figure 2.1**).

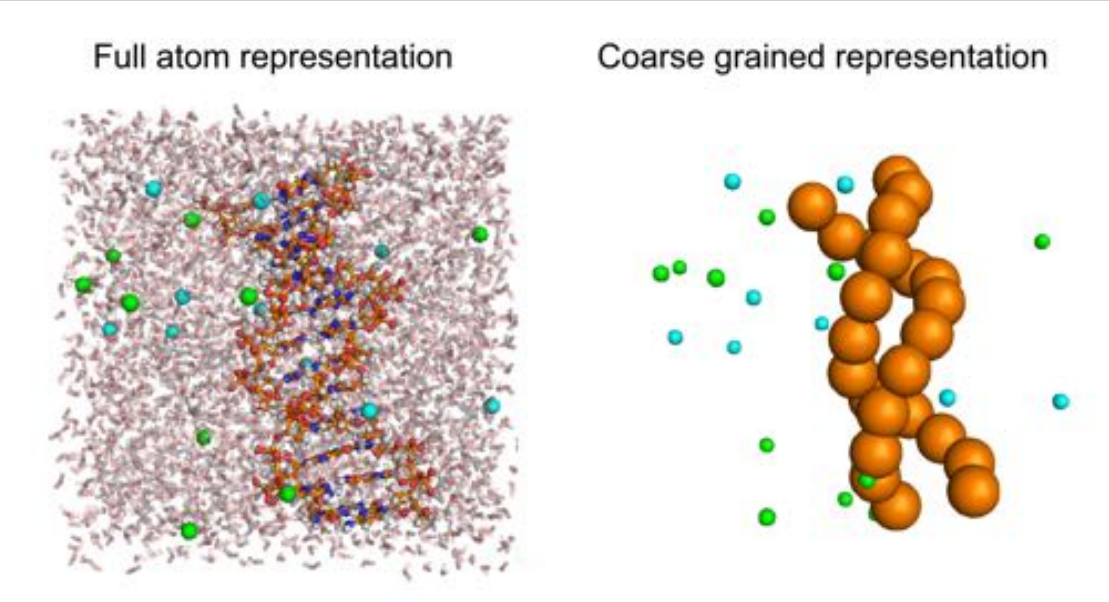


Figure 2.1: Full and coarse-grained representation of a DNA strand in a water solution with ions.

Different approximations can be made:

- Firstly, the solvent can be represented implicitly by an infinite dilute aqueous medium with a relative dielectric constant, typically taken as that of the water at 298K. This assumption of a very dilute solution will provide the only properties needed (temperature, viscosity and density) to mimic the hydrodynamic behaviors on long scale and time scales and allows to focus on the determination of large scale properties.
- Then, the mesoscopic colloids composed by group of atoms are replaced by impenetrable and solvent excluded spherical objects or pseudo-atoms. The internal microscopic properties of the colloids are not considered except for the acid/base properties of the surface with the presence of titrating sites (see section 2.4.) and for a dielectric discontinuity (see section 2.5.).
- Finally, ions, counterions and salt particles are described by spherical objects with a fixed radius and a positive or negative charge on their centers. This representation allows to consider the effect of salt on aggregation as well as to take into account electro-neutrality. In addition, ion contribution can be computed in the solvent properties *via* the dielectric constant and when aggregation processes are considered in the attachment efficiency parameter.

Despite the fact that the first coarse-grained model has been developed almost a half-century ago [21–25], this approach has proven in the last ten years to be a powerful tool to describe complex system and especially protein and polymer conformations at different multiscale. During this decade, the number of publications on coarse-grained model increased several times and in 2013, Michael Levitt, Ariel Warshel, and Martin Karplus has been awarded for "The development of multiscale models for complex chemical systems" by a Nobel prize in chemistry [26, 27]. The Nobel committee recognized their early works on the computing of large biomolecular systems based on a coarse-grained description of proteins.

In the literature, two different types of coarse-grained model have been developed. The first one corresponds to a model deriving from the specific characteristic of a well-known system or experiment. The medium characteristics, the polymer structures as well as the surface charge properties have to be reproduced according to the system under investigation. Typically, these specific properties can be obtained from atomistic simulations and/or experimental methods. This model allows to equilibrate specific systems and to investigate large scale behaviors. The second coarse-grained model approach (modelling) is more generic without any connection to a specific system or an experiment. General features that are needed as input parameters are, in our case, NP sizes, surface charge density or ion concentrations. Systematic and statistical studies can be performed in order to understand general mechanisms, and variations in experimental and theoretical observations. In this thesis work, generic coarse-grained models are considered and parametrized to mimic the nanoparticle behavior in aquatic systems from surface charge behavior to aggregation processes.

2.2 Force field model an interaction potentials

The behavior of particles in colloidal suspensions is mainly controlled by the nature of the interaction forces between them. Interactions are directly and indirectly derived from the longand short-range forces. In this context, a proper force field definition is required to reproduce in the best way the interactions between a system of atoms or coarse-grained particles. A force field is generally defined by functional forms and parameter sets which both are typically determined and parametrized *via* empirical methods (physical and chemical experiments and/or quantum calculations).

The interaction potentials are commonly divided into three main contributions: (i) interactions between atoms linked by covalent bonds E_{cov} (bond E_{bond} , valence angle E_{angle} and dihedral potential $E_{dihedral}$), (ii) non-covalent interactions $E_{non-cov}$ (Van der Walls and electrostatic potentials) and (iii) excluded volume interactions E_{H-S} (hard spheres).

$$E_{tot} = E_{cov} + E_{non-cov} + E_{H-S} = E_{bond} + E_{angle} + E_{dihedral} + E_{elec} + E_{VdW} + E_{H-S}$$

$$(2.1)$$

The main "non-bonded" or non-covalent potential energies used in coarse-grained computer simulations are presented in the next section.

2.2.1 Hard sphere interactions

At "very" short range, strong repulsions occur between particles i and j, and lead to excluded volume interactions. For that purpose, particles are described by impenetrable spheres and cannot overlap each other.

$$E_{H-S} = \begin{cases} \infty, r_{ij} < R_i + R_j \\ 0, r_{ij} \geqslant R_i + R_j \end{cases}$$
 (2.2)

Here r_{ij} represents the distance between particles i and j and $R_{i,j}$ the radius of species i or j.

2.2.2 Van der Waals interactions

Van der Waals forces combine weak intermolecular attractive and repulsive forces and derive their origin from fluctuating polarizations of electronic clouds. Van der Waals interactions may be categorized in three different contributions (i) dipole-dipole interactions called also Keesom force (attractive or repulsive) (ii) dipole-induced dipole interactions called also polarization or Debye force (attractive) and (iii) induced dipole-induced dipole interactions called also dispersion or London forces (attractive). The van der Waals energy E_{VdW} between two objects separated by a distance r can be written as:

$$E_{VdW}(r) = \frac{1}{(4\pi\varepsilon_{VdW})^2 r^6} \sum \beta$$
 (2.3)

where ε_{VdW} represents the energy depth at minimum and β the specific parameter of each forces. Van der Waals interactions have an inverse sixth power dependence which describes the attraction at short ranges. However, the Pauli exclusion principle that characterizes repulsion at short ranges is not taken into account in equation 2.3 and is generally mathematically added to the model without theoretical justification. This approximation is proportional to an inverse twelfth power factor which is more convenient for computing efficiency (r^{12} is the square root of r^6). Therefore, both attractive and repulsive van der Waals interactions are generally described *via* Lennard-Jones potential:

$$E_{VdW}(r) = E_{LJ}(r) = \varepsilon_{VdW} \left(\left(\frac{r_0}{r} \right)^{12} - 2 \left(\frac{r_0}{r} \right)^6 \right)$$
 (2.4)

where r_0 corresponds to the minimum energy distance between two particles. When the hard sphere interaction model is taken into account, r_0 is equal to the sum of the two radii of the interacting particles.

2.2.3 Electrostatic interactions

The presence of charged particles in solution induces long-range electrostatic interactions between them [18, 19]. They are playing key roles on the particle behavior in aquatic systems. Coulomb's law is commonly employed to describe the potential energy between different or similar species. In a medium, the Coulomb potential energy of two charges q_i and q_j , separated by a distance r_{ij} , is defined as follow:

$$E_{elec}^{ij}(r_{ij}) = \frac{q_i q_j}{4\pi\varepsilon_0 \varepsilon_r r_{ij}} = \frac{z_i z_j e^2}{4\pi\varepsilon_0 \varepsilon_r r_{ij}}$$
(2.5)

where e represents the elementary charge, $z_i(i,j)$ the amount of charges, ε_0 the vacuum permittivity and ε_r the dielectric constant of the medium. Electrostatic interactions are inversely proportional to the distance between charges and represent the energy required to bring q_i from

the infinity to a distance r from q_i . The solvent is implicitly taken into account through its dielectric constants. The full Coulomb potential is the sum of whole possible interactions between charges present in solution (titrating sites, counterions, salt particles, colloids):

$$E_{elec}^{Tot}(r_{ij}) = \sum_{i} \sum_{j} E_{elec}^{ij}(r_{ij} = \sum_{i} \sum_{j} \frac{q_i q_j}{4\pi\varepsilon_0 \varepsilon_r r_{ij}} = \frac{z_i z_j e^2}{4\pi\varepsilon_0 \varepsilon_r r_{ij}}$$
(2.6)

The interaction is considered attractive between opposite charges $(E_{elec}^{Tot}(r) < 0)$ and repulsive between similar charges $(E_{elec}^{Tot}(r) > 0)$.

2.3 Periodic boundary condition

Nowadays, computer simulations can handle a number of freedom degrees from a few hundred to a few millions. For most simulations, this limit is found around a few hundred to a few thousand particles, clearly far away from experimental or environmental sample concentrations. Periodic boundary conditions allow a system composed by a small number of particles to be representative of an infinite bulk solution. The initial cubic simulation box composed by N-particles is reproduced in all directions to create a periodicity. In three dimensions, 26 identical copies of the simulation region surround the simulation box. If a particle leaves the box from a given side, it will return in the simulation box by the opposite side as shown in **Figure 2.2**. The number of particles in the central box remains constant during all the simulation.

In addition, to calculate the pairwise interactions between particles in an efficient way, the minimum image convention, which consider the minimum distance between two particles, is generally used. A particle interaction is determined with the nearest neighbor in the periodic array (particle or image). For instance, in **Figure 2.2**, particles 2 and 3 will interact with the particle image 4 et 3 while particle 1 with particle 4 and 5.

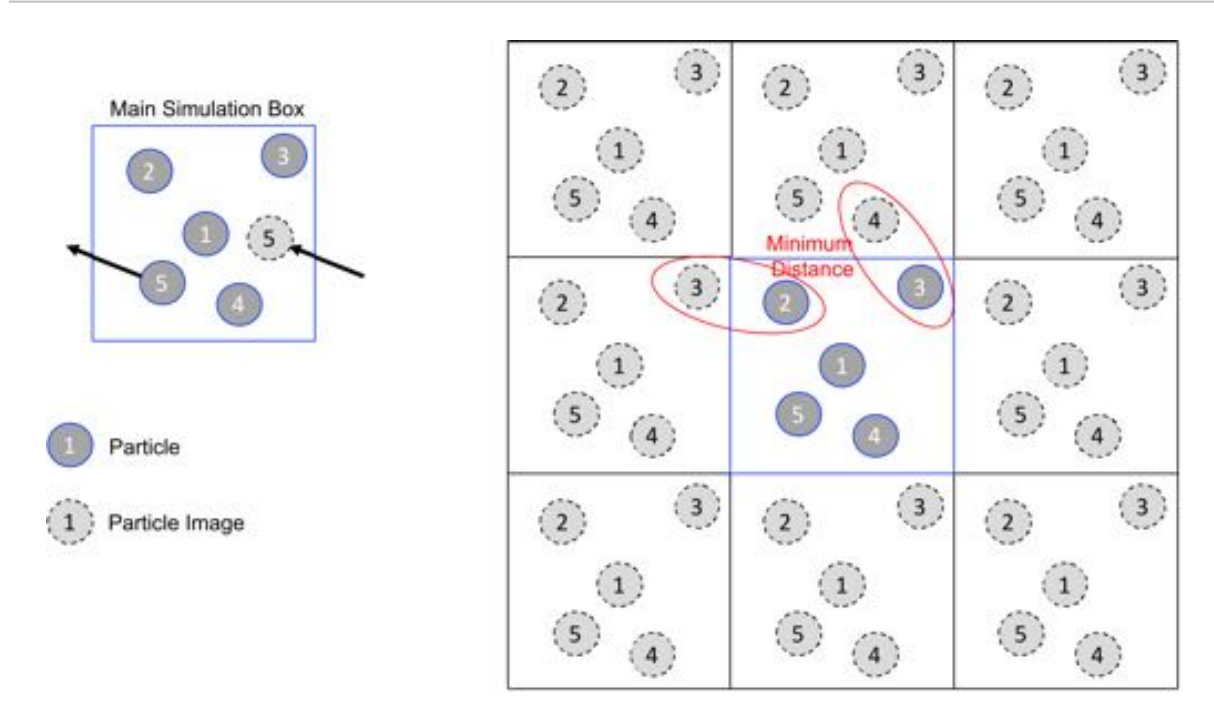


Figure 2.2: Periodic boundary conditions and minimum image convention.

2.4 Surface charge properties

As already mentioned, surface properties of colloids and nanoparticles in particular are essential in controlling environmental processes such as aggregation.

2.4.1 Origin of the surface charge

Most of the particles in contact with an aqueous media are "coated" with electric charges on their surfaces so as to reduce the interfacial energy. Resulting charge sign and density arise from the surface group properties such as acid base properties as well as the surrounding environment property such as pH. Three different mechanisms can explain the presence of charges on surfaces and are discussed in the next section.

Surface ionization

The surface charge at the interface of two phases results from the chemical reactions occurring at the surface. Many colloidal particles hold ionizable functional groups on the surface: $-\mathrm{OH}$, $-\mathrm{OPO_3H}$, $-\mathrm{COOH}$, $-\mathrm{NH_2}$. In contact with water, the oxide and amine groups react with protons $\mathrm{H^+}$ and hydroxides $\mathrm{OH^-}$ of the bulk solution. The functional groups are then pro-

tonated, deprotonated or not dissociated as a function of the pH and the chemical equilibrium constants (**Figure 2.3.(a**)). Consequently, the surface is generally positively charged at low pH and negatively charged at high pH, as reported by the following chemical equilibria:

$$M - H_2^+ \stackrel{K_{a1}^0}{\rightleftharpoons} M - H + H^+ \stackrel{K_{a2}^0}{\rightleftharpoons} M^- + 2H^+ \tag{2.7}$$

$$M - H \stackrel{K_{a2}^0}{\rightleftharpoons} M^- + H^+ \tag{2.8}$$

With $K^0_{a1,a2}$ the equilibrium constants of diprotic reactions.

Biological surfaces bring an interesting example of this process with the presence of both carboxylic and amine groups and the surface charge may be reversed according to the solution media and surface properties. This process allows the possibility to have positive, negative charges, or a neutral particle. However, monofunctional ionic groups, for example, latex particles result from the presence of carboxylic and sulphate groups only. With pH changes, the degree of ionization of the surface can approach zero but no charge reversal is observed.

Dissolution or adsorption processes

The second case of surface charge acquisition includes the surface modification by adsorbing charged particles on the colloid or nanoparticle surface or by releasing ions from the crystal lattice. For the latter, the ions available on the lattice surface has a greater tendency to "escape" due to the limited crystal solubility in water (**Figure 2.3.(c**)). One typical example of this dissolution process is silver iodide AgI which have a very low solubility in water, especially iodide. In contrast, silver particles have a greater tendency to dissolve in the aqueous solution, leaving a negative charge on the surface.

On the other hand, a surface charge may be created or altered by adsorbing an object on a neutral or already charged particle. Various mechanisms might occur, for instance, the adsorption of polyelectrolytes or surfactants on a nanoparticle, strong covalent bond between metal oxydes and biomacromolecules (humic acid) and condensation processes of ions from the so-

lution. All these processes are strongly related to the properties of the NP surface. Moreover, the salt properties can have a strong infleunce on these mechanisms via screening effects. Ion condensation processes are generally emphasized in the presence of multivalent ions such as Ca^{2+} , Mg^{2+} , Fe^{3+} , Al^{3+} , etc. However, when the pristine NP surface is neutral, some specific and favorable conditions are required to complete the surface modification, especially non-electrostatic interactions (VdW interactions).

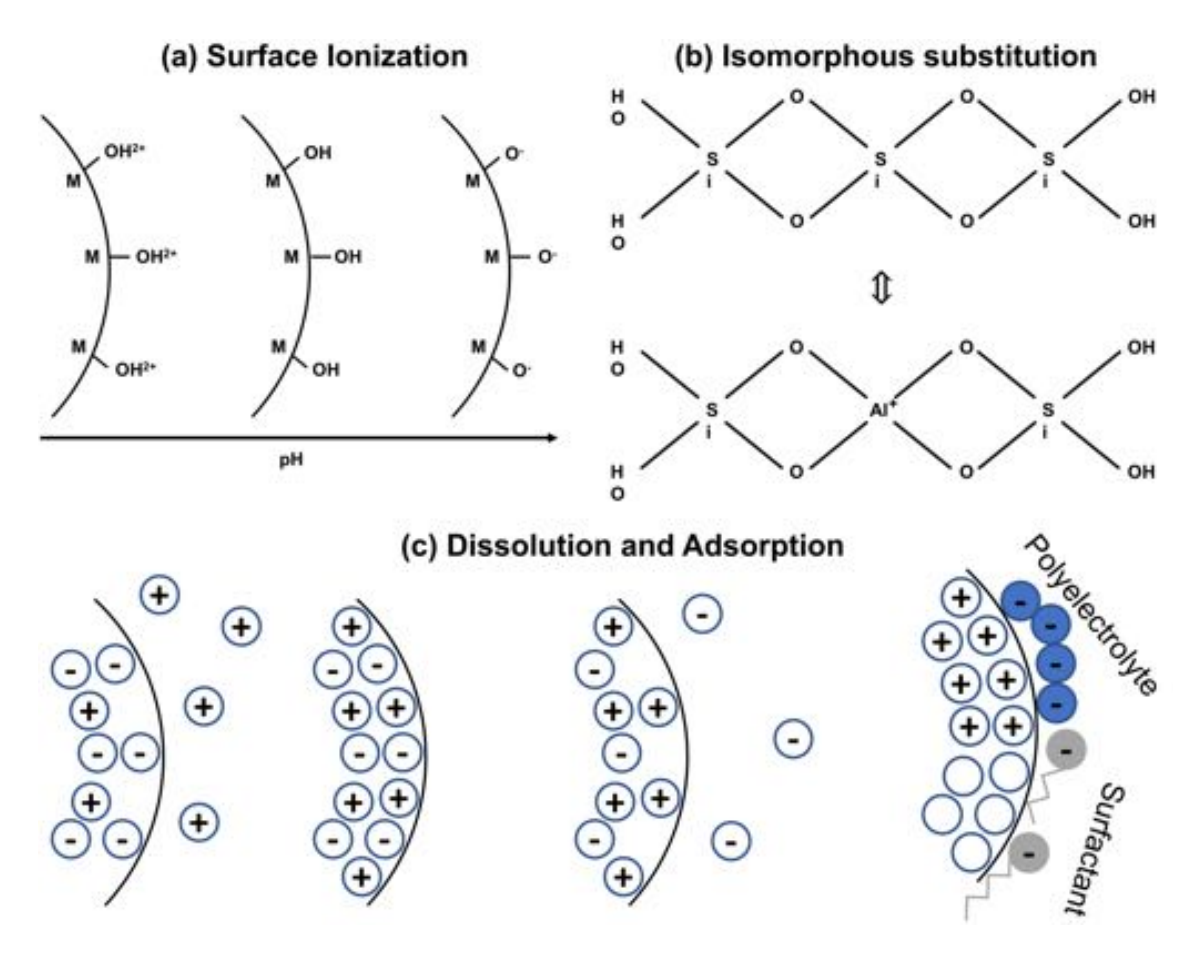


Figure 2.3: Origin of surface charges. (a) Surface ionization, (b) Isomorphous substitution and (c) dissolution/adsorption processes.

Isomorphous substitution

The third mechanism concerns the lattice defects arising from isomorphous substitution in the crystal structure. This charge acquisition process is quite different as it consits as an internal modification of the materials resulting in an "inherent" excess surface charge. The best-known example is kaolinite, a tetrahedral silica layer, which is alternated with an octahedral alumina layers. In both layers, some Si^{4+} and Al^{3+} atoms may be respectively replaced by Al^{3+} and Mg^{2+} and as shown in **Figure 2.3.(b)**, a negative charge is emerging from the surface. A similar mechanism is observed for many clay minerals in water resulting in a general negative surface charge.

2.4.2 Point of Zero Charge versus IsoElectric Point

In many situations, pH is playing a key role in the protonation/deprotonation of a surface. Two characteristic pH values can be defined from the surface charging process. Both of them describe a situation where the net surface charge is equal to zero. The first one, call the *Point of Zero Charge* (PZC) corresponds to pH conditions where all the titrating sites on the surface are neutral, while the second, the *IsoElectric Point* (IEP or pI), represents a pH value for which the number of negatively charged surface groups is counter balanced by the positives ones. These two points coincide only when no specific ion adsorptions occur. The PZC is generally determined by titration techniques, whereas IEP is determined *via* ζ potential methods [28–30].

2.4.3 Henderson-Hasselbach equation

The acid/base properties of an isolated site are commonly described by the Henderson-Hasselbach equation [31–33]. As mentioned previously under specific conditions, positive or negative charges originate from a titrating site. The dissociation of an isolated acid in an aqueous media is given by the equation 2.9.:

$$HA \stackrel{K_a^0}{\rightleftharpoons} A^- + H^+ \tag{2.9}$$

and the associating equilibrium constant is defined according to the mass action law:

$$K_a^0 = \frac{[\mathrm{H}^+][\mathrm{A}^-]}{[\mathrm{HA}]}$$
 (2.10)

Where $[H^+]$, $[A^-]$ and [HA] are the concentrations of dissociated hydrogen and dissociate/non-dissociate acids, respectively. The degree of ionization is then defined as:

$$\alpha_p = \frac{[\mathbf{A}^-]}{[\mathbf{H}\mathbf{A}] + [\mathbf{A}^-]} \tag{2.11}$$

And finally lead to the Henderson-Hasselbach equation:

$$pH = pK_a^0 + log_10(\frac{1 - \alpha_p}{\alpha_p})$$
(2.12)

For an amphoteric system, diprotic reactions are defined following the equations 2.7 et 2.8 and the Henderson-Hasselbach equation are rewritten as follow:

$$pH = pK_{amoy}^0 \pm log_{10}(\frac{1 - \alpha_p}{\alpha_p})$$
(2.13)

where $pK_{amoy}^0 = \frac{pK_{a1}^0 + pK_{a2}^0}{2}$. The plus and minus signs correspond respectively to the degree of proton association and dissociation.

2.4.4 Surface titrating site and Tanford-Kirkwood model

From a modelling point of view, the model of Tanford and Kirkwood (TK) [34, 35] takes into account the fact that charges are not uniformly distributed on the surface but as a discrete point-charge representation. TK model describes charge objects such as macroions, nanoparticles or biomolecules (globular protein) as impenetrable spheres (**Figure 2.4**). Discrete charges are then mapped by points close to the surface with an internal dielectric constant which can be different from the solvent. Due to its ability to take into account different dielectric constants, TK model has been chosen to represent the discrete charges arising on the nanoparticle surface and dielectric discontinuity between the nanoparticle and the dispersing medium.

Tanford-Kirkwood model

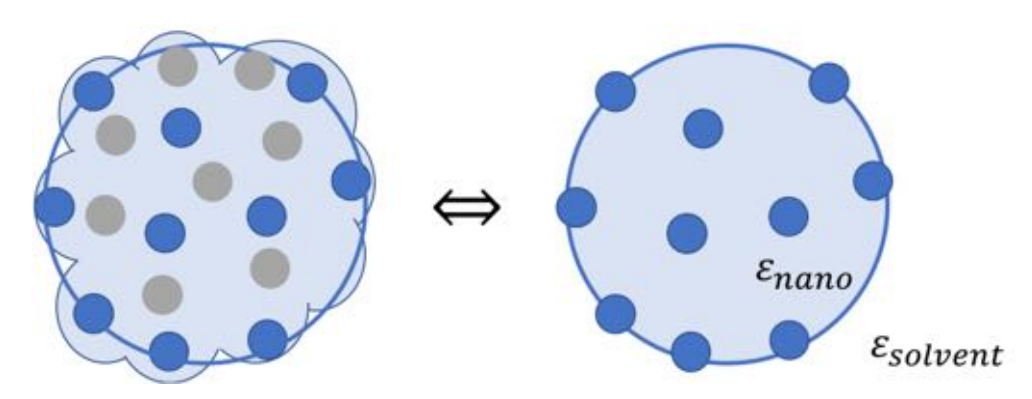


Figure 2.4: Representation of the Tanford and Kirkwood model.

Different environmental and experimental scenarios may be considered to describe the site distribution on the nanoparticle surface and can be classified in two different categories (i) site distribution (homogeneous/heterogeneous or patches) and (ii) site arrangement (homogeneous or heterogeneous).

Titrating surface sites can be distributed all around the nanoparticle surface, heterogeneous and homogeneous distribution (Figure 2.5.(b) and 2.5.(c)) or present in confined area on the surface, resulting in patch distributions (**Figure 2.5.(d**), (e) and (f)). Heterogeneous/homogeneous distributions refer to pristine particle while patches to the coexistence of different materials or when a crystal plane is not large enough to neglect boundary conditions. The presence of multiple patches illustrates different coexistence zones [36, 37]. Two different arrangements are also considered: a heterogeneous disposition resulting from defect or chemical impurity on a crystal plan, material coexistence or by a passivation [38] of the surface and a homogeneous arrangement corresponding to a perfect crystal organization. Surface sites are usually randomly distributed on the surface (or in patches) and the excluded volume is taken into consideration to generate the heterogeneous arrangement. For the homogeneous case, a reorganization of a heterogeneous surface is performed by adjusting the site position using a Metropolis criterion in Monte Carlo simulation (see below, section 2.5) to obtain an optimal configuration. Both arrangements are also adopted for patch distribution. It should be noted that the surface charge can also be described by an uniform surface charge density resulting from the presence of a single fixed charge at the center of the nanoparticle (**Figure 2.5.(a**)).

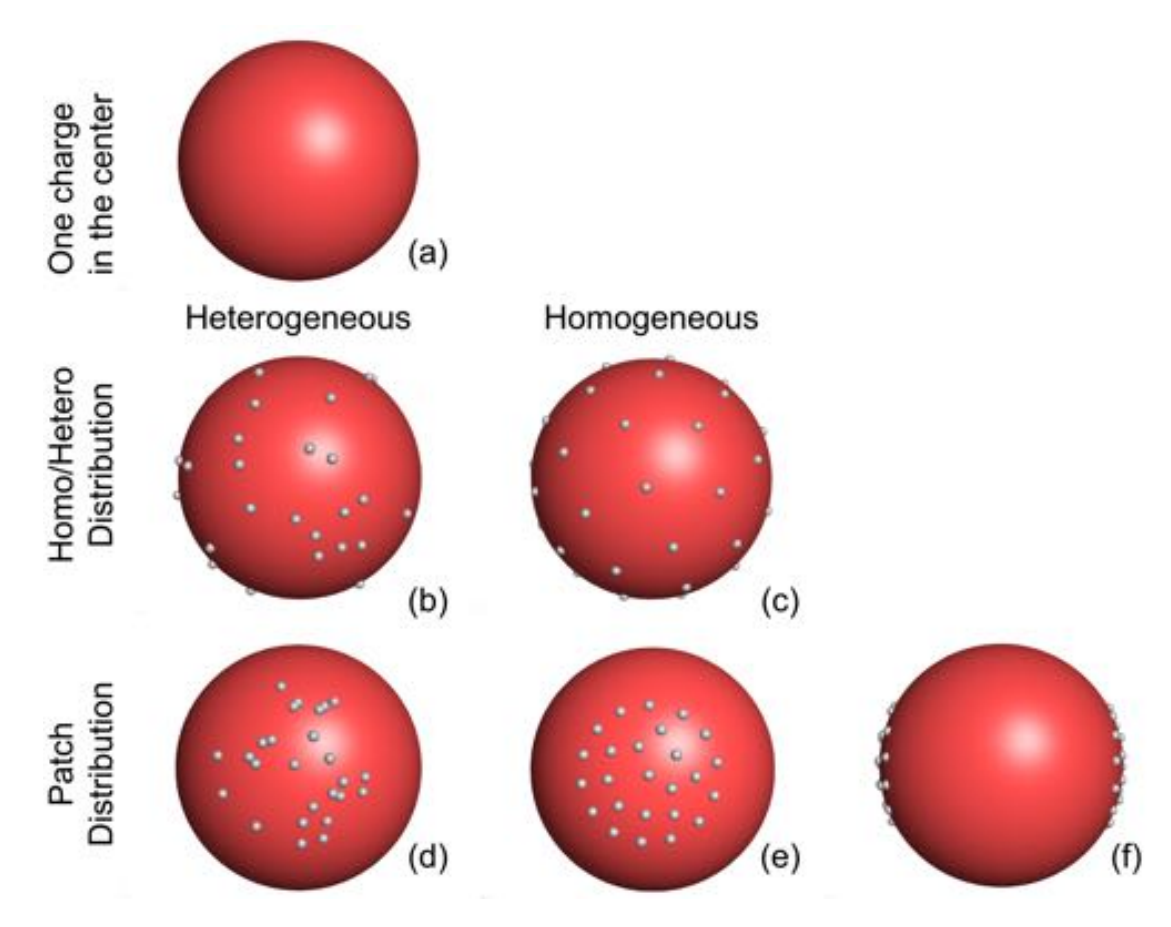


Figure 2.5: Spatial distributions of surface discrete charges. (a) homogeneous, (b) heterogeneous and (c) patch distributions.

2.4.5 Electrical double layer models

Independently of the origin of the surface charge, the contact with a dispersing medium composed of water and ions will lead to a characteristic structuration of the solvent [39]. If we consider the water described by a continuum model, and Stern Grahame approach [19], the electric double layer refers to two parallel charged layers: (i) the surface charge and (ii) a second layer composed by opposite charged ions (*counterions*) attracted to the surface. A corresponding excess of counterions in the solution automatically counterbalances the charge arising from the surface in order to keep the electroneutrality of the solution. This ion distribution description was widely studied and theoretical models with different complexity levels were developed such as the models of Helmholtz, Gouy-Chapman, Stern or Grahame.

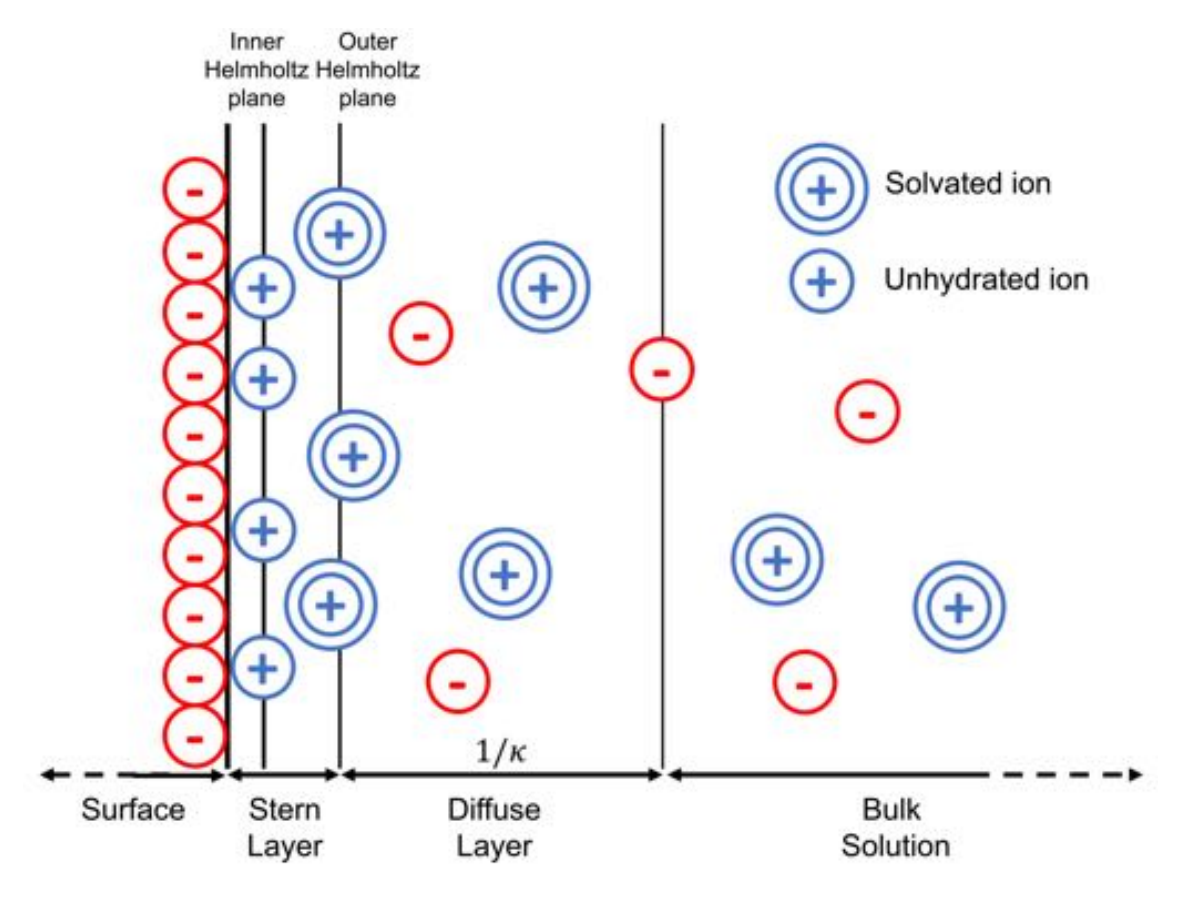


Figure 2.6: Model of Stern-Grahame of the electrical double layer.

According to Helmholtz, the double layer can be mathematically represented as a capacitor with both negative and positive charges distributed on two different planes (electrode and electrolyte) separated by a fixed distance l_H , the Helmholtz plane. l_H is approximately equal to 2 to 3 Å. The differential capacitance C_H can be calculated and is independent on the charge density, the resulting electrostatic potential $\Delta\Phi$ and the ion properties, but is dependent on the dielectric properties and the thickness of the double layer l_H :

$$C_H = \frac{dq}{d\Delta\Phi} = \frac{\varepsilon_0 \varepsilon_r}{l_H} \tag{2.14}$$

However, even if the charge is confined on the surface, the ions are considered as mobile in the solution and may be adsorbed on the surface due to electrostatic attractions.

The model of Gouy-Chapman introduces a diffuse layer in the theory for a low concentration of electrolytes by taking into account mobile ions in the solution represented by point-charges. Ions are then non-homogeneously distributed in the solution as a function of the electrostatic attractions to the charged surface (surface charge density and potential) and the random motion of ions originating from the thermal dispersion occurring in the solution. The distribution of these mobile ions around surface charge are generally predicted using Poisson-Boltzmann theory. From electrostatic theory, the electrostatic potential at any point r, $\Phi(r)$ is related to the charge density $\rho(r)$ through the Poisson's equation as followed:

$$\nabla^2 \Phi(r) = -\frac{\rho(r)}{\varepsilon_0 \varepsilon_r} \tag{2.15}$$

With
$$\nabla^2 = \frac{\delta^2}{\delta x^2} + \frac{\delta^2}{\delta y^2} + \frac{\delta^2}{\delta z^2}$$
 the Laplacian.

In an electrolyte solution, the local concentration of ions i at a position r may be expressed by a Boltzmann distribution as:

$$n_i(r) = n_{i0} exp\left(-\frac{q_i \Phi(r)}{k_b T}\right)$$
 (2.16)

With n_{i0} defined as the concentration of species i in the bulk solution at $\Phi(r) = 0$, k_B the Boltzmann constant and T the temperature. The charge q_i can be replaced by $z_i e$ as already showed in section 2.5. $n_i(r)$ is also related to the electrostatic potential of the solution.

The charge density $\rho(r)$ may be related then to the local ion concentration:

$$\rho(r) = \sum_{i} q_i n_i(r) = \sum_{i} q_i n_{i0} exp\left(-\frac{q_i \Phi(r)}{k_b T}\right)$$
 (2.17)

The generalized Poisson-Boltzmann (PB) equation is then finally obtained by combining the equation 2.15, 2.16 and 2.17 and a nonlinear equation is obtained:

$$\nabla^2 \Phi(r) = -\frac{1}{\varepsilon_0 \varepsilon_r} \sum_i q_i n_{i0} \left(exp - \frac{q_i \Phi(r)}{k_b T} \right)$$
 (2.18)

In general, the Poisson Boltzmann equation does not have analytical solutions. However, the resolution of the PB equation remains possible for simple case such as flat and spherical surfaces uniformly charged by considering some approximations. In the Debye-Hückel theory, the approximation consists to linearize the PB equation.

At low electric potential ($\Phi(r)$ < 26 mV at 298 K), the electrical energy $q_i\Phi(r)$ becomes smaller compared to the thermal energy of the system k_bT . The exponential may then be replaced by a Taylor series as follow:

$$\nabla^2 \Phi(r) = -\frac{1}{\varepsilon_0 \varepsilon_r} \left(\sum_i q_i n_{i0} - \sum_i q_i^2 n_{i0} \frac{\Phi(r)}{k_b T} + \sum_i q_i n_{i0} \frac{1}{2!} \left(exp\left(-\frac{q_i \Phi(r)}{k_b T} \right) \right)^2 \right)$$
(2.19)

If we maintain the first order of the Taylor series and due to the electroneutrality of the system ($\sum_i q_i n_{i0} = 0$), the Poisson-Boltzmann equation may be rewritten as:

$$\nabla^2 \Phi(r) = \kappa^2 \Phi(r) \tag{2.20}$$

with κ the Debye screening parameter defined as $\kappa^2 = \frac{e^2}{\varepsilon_0 \varepsilon_r k_b T} \sum_i n_{i0} z_i^2$. The Debye parameter, and more specifically the inverse κ^{-1} or λ , is the most important quantity of the Debye-Hückel theory. κ^{-1} , also called the Debye screening length, has the unit of length and referred to the distance over which the electrostatic interactions of the surface charge are non-significant. κ^{-1} commonly defines the thickness of the double layer model and the size of the diffuse layer.

Finally, an analytical solution is found to solve the linearized Poisson-Boltzmann equation using proper boundary conditions and the electric potential is given by:

$$\Phi(r) = \frac{z_i e}{4\pi\varepsilon_0 \varepsilon_r} \frac{exp(-\kappa r)}{r}$$
(2.21)

The screened Coulomb potential between two points charges i and j is then deduced:

$$E_{elec}^{ij}(r) = z_i e \Phi_j(r) = \frac{z_i z_j e^2 exp(-\kappa r)}{4\pi \varepsilon_0 \varepsilon_r r}$$
(2.22)

However, the Gouy-Chapman and Debye-Hückel theories have multiple shortcomings. In practice, due to the assumptions made, the model is only valid for low electric potential and low electrolyte concentrations. If electrolyte concentration increases, values obtained from the Gouy-Chapman model are a little bit higher than the experimental measured values. Moreover, quite simple modifications to the theory can be made such as considering finite charge size for ion description as developed in the model of Stern. Ions are not considered as point charges but described by finite size spheres with a charge located at their center. Such spheres represent the hydrated layer around the ions. Hence, the model of Stern is a combination of Helmholtz and Gouy-Chapman models. The interaction potential is thus described by two contributions:

- a linear potential due to an inaccessible region between surface and ion charge, similar to the Helmholtz distance. This distance defines the minimum distance between both charges and is generally known as the Stern layer or Stern plane.
- the second represents the diffuse layer with an exponential decrease of the potential (Poisson-Boltzmann distribution), similar to the Gouy-Chapman theory.

Although, the model of Stern provides a good description of the electrical double layer around surface charge in many situations, some refinements can be made. For instance, Grahame included in his model the possibility for ions (of same, neutral or opposite charge) to lose their hydrated shell and to be adsorbed on the surface. The Stern layer is then subdivided in two different layers (i) a first one composed of ions not fully solvated, called inner Helmholtz layer. The center of this adsorbed layer defines the inner Helmholtz plane, which represents the closest approach of solvated ions to the surface (ii) and a second one, named outer Helmholtz layer, equivalent to the Stern layer, and represents the limit with the diffuse layer.

2.5 Statistical mechanics and Monte Carlo simulations

2.5.1 Statistical mechanics

Most of computer simulations are based on the assumption that classical physical laws can be employed to describe the displacement of many-atoms (or particles) systems. However, the macroscopic properties or observables (temperature, pressure, density, viscosity, thermal expansion, ...) of such systems are not all directly linked to the properties obtained from the modelling and do not correspond to properties measured in real experiments. From this point, statistical mechanics represent an interesting tool in order to establish links between the macroscopic properties and the microscopic description of a system [3, 40–42]. For instance, the temperature of a gas is related to the average kinetic energy of all particles.

In statistical mechanics, the microscopic description of a system is generally defined by the positions p and the momenta q of all particles. For a system composed of N identical particles in a three-dimension space, 6N coordinates are then defined to describe the state of the system, commonly called the *phase space*. Thus, at any time t, all the positions and momenta are totally known.

On the other hand, a system at a thermodynamic equilibrium is described by a limited number of macroscopic properties (such as pressure P, temperature T, number of particles N, volume V, density, chemical potential μ , ...) and are specific to a statistical ensemble with a particular microscopic function, called partition or microscopic function. In statistical physics, three different ensembles may be considered (**Table 2.1**). Firstly, a micro-canonical ensemble isolated to external interactions with a constant energy (N, V and E fixed) and with a microscopic function related to the number of microscopic states. Secondly, a canonical ensemble closed and in thermal equilibrium with an external thermostat (N, V and T fixed) and with a canonical partition function related to the Boltzmann distribution. Finally, a grand canonical ensemble connected to external reservoirs of particles and energies characterized by a chemical potential (μ , V and T fixed) and with a grand canonical partition function related to the variation of energy.

Finally, the observable values (temperature, entropy, free energy, particle numbers, ...) are deduced from these specific partition functions and strongly correlated to the microscopic states (position, momenta).

Table 2.1: Resume of the different ensembles in statistical mechanics with their independent variables and their partition or microscopic functions

	Microcanonic	Canonic	Grand-canonic
Independent variables	E,N and V	N,V and T	μ ,V and T
Microscopic or partition function	Number of micro-states	$Z = \sum_{k} exp(-\beta E_k)$	$\Xi = \sum_{i} exp(-\beta(E_i - \mu N_i))$

2.5.2 Monte Carlo Metropolis simulation method and procedure

Basic principles of Monte Carlo simulation

Monte Carlo (MC) simulations refer to a class of computational algorithms used to solve deterministic and probabilistic problem [3]. Thus, MC modelling is strongly related to statistical concepts and can be applied to a wide range of fields, from physical systems to financial mathematics or from quantum mechanics to computational biology. The designation "Monte Carlo" alludes to the casinos and in particular gambling games occurring in Monaco and in terms to being specific to the randomness and the probabilities of these games. (Pseudo)random numbers and in particular repeated random sampling are the basis of Monte Carlo calculations. In statistical physics, Monte Carlo simulations are an interesting alternative to molecular dynamic [43]. Indeed, they can take into account systems with a large number of degree of freedom and with multiple unknown parameters. They can also explore a large range of different conformations and in particular get an insight into specific local minimum energy by considering different random moves and possible barrier crossings. Moreover, the variation of particle numbers in grand canonical ensemble is taking over by Monte Carlo methods. In this thesis, MC simulations are used to simulate Brownian motions of particles, titration processes of nanoparticle surfaces (deprotonation-protonation), ion condensation and nanoparticle aggregation (attachment efficiency).

Random sampling method

The basic Monte Carlo technique is the random sampling [3], for instance, to evaluate the

surface of a lake (for instance Lake Geneva, **Figure 2.7**). A way to calculate this surface is to randomly throw X rocks (points) in the land (rectangle) which contains the lake with a well-known surface ($size_{land}$). Then, the lake size $size_{lake}$ can be estimated by counting the number N of rocks present in the land ($size_{lake} = size_{land} \times \frac{X-N}{X}$).



Figure 2.7: Monte Carlo scheme to evaluate the size of the Lake Geneva.

However, to improve the quality of the surface estimation, the random number generator needs to cover all the surface with the same probability to explore each point of the surface. Moreover, the accuracy increases with the number of trials.

Metropolis method

Random sampling was adapted by Nicholas Metropolis et al. in 1953 [44] which take into account the concept of the importance of sampling in order to improve the variance of the system. The general idea of this concept is that specific values in a simulation, determined from an equilibrated random generator, are more interesting than others for the estimation of an integral, or a macroscopic value in our case. Metropolis employed this strategy in order to sample points of the phase space where the Boltzmann factor is large and consequently with an interest to be explored. Many regions of the phase space remain interest-free due to too high energies and with a probability of occurrence near to zero. Metropolis criterion allows to save computational resources by exploring regions of main interests.

The main difference between simple Monte Carlo simulations and the Metropolis algorithm resides on the probability distribution chosen to characterize the system. Instead of a random draw, configurations are selected with a Boltzmann probability. The exploration of the phase space is then obtained by generating a first representative conformation a followed by perturbations (particle translation, charge modification, ...) to obtain a new conformation b.

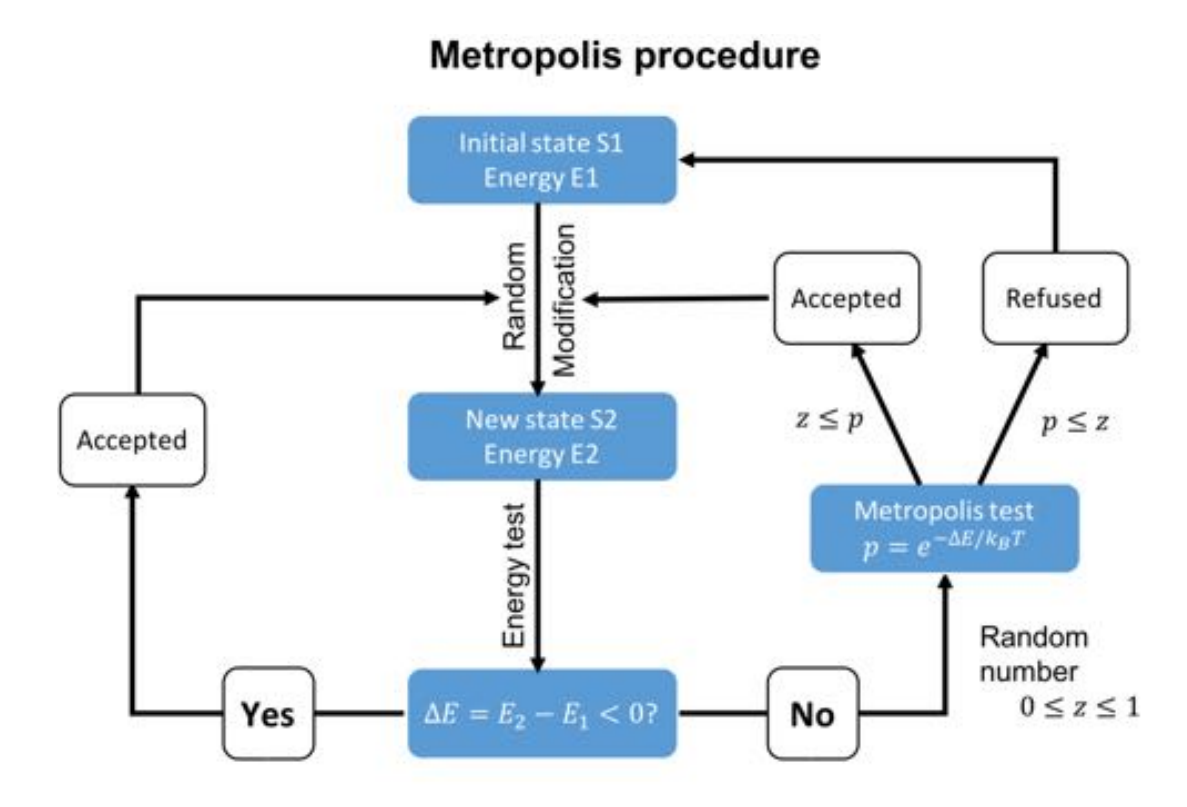


Figure 2.8: Scheme of the general Metropolis procedure.

The probability of accepting the new state is related to the energy variation between the two states ($\Delta E = E_2 - E_1$). If the new energy is lower than the initial energy then the step is accepted according to the fact that a low energy state is more favorable. Otherwise, the Boltzmann factor is calculated ($p = exp\left(-\frac{\Delta E}{k_bT}\right)$) and compared to a random number z ($z \in [0,1]$). If the probability p is higher than z, then the new state is accepted. If not, the new state is rejected.

The Metropolis criterion allows the possibility of finding local minima potential energy during the exploration of phase space by considering higher energy transition. Energy barrier crossings are then able leading to the exploration of other part of the phase space.

Monte Carlo procedures

All along this work, Monte Carlo is used in various ways. Firstly, MC-Metropolis simulations are performed to generate the site distribution on the nanoparticle. The initial heterogeneous configuration is created using Monte Carlo modelling with a random site distribution on

Table 2.2: Aci	d/base reactions a	t the NP	surface and	associated	energy changes ΔE

Initial charge	Possible charge	Acid/base chemical reaction	ΔE
0	+1	$Site - H + H^{+} \stackrel{1/K_{a1}^{0}}{\rightleftharpoons} Site - H_{2}^{+}$	$\Delta E_{elec} + (pH - pK_{a1}^0)ln(10)$
	-1	$Site - H \stackrel{1/K_{a2}^0}{\rightleftharpoons} Site^- + H^+$	$\Delta E_{elec} - (pH - pK_{a2}^0)ln(10)$
+1	0	$Site - H_2^+ \stackrel{K_{a_1}^0}{\rightleftharpoons} Site - H + H^+$	$\Delta E_{elec} - (pH - pK_{a1}^0)ln(10)$
	-1	$Site - H_2^+ \stackrel{K_{a1}^0 K_{a2}^0}{\rightleftharpoons} Site^- + 2H^+$	$\Delta E_{elec} - (2pH - pK_{a1}^0 - pK_{a2}^0)ln(10)$
-1	0	$Site^- + H^+ \stackrel{1/K_{a2}^0}{\rightleftharpoons} Site - H$	$\Delta E_{elec} + (pH - pK_{a2}^0)ln(10)$
	+1	$Site^- + 2H^+ \stackrel{1/(K_{a1}^0 K_{a2}^0)}{\rightleftharpoons} Site - H_2^+$	$\Delta E_{elec} + (2pH - pK_{a1}^{0} - pK_{a2}^{0})ln(10)$

the nanoparticle surface. To obtain homogenous surface, the site distribution is adjusted through MC methods according to the Metropolis criterion.

Secondly, the conformation phase of surface charges is investigated *via* Monte Carlo Metropolis simulations. At each MC step, one site is randomly chosen and its charge is changed (one or two new states are possible). Then the step is accepted or not as a function of the Metropolis selection criterion. This acceptance criterion is sensitive to the total electrostatic energy variation of the system as defined in **Table 2.2**. However, minimum local energies are considered by comparing the Boltzmann factor to a random number between zero and the unity. An equilibrium period is performed at each pH of the simulation in order to stabilize the system from the initial values and achieve the better level of energy convergence.

For condensation studies, a similar approach is performed. The site and ion distributions are created using Monte Carlo sampling and depending on the surface charge density, site distribution, ion concentration and composition, importance of ion condensation can be evaluated. Then, the ions of the solution (except the nanoparticle) are randomly moved at each step of the simulation in order to mimic the Brownian motion resulting from the interactions with water particles. Finally, the energy variation ΔE is calculated and the step is accepted or not according to the Metropolis test.

MC modelling was also performed in the hetero-aggregation studies. In addition to the initial conformation of the simulation box, Brownian motion of particles and objects as well as the sticking probability tests were achieved using simple Monte Carlo algorithms.

2.6 Particle aggregation

2.6.1 Smoluchowski theory

Aggregation or coagulation refers to the formation of structures between particles (here nanoparticles) and is an important process to characterize the stability of nanomaterials in aquatic systems [10, 45, 46]. During this process, the particles can interact or attach to each other to form aggregates. These structures are also referred as particle clusters, flocs or aggregates and mechanisms as clustering, flocculation or coagulation. However, flocculation is a type of aggregation which is induced by addition of polymers. Generally, particle aggregation is an one-way process which is irreversible. Aggregate size progressively grows until reaching a size which allows the aggregate to be removed from the water column *via* sedimentation. Particle behavior is mainly controlled by the surface properties of the particle and resulting electrostatic interactions between particles [47–49]. In this context, the DLVO theory represents a valuable tool to describe these electrostatic interactions. However, the solution properties and especially the salt properties play a key role in these processes. Moreover, aggregation kinetics is an interesting characteristic for the evaluation of the stability of a colloidal suspension.

In the last century, the aggregation processes have been largely described and studied using experimental methods [50–54], and numerical/theoretical models [9,55–58] in various and different domains such as aerosol coalescence, star formations, flocculation, blood coagulation or volcanic eruption. Most of these studies were based on the study made by Marian von Smoluchowski in the beginning of the 19th century [59]. He developed a mathematical kernel of equations to characterize the second-order rate processes of aggregation of spherical particles. Thus, each possible reaction between particles is then described by a unique equation and aggregation constant characterizing the formation rate of aggregate of size k and defined as follow:

$$\frac{dn_k}{dt} = \frac{1}{2} \sum_{i=k-i-1}^{k-1} k_{ij}^{agg} n_i n_j - n_k \sum_{i=1}^{\infty} k_{ik}^{agg} n_i$$
 (2.23)

With k_{ij}^{agg} the kinetic aggregation rate, and $n_{i,j,k}$ the respective numerical concentration of aggregate of size i,j, and k. The first part of the equation represents the rate formation of aggregate k resulting from the collision of particle of size i and j, while the second corresponds to the disappearance of this aggregate size resulting from the collision with particles of size i. The aggregation kinetic rate can be split in two different contributions and can be rewritten as:

$$k_{ij}^{agg} = \alpha_{ij} k_{ij}^{coll} \tag{2.24}$$

The first part of this equation represents the attachment efficiency α_{ij} which corresponds to the probability of efficient collision between particle i and j. This parameter is described in more detail in the next section. The second part of the aggregation kinetic rate is the collision rate constant k_{ij}^{coll} which represents the physical contribution in the aggregation process. This contribution is strongly related to the system properties (temperature, particle size, density, ...) and also to the transport model [18]. The particles may undergo Brownian motion (perikinetic) and/or specific force field such as laminar shear (orthokinetic aggregation) or gravity (differential settling). The different contributions are largely dependent on the size of the particles. The aggregation kinetic rate can be calculated according to the equation presented in **Table 2.3**.

Table 2.3: Aggregation kinetic rates as a function of the different transport models

Transport model	Kinetic rate constant		
Transport moder	Heterodisperse solution	Monodisperse solution	
Perikinetic	$\frac{2k_bT}{3\mu_s}\frac{(r_i+r_j)^2}{r_ir_j}$	$rac{8k_bT}{3\mu_s}$	
Orthokinetic	$\frac{4}{3}G(r_i+r_j)^3$	$rac{16}{3}Gr_i^3$	
Differential settling	$\pi(r_i + r_j)^2 \nu_{s,i} - \nu_{s,j} $	0	

Where G is the shear rate, μ_s the viscosity of the solvent and $v_{i,j}$ the settling velocity. In addition to this theory, several models were also numerically developed in 2D and 3D, such as the Witten and Sander Diffusion Limited Aggregation [60–62] and the Cluster-Cluster Ag-

gregation models [63] [64, 65] which allow to determine the time evolution of the density as well as the aggregate properties of a specific system (size, fractal dimension, ...).

2.6.2 Attachment efficiencies

The attachment efficiency (α) , also called sticking probability, is a unitless number which describes the probability to have an effective collision between two particles or aggregates. α is comprised between zero and the unity. Zero corresponds to a stable solution of particles without aggregation (predominance of repulsive forces) while $\alpha_{ij}=1$ represents a system where each contact between particles is efficient and create a permanent bond (predominance of attractive forces). Commonly, the attachment efficiency is defined as the ratio between the aggregation rate of the system studied k_{eff} and the aggregation rate k_{max} when all the collisions are expected to be efficient (generally at high ionic strength) as follow:

$$\alpha = \frac{k_{eff}}{k_{max}} \tag{2.25}$$

However, the estimation of attachment efficiencies remains challenging and strongly dependent on the complexity of the system. Moreover, as shown in **Figure 2.9**, several attachment efficiencies can describe aggregation at different scales of the process in particular when two types of particles are considered. At the very early stages, during the formation of dimer and trimer, an α_{homo} or α_{hetero} is considered, while at long-time scale a α_{global} has to be considered to describe the formation of large heteroaggregates. Between the short and long-time heteroaggregation process, other attachment efficiencies can be considered which complicate the description of heteroaggregation processes.

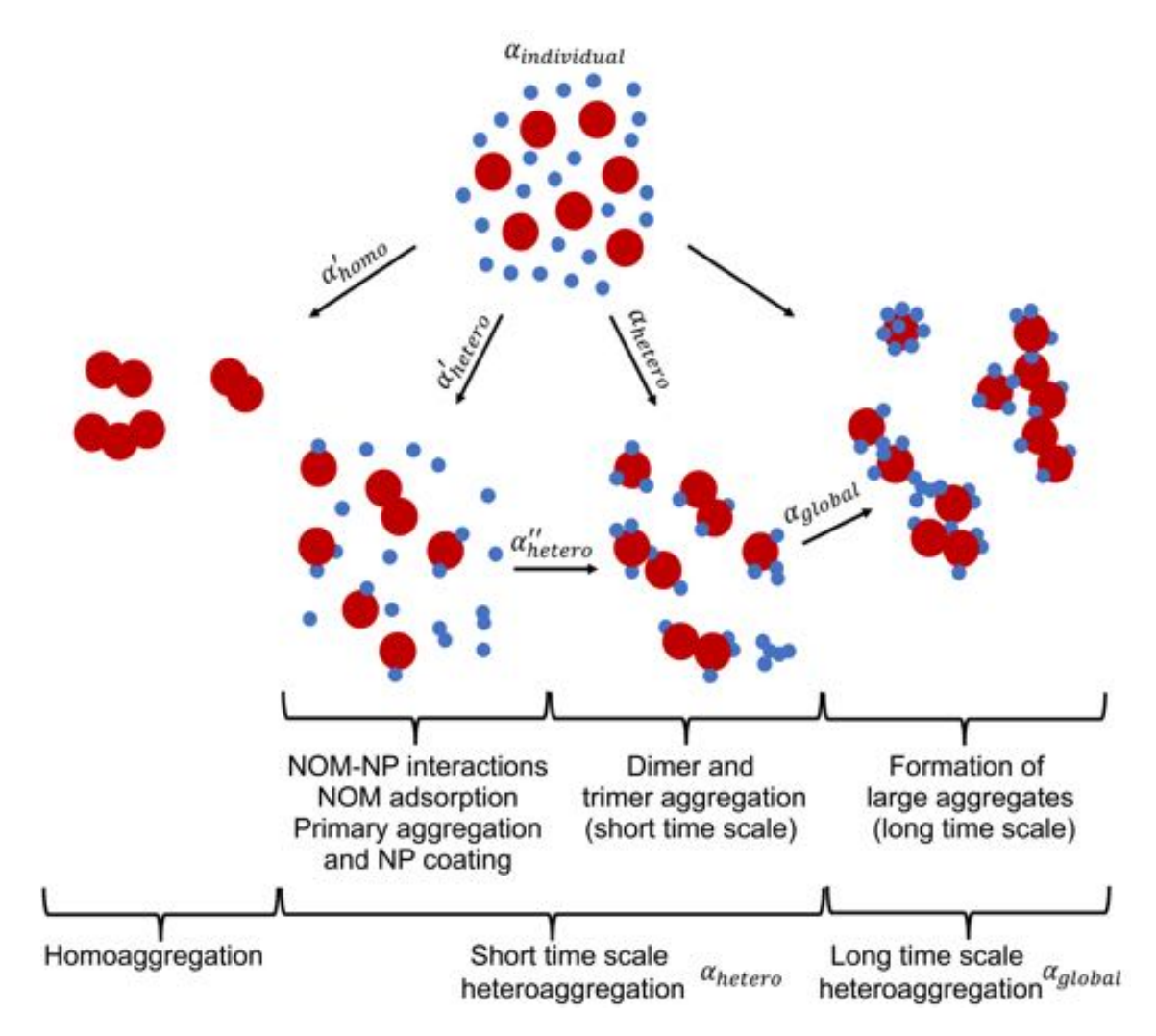


Figure 2.9: Description of homo- and heteroaggregation processes and corresponding attachment efficiencies.

The aggregate size and structure, and the aggregate surface chemistry will evolve all along the process and will modify the attachment efficiency values. In **Figure 2.10**, some examples of homo- and heteroaggregates obtained with our model are presented. In some specific systems, the surface of a nanoparticle can be recovered by organic matter and the attachment efficiency value will be totally different at short and long time scales. Such issues are discussed in details in **chapter 5**.

Different aggregate structures obtained from simulations

Figure 2.10: Various homo- and heteroaggregate structures obtained from the Monte Carlo aggregation model at different MC steps and for diverse initial properties.

Bibliography

- [1] Harvey Gould, Jan Tobochnik, and Wolfgang Christian. *An Introduction to Computer Simulation Methods: Applications to Physical Systems*. Addison-Wesley, San Francisco, 3 edition edition, January 2006.
- [2] Daan Frenkel. Introduction to Monte Carlo Methods. In *Computational Soft Matter: from Synthetic Polymers to Proteins*, volume 23, pages 29–60. NIC Series, Jülich, 2004.
- [3] Daan Frenkel and Berend Smit. *Understanding Molecular Simulation: From Algorithms to Applications*. Academic Press, October 2001.
- [4] Michael P. Allen and Dominic J. Tildesley. *Computer Simulation of Liquids: Second Edition*. Oxford University Press, August 2017. Google-Books-ID: WFExDwAAQBAJ.
- [5] Joan Estelrich, Manuel Quesada-Perez, Jacqueline Forcada, and Jose Callejas-Fernandez. Introductory Aspects of Soft Nanoparticles. In *Soft Nanoparticles for Biomedical Applications*. The Royal Society of Chemistry, Cambridge, 2014.
- [6] Marianne Seijo, Serge Ulrich, Montserrat Filella, Jacques Buffle, and Serge Stoll. Modeling the Adsorption and Coagulation of Fulvic Acids on Colloids by Brownian Dynamics Simulations. *Environmental Science & Technology*, 43(19):7265–7269, October 2009.
- [7] Nicole C. Mueller and Bernd Nowack. Exposure Modeling of Engineered Nanoparticles in the Environment. *Environmental Science & Technology*, 42(12):4447–4453, June 2008.
- [8] Joris T. K. Quik, Dik van De Meent, and Albert A. Koelmans. Simplifying modeling of nanoparticle aggregation–sedimentation behavior in environmental systems: A theoretical analysis. *Water Research*, 62:193–201, October 2014.
- [9] A. A. Markus, J. R. Parsons, E. W. M. Roex, P. de Voogt, and R. W. P. M. Laane. Modeling aggregation and sedimentation of nanoparticles in the aquatic environment. *Science of The Total Environment*, 506–507:323–329, February 2015.
- [10] Biplab Mukherjee and James W. Weaver. Aggregation and Charge Behavior of Metallic and Nonmetallic Nanoparticles in the Presence of Competing Similarly-Charged Inorganic Ions. *Environmental Science & Technology*, 44(9):3332–3338, May 2010.

- [11] Gregory V. Lowry, Kelvin B. Gregory, Simon C. Apte, and Jamie R. Lead. Transformations of Nanomaterials in the Environment. *Environmental Science & Technology*, 46(13):6893–6899, July 2012.
- [12] M. Baalousha, Y. Nur, I. Römer, M. Tejamaya, and J. R. Lead. Effect of monovalent and divalent cations, anions and fulvic acid on aggregation of citrate-coated silver nanoparticles. *Science of The Total Environment*, 454-455:119–131, June 2013.
- [13] Fatehah Mohd Omar, Hamidi Abdul Aziz, and Serge Stoll. Aggregation and disaggregation of ZnO nanoparticles: Influence of pH and adsorption of Suwannee River humic acid. *Science of The Total Environment*, 468–469:195–201, January 2014.
- [14] Fabrice Carnal, Arnaud Clavier, and Serge Stoll. Modelling the interaction processes between nanoparticles and biomacromolecules of variable hydrophobicity: Monte Carlo simulations. *Environ. Sci.: Nano*, 2(4):327–339, 2015.
- [15] Fanyao Qu and Paulo Cesar Morais. An Oxide Semiconductor Nanoparticle in an Aqueous Medium: A Surface Charge Density Investigation. *The Journal of Physical Chemistry B*, 104(22):5232–5236, June 2000.
- [16] A. Martin-Molina, M. Quesada-Perez, F. Galisteo-Gonzalez, and R. Hidalgo-Alvarez. Charge inversion of latex particles in the presence of electrolyte. *Progress in Colloid and Polymer Science*, 123:114–118, 2004.
- [17] Makio Naito, Masuo Hosokawa, Toyokazu Yokoyama, and Kiyoshi Nogi. *Nanoparticle Technology Handbook*. Elsevier, October 2007. Google-Books-ID: 6fvcH6SLSMIC.
- [18] M. Elimelech, R. Williams, J. Gregory, and X. Jia. *Particle deposition and aggregation: Measurement, modelling and simulation*. Butterworth-Heinemann, 1998.
- [19] John Gregory. *Particles in water: properties and processes*. IWA Publishing, London, 2005.
- [20] Valentina Tozzini. Coarse-grained models for proteins. *Current Opinion in Structural Biology*, 15(2):144–150, April 2005.
- [21] Cesar A. López, Andrzej J. Rzepiela, Alex H. de Vries, Lubbert Dijkhuizen, Philippe H. Hünenberger, and Siewert J. Marrink. Martini Coarse-Grained Force Field: Extension to Carbohydrates. *Journal of Chemical Theory and Computation*, 5(12):3195–3210, December 2009.

- [22] Hender Lopez and Vladimir Lobaskin. Coarse-grained model of adsorption of blood plasma proteins onto nanoparticles. *The Journal of Chemical Physics*, 143(24):243138, December 2015.
- [23] Alan R. Denton. Coarse-Grained Modeling of Charged Colloidal Suspensions: From Poisson-Boltzmann Theory to Effective Interactions. *arXiv:1212.1758 [cond-mat]*, December 2012.
- [24] Gregory A. Voth. *Coarse-Graining of Condensed Phase and Biomolecular Systems*. CRC Press, September 2008. Google-Books-ID: skNKAXfeXUMC.
- [25] Helgi I. Ingolfsson, Cesar A. Lopez, Jaakko J. Uusitalo, Djurre H. de Jong, Srinivasa M. Gopal, Xavier Periole, and Siewert J. Marrink. The power of coarse graining in biomolecular simulations. Wiley Interdisciplinary Reviews. Computational Molecular Science, 4(3):225–248, May 2014.
- [26] Michael Levitt and Arieh Warshel. Computer simulation of protein folding. *Nature*, 253(5494):694–698, February 1975.
- [27] A. Warshel and M. Levitt. Theoretical studies of enzymic reactions: Dielectric, electrostatic and steric stabilization of the carbonium ion in the reaction of lysozyme. *Journal of Molecular Biology*, 103(2):227–249, May 1976.
- [28] Frédéric Loosli, Philippe Le Coustumer, and Serge Stoll. TiO2 nanoparticles aggregation and disaggregation in presence of alginate and Suwannee River humic acids. pH and concentration effects on nanoparticle stability. *Water Research*, 47(16):6052–6063, October 2013.
- [29] Márta Szekeres and Etelka Tombácz. Surface charge characterization of metal oxides by potentiometric acid–base titration, revisited theory and experiment. *Colloids and Surfaces A: Physicochemical and Engineering Aspects*, 414:302–313, November 2012.
- [30] Etelka Tombácz and Márta Szekeres. Interfacial AcidBase Reactions of Aluminum Oxide Dispersed in Aqueous Electrolyte Solutions. 1. Potentiometric Study on the Effect of Impurity and Dissolution of Solid Phase. *Langmuir*, 17(5):1411–1419, March 2001.
- [31] Lawrence J. Henderson. Concerning the Relationship between the Strength of Acids and their Capacity to Preserve Neutrality. *American Journal of Physiology*, 21:173–9, 1908.

- [32] K. A. Hasselbach. Die Berechnung der Wasserstoffzahl des Blutes aus der freien und gebundenen Kohlensäure desselben, und die Sauerstoffbindung des Blutes als Funktion der Wasserstoffzah. *Biochemische Zeitschrift*, 78:112–114, 1916.
- [33] D. C. Rapaport. *The Art of Molecular Dynamics Simulation*. Cambridge University Press, April 2004. Google-Books-ID: iqDJ2hjqBMEC.
- [34] Fernando LuífS B. Da Silva, Bo Jönsson, and Robert Penfold. A critical investigation of the Tanford-Kirkwood sheeme by means of Monte Carlo simulations. *Protein Science : A Publication of the Protein Society*, 10(7):1415–1425, July 2001.
- [35] James J. Havranek and Pehr B. Harbury. Tanford–Kirkwood electrostatics for protein modeling. *Proceedings of the National Academy of Sciences of the United States of America*, 96(20):11145–11150, September 1999.
- [36] J. M. Cases and B. Mutaftschiev. Adsorption et condensation des chlorhydrates d'alkylamine à l'interface solide-liquide. *Surface Science*, 9(1):57–72, 1968.
- [37] Sydney Ross and James P. Olivier. On physical absorption, 1964.
- [38] Kazuomi Nagashima and Frank D Blum. Proton Adsorption onto Alumina: Extension of Multisite Complexation (MUSIC) Theory. *Journal of Colloid and Interface Science*, 217(1):28–36, September 1999.
- [39] James A. Davis, Robert O. James, and James O. Leckie. Surface ionization and complexation at the oxide/water interface: I. Computation of electrical double layer properties in simple electrolytes. *Journal of Colloid and Interface Science*, 63(3):480–499, March 1978.
- [40] David Chandler. Introduction to Modern Statistical Mechanics. *Introduction to Modern Statistical Mechanics, by David Chandler, pp. 288. Foreword by David Chandler. Oxford University Press, Sep 1987. ISBN-10: 0195042778. ISBN-13: 9780195042771*, page 288, September 1987.
- [41] E. Luijten. Introduction to Cluster Monte Carlo Algorithms. In *Computer Simulations in Condensed Matter Systems: From Materials to Chemical Biology Volume 1*, volume 703 of *Lecture Notes in Physics*, pages 13–38. Springer-Verlag, Berlin, 2006.
- [42] Alexei R. Khokhlov, Alexander Yu Grosberg, and Vijay S. Pande. *Statistical Physics of Macromolecules*. Polymers and Complex Materials. AIP-Press, 1994.

- [43] William L. Jorgensen and Julian Tirado-Rives. Monte Carlo vs Molecular Dynamics for Conformational Sampling. *The Journal of Physical Chemistry*, 100(34):14508–14513, January 1996.
- [44] N. Metropolis, A.W. Rosenbluth, M.N. Rosenbluth, A.H. Teller, and E. Teller. Equation-of-state calculations by fast computing machines. *Journal of Chemical Physics*, 21:1087–92, 1953.
- [45] Laura-Jayne A. Ellis, Eugenia Valsami-Jones, Jamie R. Lead, and Mohammed Baalousha. Impact of surface coating and environmental conditions on the fate and transport of silver nanoparticles in the aquatic environment. *Science of The Total Environment*, 568:95–106, October 2016.
- [46] Amro M. El Badawy, Todd P. Luxton, Rendahandi G. Silva, Kirk G. Scheckel, Makram T. Suidan, and Thabet M. Tolaymat. Impact of Environmental Conditions (pH, Ionic Strength, and Electrolyte Type) on the Surface Charge and Aggregation of Silver Nanoparticles Suspensions. *Environmental Science & Technology*, 44(4):1260–1266, February 2010.
- [47] B. Derjaguin and L. Landau. Theory of the stability of strongly charged lyophobic sols and of the adhesion of strongly charged particles in solutions of electrolytes. *Progress in Surface Science*, 43(1):30–59, May 1993.
- [48] B. V. Derjaguin. Theory of the stability of strongly charged lyophobic sols and the adhesion of strongly charged particles in solutions of electrolytes. *Acta Physicochim. USSR*, 14:633–662, 1941.
- [49] J. Th. G. Overbeek and E. J. W. Verwey. *Theory of the Stability of Lyophobic Colloids:* The interaction of Sol Particles Having an Electric Double Layer. 1948.
- [50] Mohammed Baalousha. Aggregation and disaggregation of iron oxide nanoparticles: Influence of particle concentration, pH and natural organic matter. *Science of The Total Environment*, 407(6):2093–2101, March 2009.
- [51] Geert Cornelis, Liping Pang, Casey Doolette, Jason K. Kirby, and Mike J. McLaughlin. Transport of silver nanoparticles in saturated columns of natural soils. *Science of The Total Environment*, 463-464:120–130, October 2013.

Model, Theory and simulation methods

- [52] Jose Garcia, Jasmina Markovski, J. McKay Gifford, Onur Apul, and Kiril D. Hristovski. The effect of metal (hydr)oxide nano-enabling on intraparticle mass transport of organic contaminants in hybrid granular activated carbon. *Science of The Total Environment*, 586:1219–1227, May 2017.
- [53] Minghua Li, Suman Pokhrel, Xue Jin, Lutz Mädler, Robert Damoiseaux, and Eric M. V. Hoek. Stability, Bioavailability, and Bacterial Toxicity of ZnO and Iron-Doped ZnO Nanoparticles in Aquatic Media. *Environmental Science & Technology*, 45(2):755–761, January 2011.
- [54] Antonia Praetorius, Martin Scheringer, and Konrad Hungerbühler. Development of Environmental Fate Models for Engineered Nanoparticles—A Case Study of TiO2 Nanoparticles in the Rhine River. *Environmental Science & Technology*, 46(12):6705–6713, June 2012.
- [55] Alexandre Albanese and Warren C.W. Chan. Effect of Gold Nanoparticle Aggregation on Cell Uptake and Toxicity. *ACS Nano*, 5(7):5478–5489, July 2011.
- [56] Arturo A. Keller, Hongtao Wang, Dongxu Zhou, Hunter S. Lenihan, Gary Cherr, Bradley J. Cardinale, Robert Miller, and Zhaoxia Ji. Stability and Aggregation of Metal Oxide Nanoparticles in Natural Aqueous Matrices. *Environmental Science & Technology*, 44(6):1962–1967, March 2010.
- [57] Lauren E. Barton, Mathieu Therezien, Melanie Auffan, Jean-Yves Bottero, and Mark R. Wiesner. Theory and Methodology for Determining Nanoparticle Affinity for Heteroaggregation in Environmental Matrices Using Batch Measurements. *Environmental Engineering Science*, 31(7):421–427, June 2014.
- [58] M E Costas, M Moreau, and L Vicente. Some analytical and numerical solutions for colloidal aggregation with fragmentation. *Journal of Physics A: Mathematical and General*, 28(11):2981–2994, June 1995.
- [59] M. V. Smoluchowski. Drei Vortrage uber Diffusion, Brownsche Bewegung und Koagulation von Kolloidteilchen. *Zeitschrift fur Physik*, 17:557–585, 1916.
- [60] P. Meakin. The structure of two-dimensional Witten-Sander aggregates. *Journal of Physics A: Mathematical and General*, 18(11):L661, 1985.
- [61] T. A. Witten and L. M. Sander. Diffusion-Limited Aggregation, a Kinetic Critical Phenomenon. *Physical Review Letters*, 47(19):1400–1403, November 1981.

- [62] D. Elderfield. Smoluchowski and beyond: a field theoretical study of coagulation/fragmentation processes. *Journal of Physics A: Mathematical and General*, 20(3):L135, 1987.
- [63] Paul Meakin, Tamás Vicsek, and Fereydoon Family. Dynamic cluster-size distribution in cluster-cluster aggregation: Effects of cluster diffusivity. *Physical Review B*, 31(1):564–569, January 1985.
- [64] Hailing Xiong, Hang Li, Weiping Chen, Jian Xu, and Laosheng Wu. Application of the Cluster–Cluster Aggregation model to an open system. *Journal of Colloid and Interface Science*, 344(1):37–43, April 2010.
- [65] M. Kolb and H. J. Herrmann. Surface fractals in irreversible aggregation. *Physical Review Letters*, 59(4):454–457, July 1987.

CHAPTER 3

Surface Charging Behavior of Nanoparticles. Effects of Site Distribution and Density, Dielectric Constant and pH Changes. A Monte Carlo Approach.

3.1 Introduction

In this chapter, Monte Carlo simulations are performed in order to describe the charging behavior of metal oxide nanoparticles thus enabling a novel and original approach to predict nanoparticle reactivity and possible interactions with biological and environmental molecules such as NOM. The charging behavior of spherical nanoparticles is investigated by adjusting the pH of the medium and the influence of surface site distribution (heterogeneous, homogeneous and patches), density and dielectric constant as well as acid/base properties of the surface sites and $\Delta p K_a^0$ values (difference between two successive deprotonation constants) and is systematically studied using a grand canonical Monte Carlo method. A one pK_a^0 (also referred to as $1-pK_a^0$) and a two pK_a^0 models $(2-pK_a^0)$ are considered in order to mimic simple and multiple deprotonation processes of one fixed nanoparticle as presented in **Table 2.2 (Chapter 2**).

3.2 Main results

3.2.1 $1 - pK_a^0$

Influence of NP surface site distribution.

As shown in **Figure 3.1**, NP deprotonation process is more effective for homogeneous and heterogeneous site distribution. This is due to larger distances between nearest neighbors and lower electrostatic repulsions between negatively charged sites. The homogeneous surface is the most efficient configuration for efficient site deprotonation (or surface charging process).

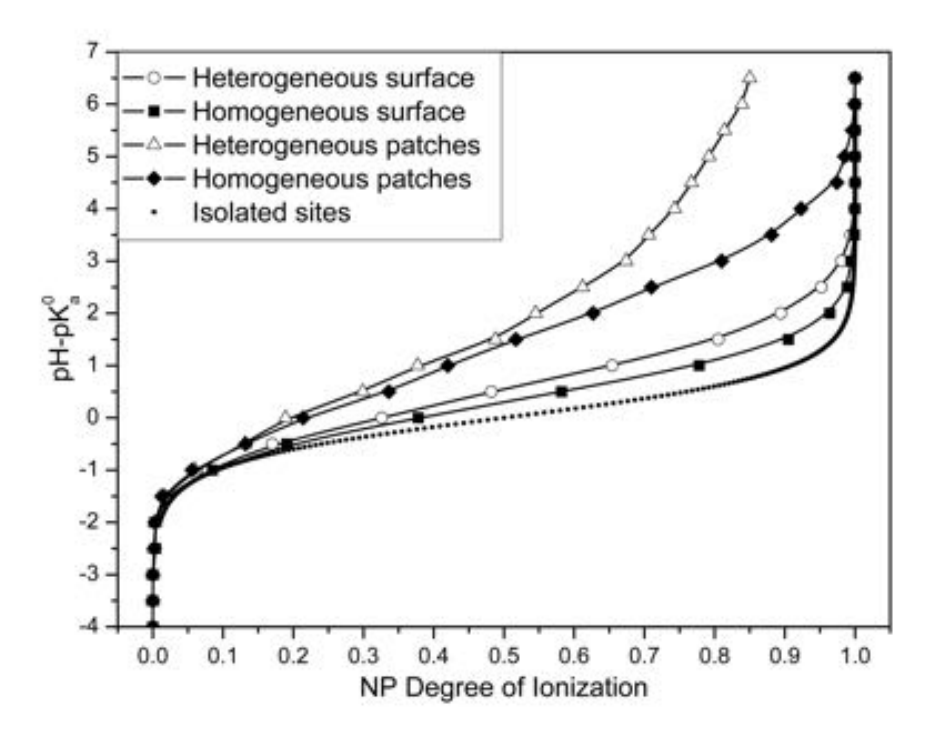


Figure 3.1: Monte-Carlo titration curves for a NP with 50 sites and with different surface distributions $(1 - pK_a^0 \text{ model})$. For the sake of clarity, titration curves are compared with the corresponding ideal (isolated) case, i.e. in absence of electrostatic interactions between sites.

Nevertheless, there is a significant difference compared to isolated monomers. At a given $pH - pK_a^0$, the ionization is less important due to electrostatic repulsions. For patch distribu-

Chapter 3: Surface Charging Behavior of Nanoparticles

tions, distances between sites are smaller and the charging process is less efficient. Furthermore, in the case of heterogeneous patches, distances between some sites are so close that deprotonation is not completely achieved even for high pH $-pK_a^0$ values.

Influence of NP surface site distribution.

As shown in **Figure 3.2**, the decrease of the surface charge density is also playing an important role on the deprotonation process with differences of several pH $- pK_a^0$ units at high ionization degrees. With the decrease of the surface site density, deprotonation processes become easier and curves are shifted to the isolated monomer situation.

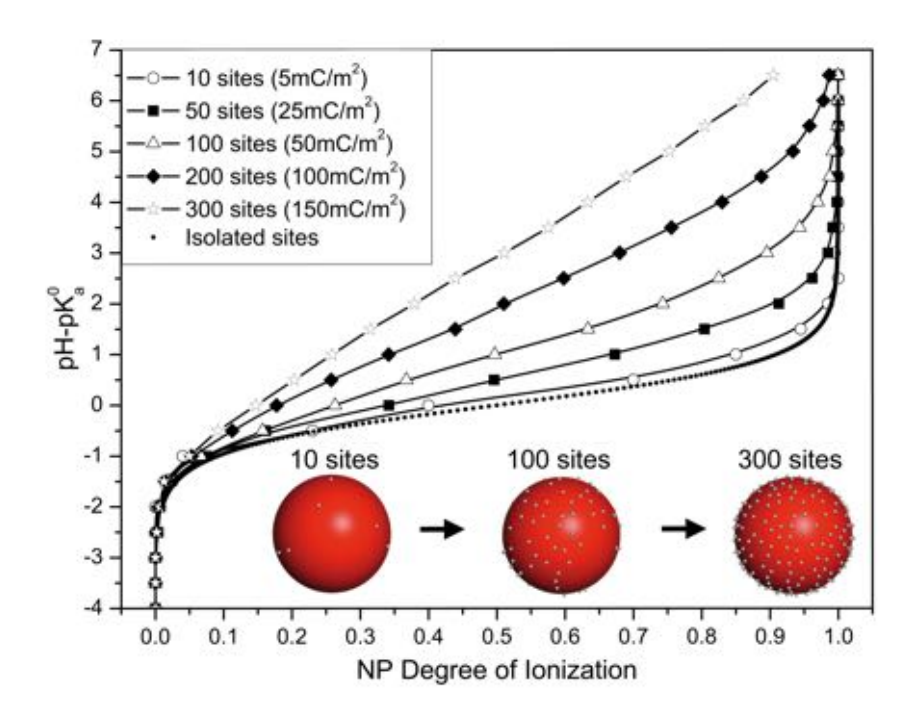


Figure 3.2: Monte-Carlo titration curves for a heterogeneous surface with different charge densities (10, 50, 100, 200 and 300 sites). The corresponding charge densities in mC/m² are given in the inset.

As observed now in **Figure 3.3**, the dielectric constant variation is also found to play an important role. The "soft" NPs dielectric constant constitutes an intermediate case. For low dielectric constant values (hematite), since sites are less electrostatically screened, the repulsion between them are stronger and the deprotonation is more difficult. On the contrary, site interactions are much more reduced for larger values of dielectric constant (titanium dioxide)

and the deprotonation process with $pH - pK_a^0$ increase is more efficient.

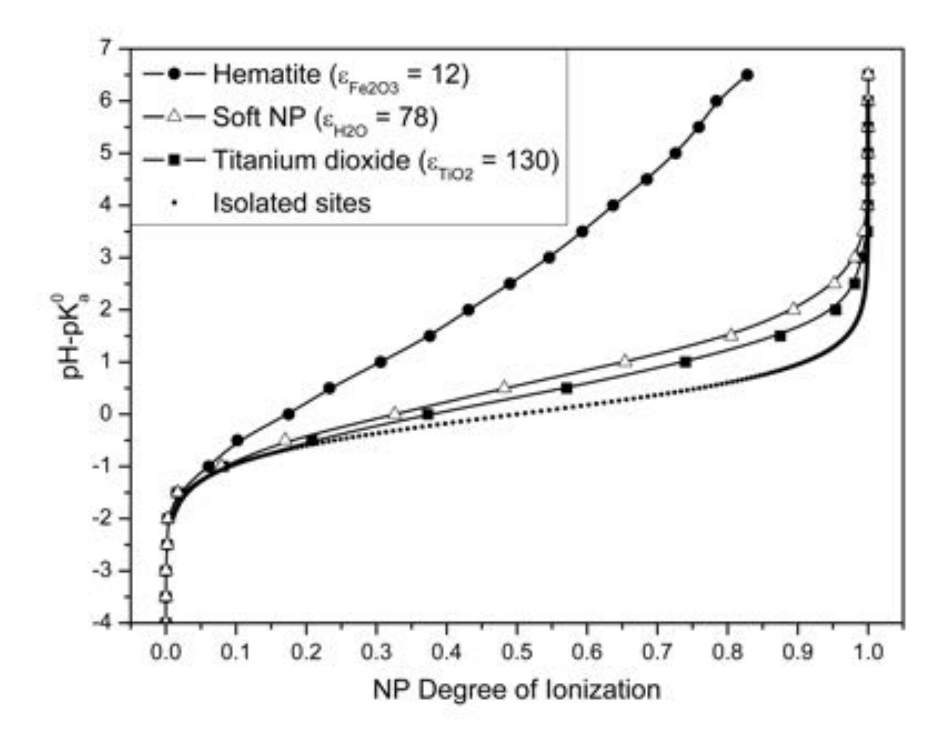


Figure 3.3: Monte-Carlo titration curves for a heterogeneous surface with 50 sites (25mC/m²) and with various dielectric constants. The dielectric constant is found to play an important role on the NP charging behavior by controlling the electrostatic repulsions between the different sites.

3.2.2 $2 - pK_a^0$

Influence of $\varDelta pK_a^0$ and dielectric constant variation.

As shown in **Figure 3.4.(a)**, the $\Delta p K_a^0$ value has important effect on the NP charging behavior. We start with a fully positively charged which is gradually deprotonated by increasing the $pH-pK_a^0$ value. Then a second deprotonation step is induced towards the formation of negative charges by increasing further the $pH-pK_a^0$ value and, consequently, the NP degree of ionization is increasing again. At low $\Delta p K_a^0$ values ($\Delta p K_a^0 < 2$), in agreement with the acid/base properties of the sites, and when $pH-pK_a^0$ is equal to zero, the NP degree of ionization is still important due to the presence of both positive and negative charges, which are predominant

Chapter 3: Surface Charging Behavior of Nanoparticles

regarding the neutral sites. As a result an isoelectric point is obtained here and an equivalent number of positive and negative charges is obtained at the NP surface. As shown in **Figure 3.4**, small $\Delta p K_a^0$ values result in the dynamic coexistence of the three possible charge transition states (1 to 0, 0 to -1 and 1 to -1) as well as the concomitant presence of positive and negative sites (opposite charges). The number of opposite charges, in particular when, pH $-pK_a^0=0$ is a function of $\Delta p K_a^0$ and increases with the decrease of $\Delta p K_a^0$. At high $\Delta p K_a^0$ ($\Delta p K_a^0 \geq 2$), the corresponding situation is now representative of a point of zero charge, since the number of positive and negative charges are close to 0. In such condition, the deprotonation process is a step by step mechanism (as observed in both **Figure 3.4.(a)** and **Figure 3.4.(b)**): the positive charges are first switched off before the emergence of negative charges.

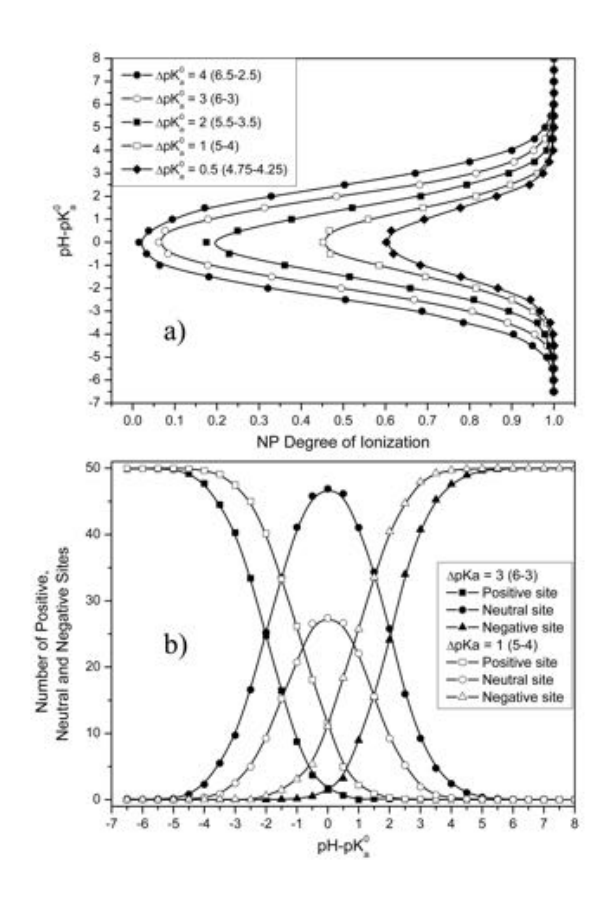


Figure 3.4: a) pH $-pK_a^0$ as a function of NP degree of ionization and b) number of charge type as a function of pH $-pK_a^0$ for a heterogeneous surface NP with variable ΔpK_a^0 values $(2-pK_a^0$ model). Values of pK_{a1}^0 and pK_{a1}^0 are given in the brackets.

In **Figure 3.5.(a)** are presented the effective NP surface charge variations as a function of the $pH - pK_a^0$ values and for different ΔpK_a^0 values.

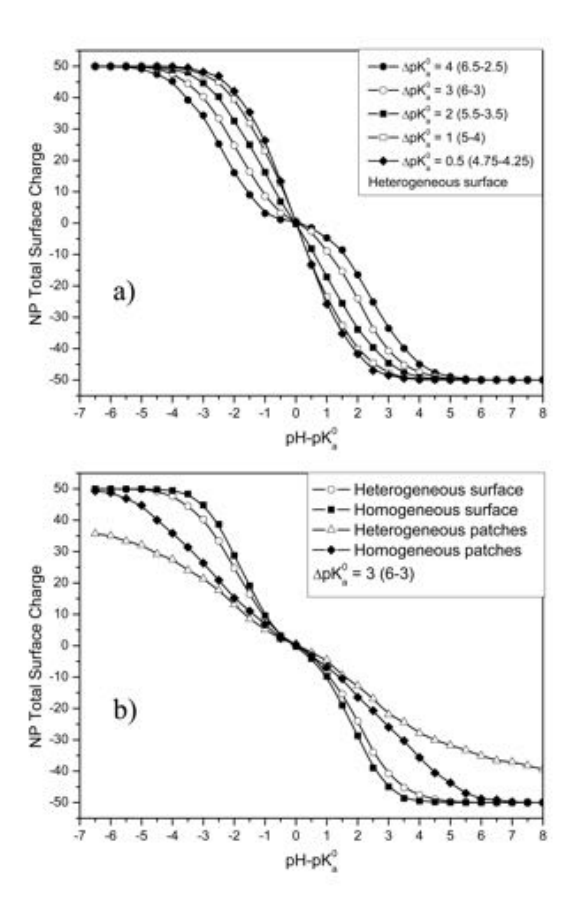


Figure 3.5: a) Variation of the total surface charge for different $\Delta p K_a^0$ considering a heterogeneous surface and b) for different site distributions with $\Delta p K_a^0 = 3$ ($2 - p K_a^0$ model). The presence of an isoelectric point results in sharp transitions between the positive and negatively charged domains. Values of $p K_{a1}^0$ and $p K_{a2}^0$ are given in the brackets.

The general shape is quite similar to the experimental titration curves, which are obtained via experimental potentiometric titrations. It should be noted that i) when the NP total charge is zero all the curves cross each other at the same point i.e. when $pH - pK_a^0 = 0$ and ii) a sharp transition is observed in presence of an isoelectric point from positive to negatively charged NPs.

When $\Delta p K_a^0 = 3$ (**Figure 3.4.(b**)) it is found that the shape of the curves is also controlled by the surface site distribution. This constitutes an important outcome in the interpretation of

Chapter 3: Surface Charging Behavior of Nanoparticles

experimental data. Heterogeneous and homogeneous distributions exhibit plateau values at the beginning and at the end of the titration processes whereas patch distributions show more linear charge variations.

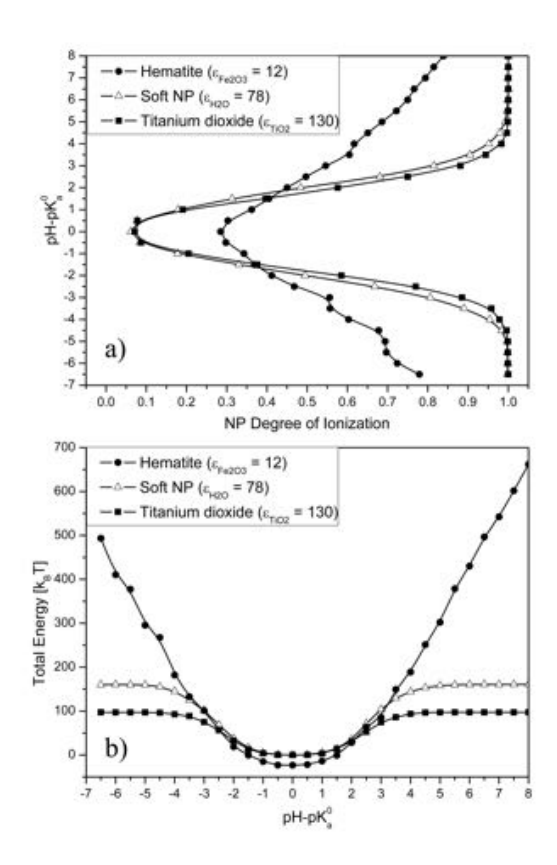


Figure 3.6: a) pH $-pK_a^0$ as a function of NP degree of ionization and b) total energy as a function of pH $-pK_a^0$. The effect of the dielectric constant is investigated here for a heterogeneous surface $(2-pK_a^0 \text{ model})$ with N=50.

Complementary calculations are then carried out to understand the influence of the dielectric constant. We are considering the case with $\Delta p K_a^0 = 3$ with heterogeneous surface distribution. As shown in **Figure 3.6.(a)**, two different behaviors are observed by adjusting the dielectric constant. On the one hand, for titanium dioxide and "soft" NPs, having relatively high dielectric constants, most of the charges are switched-off when pH $-pK_a^0 = 0$ and a point of zero charge is obtained. NPs ionization degree at low and high pH values are equal to one hence indicating fully charged surfaces. The variation of the total energy (**Figure 3.6.(b)**) also exhibits specific profiles with values equal to zero at the PZC. On the other hand, at low dielectric con-

stant, sites are electrostatically less screened and partial protonation or deprotonation process is achieved. In addition when $pH - pK_a^0 = 0$, NPs exhibit a mixture of positive, negative and neutral sites on their surface, which is much more representative of an isoelectric point model. Total energies in **Figure 3.6.(b)** support the observed differences and that such a system is less stable from an electrostatic point of view when low or high dielectric constant are considered.

3.3 Conclusions

In this chapter, we have demonstrated that Monte Carlo simulations constitute a powerful approach to get an insight into the charging behavior of metal oxide type NPs, isolate the influence of several important parameters such as acid base properties of surface sites, charge density, surface site distribution and dielectric constant and elucidate the possible transformation and properties of NPs in a changing environment. In particular it was shown that the site distribution is playing a key role and that the homogeneous distribution is the most efficient one to obtain high ionization degrees when the $1-pK_a^0$ model is considered. Acid/base properties are also found to play key roles in particular for the $2-pK_a^0$ model. It was also found that the presence of an isoelectric point or point of zero charge resulted from two different charging process.

Paper I

Reprinted from A. Clavier, M. Seijo, F. Carnal, S. Stoll *Phys. Chem. Chem. Phys.*, **2015** vol. 17, 4346 Copyright (2015), with permission of the *Royal Society of Chemistry*



PCCP



PAPER



Cite this: *Phys. Chem. Chem. Phys.*, 2015, **17**, 4346

Surface charging behavior of nanoparticles by considering site distribution and density, dielectric constant and pH changes — a Monte Carlo approach

Arnaud Clavier, Marianne Seijo, Fabrice Carnal and Serge Stoll*

Monte Carlo simulations are used to describe the charging behavior of metal oxide nanoparticles thus enabling a novel and original approach to predict nanoparticle reactivity and the possible interactions with biological and environmental molecules. The charging behavior of spherical nanoparticles is investigated by adjusting the pH of the media and the influence of surface site distribution, density and dielectric constant as well as the acid/base properties of the surface sites and $\Delta p K_a^0$ values (difference between two successive deprotonation constants) is systematically studied using a grand canonical Monte Carlo method. A primitive Coulomb model is applied to describe the interaction energies between the explicit discrete sites. Homogeneous/heterogeneous surfaces and patches with homogeneous and heterogeneous distributions are considered in order to reproduce possible site distributions of metal oxide nanoparticles. Two models are used. In the 1-p K_a^0 model (one deprotonation step) the results indicate that the deprotonation process is controlled by inter-site distances which are defined by site distributions and densities. It is shown that the homogeneous surface is the most efficient site distribution to obtain high ionization degrees. In the $2-pK_a^0$ model (two deprotonation steps), the $\Delta p K_a^0$ value is found to control the surface charge properties with regard to pH changes. By considering the variation of the total nanoparticle surface charge as a function of pH our results help in the distinction between the zero charge and the isoelectric point and interpretation of experimental NP titration curves.

Received 17th October 2014, Accepted 23rd December 2014

DOI: 10.1039/c4cp04733h

www.rsc.org/pccp

Introduction

Manufactured nanoparticles (NPs), which are more and more present in our direct environment are expected, *via* the development of nanotechnologies, to revolutionize our everyday life as well as many important research areas such as medicine, energy, drug design, catalytic surfaces and advanced material design. However, this huge development is expected to increase the (accidental) release and concentration of NPs in environmental compartments such as air, soil and aquatic systems. Unfortunately, the impact of NPs on ecosystems and human health is nowadays not clearly known. The large specific surface areas of NPs result in high chemical reactivity whereas NP sizes result in high diffusion capacity and such properties give them the ability to cause harm in biological systems.

One important parameter controlling the chemical, physical and biological properties of NPs is related to the presence of

Environmental Physical Chemistry, F.-A. Forel Institute, Earth and Environmental Sciences, Faculty of Sciences, University of Geneva, 10 route de Suisse, CH-1290 Versoix, Switzerland. E-mail: Serge.stoll@unige.ch; Fax: +41 22 379 0329; Tel: +41 22 379 0333

surface charges resulting, for instance, from the acid/base properties of surface sites. The surface charge, sign and density also depend on the physicochemical dispersion media (mainly temperature, pH, ion concentration) and the presence of soluble species (polyelectrolytes, natural organic matter, proteins...). 11,12 As a result NPs, such as metal oxides, can be positively charged (usually this is observed at low pH), neutral, or negatively charged (at high pH). Not only the surface charge density and sign but also the acid-base site distributions of NPs have an impact on the chemical processes at the NP-solution interface such as NP coating, polyelectrolyte adsorption and protein corona formation. 13-16 The surface charge density and sign are also expected to control the stability of NPs, i.e. aggregation versus dispersion, by modifying the electrostatic repulsion between the NPs. When NPs have the possibility to aggregate they are less mobile and usually eliminated from the suspension *via* sedimentation processes.¹⁷ On the other hand, when they are present as isolated monomers or disagglomerated NPs they become more mobile and bioavailable in the soil/sediments/water and air and are thus potentially more toxic. 6-8 The knowledge of the charging behavior of NPs is then of main importance to predict the residence time of NPs in the environmental compartments.

Paper **PCCP**

The total surface charge of NPs is mainly controlled by the probability for each surface site, having acid/base properties, to be ionized 18,19 and is usually limited by the electrostatic interactions at the NP surface. The presence of ions or polyelectrolytes in the solution, on the other hand, can reduce electrostatic repulsions between sites via screening effects and promote the charging processes. In the case of metal oxide NPs, the surface charge (sign and density) will depend on proton binding reactions and chemical equilibrium, which can change as a function of pH and ionic strength.20,21 In contrast to isolated monomers in solution, electrostatic repulsions between sites strongly influence the deprotonation reactions of each site and can limit the effective charge of the NPs.

The surface charge density, net specific surface proton excess and related properties of NPs can be investigated using experimental methods, 11 theoretical and numerical models, 22-24 and by considering energetically homogeneous surfaces.²⁵ The surface charge of NPs can also be described by considering an Ising model²⁶ with a solution/solid interface, Monte Carlo simulations,²⁷ or a Poisson-Boltzmann approximation²⁸ for a planar geometry. Experimentally, the surface charge of NPs can be characterized indirectly by zeta-potential measurements¹¹ or directly by potentiometric acid/base titration. 29,30 Potentiometric and acid/base titrations have been used for decades to determine the surface charge density of oxides and now the method has solid theoretical and experimental foundation.³⁰

In this work we investigate the effect of surface site distribution, density and dielectric constant on the charging behavior of metal oxide NPs by considering a one pK_a^0 model (also referred to as 1-pK $_{\rm a}^{\rm 0}$) and a two p $K_{\rm a}^{\rm 0}$ model (2-p $K_{\rm a}^{\rm 0}$) to consider simple and multiple deprotonation processes. By adjusting the pH value (titration process), the surface charge density, the pK_a^0 values of the surface sites and the charging behavior (via the surface dissociation or ionization degree) are investigated in detail and in a systematic way to get an insight into the role of each parameter in an independent way. The original aspect of that work consists of studying the charging behavior of NPs not only as a function of acid/base properties of surface sites and solution pH, but also as a function of different explicit surface site distributions and specific NP properties (dielectric constant, surface charge density). Electrostatic interactions between sites are calculated using a primitive Coulomb model³¹ and focus is made on the total surface charge variation of NPs so as to help in the interpretation and understanding of experimental data such as electrophoretic mobility or potentiometric measurements made on manufactured nanoparticles. It should be noted that in a previous work we used a similar approach to investigate in detail the effect of the dielectric discontinuity on the charging process of nanoparticles using a Tanford's model.³²

The influence of pH and the many body problems are solved using Monte Carlo (MC) simulations²⁷ using the Metropolis Criterion.³³ Simulations are carried out in a grand canonical ensemble (chemical potential μ , temperature T, volume V) to obtain an equilibrium state at a fixed pH. Site distributions are classified into two categories: heterogeneous and homogeneous (perfect crystal arrangement). Spherical NPs are modeled by using two types of distribution: full surface coverage and partial surface coverage via the presence of two patches. In the first part of this paper theoretical modeling is presented then, in the Results and discussion part, the 1-p K_a^0 and 2-p K_a^0 models are discussed by adjusting the site distribution, surface charge density, dielectric constant, and pH.

Theoretical modeling

Model description

A primitive Coulomb model is used to calculate the electrostatic energy of interaction between sites by considering discrete charge distributions. The nanoparticles are described using a sphere, with an arbitrary radius of 25 Å, in an infinitely diluted aqueous solution with a continuum representation of the solvent. The spherical NP is impenetrable to the solvent. To consider the dielectric discontinuity between the NP and the solvent, the relative permittivity ε_c is adjusted to be different from the dielectric constant of water ε_w . Three different dielectric constants of NPs are studied, respectively, below, above and equal to the dielectric constant of water. For that purpose the dielectric constants of hematite NPs³⁴ (with $\varepsilon_{\text{Fe},O_2} = 12$), titanium dioxide NPs³⁴ (with $\varepsilon_{\text{TiO}_2}$ = 130) and "soft" NPs³⁴ (with ε_{w} = 78) are considered. Titrating sites are represented by fixed points placed at 0.5 Å under the surface (Fig. 1). The spatial configuration of surface discrete charge distributions in the model can represent specific experimental surface site distributions. The long-range electrostatic potential at a distance r_{ii} between sites i and j with charges z_i and z_i is given by:

$$E_{\text{Tot}} = \sum_{i=1}^{N-1} \sum_{j=i+1}^{N} \frac{z_i z_j e^2}{4\pi \varepsilon_0 \varepsilon_c r_{ij}}$$
 (1)

where ε_0 is the vacuum permittivity (8.85 × 10⁻¹² C V⁻¹ m⁻¹) and eis the elementary charge (1.60 \times 10⁻¹⁹ C).

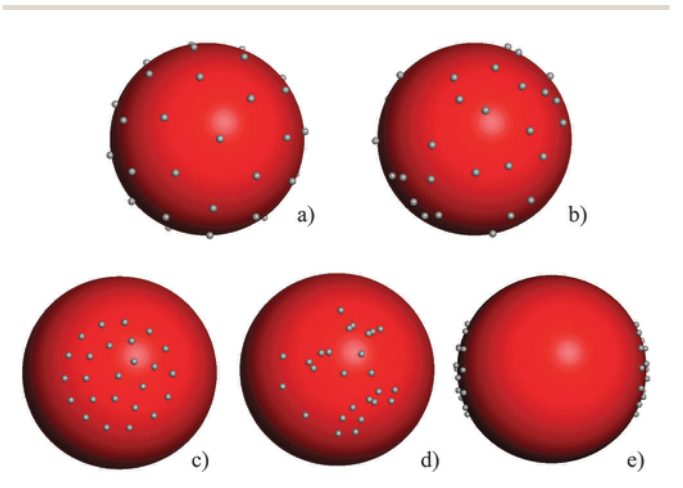


Fig. 1 NP surface discrete charge distributions: (a) homogeneous surface, (b) heterogeneous surface, (c) homogeneous patches, (d) heterogeneous patches, and (e) patches position. Each NP has 50 sites on its surface and a diameter of 5 nm. For the sake of clarity, the point-like sites are represented as having a volume on the NP surface. In the Monte Carlo simulation model the surface charge density can be adjusted as well as the NP size, dielectric constant and acid-base properties of the sites.

PCCP Paper

Henderson-Hasselbalch equation

The Henderson–Hasselbalch equation 35,36 is used to describe the acid/base properties of an isolated site. Under appropriate conditions, sites dissociate and positively or negatively charges appear on the surface. The dissociation of an isolated acid (HA) in an aqueous medium is given by HA \leftrightarrow H⁺ + A⁻. According to the mass action law, the equilibrium constant is given by:

$$K_{\rm a}^0 = \frac{[{\rm H}^+][{\rm A}^-]}{[{\rm HA}]}$$
 (2)

where $[H^+]$, $[A^-]$ and [HA] are the concentrations of dissociated hydrogen and dissociated and non-dissociated acids, respectively. The degree of ionization α is then given by:

$$\alpha_{\rm p} = \frac{[{\rm A}^-]}{[{\rm A}^-] + [{\rm HA}]}$$
(3)

and finally, the Henderson-Hasselbalch equation is defined as:

$$pH = pK_a^0 + \log_{10}\left(\frac{1 - \alpha_p}{\alpha_p}\right)$$
 (4)

For an amphoteric system, the Henderson–Hasselbalch equation is given by:

$$pH = pK_a^0 \pm \log_{10} \left(\frac{1 - \alpha_p}{\alpha_p}\right)$$
 (5)

with

$$pK_a^0 = (pK_{a1}^0 + pK_{a2}^0)/2 (6)$$

The plus sign corresponds to the degree of proton association and the minus sign to the degree of proton dissociation. $K_{\rm a}^0$ represents the intrinsic dissociation constant for a monoprotic reaction. For diprotic reactions, $K_{\rm a1}^0$ and $K_{\rm a2}^0$ are defined as:

Site
$$-H_2^+ \stackrel{K_{a_1}^0}{\Longleftrightarrow} Site - H + H^+$$
 (7)

Site
$$-H \stackrel{K_{a2}^0}{\rightleftharpoons} Site^- + H^+$$
 (8)

In this study, the different pK_a^0 values have been arbitrarily fixed but can be adjusted in the model.

Monte-Carlo metropolis procedure

For the sampling of the configuration space, MC simulations are performed according to the Metropolis algorithm. 27,33 The NPs have N ionizable sites and this number is adjusted here between N=10 and 300 to get an insight into the influence of the charge density. 2^N or 3^N charge states can be considered, corresponding to the different charge states of monoprotic and diprotic reactions as defined in Table 1. For each simulation step, one site is chosen randomly and has a random change in its charge state. Then each acid/base reaction is accepted or not according to the Metropolis selection criterion. This criterion is related to the energy variation ΔE during the protonation–deprotonation process,

$$\Delta E = E_{\rm f} - E_{\rm i} \tag{9}$$

with E_f being the energy of the new state and E_i the energy of the previous state. If the change in the total energy ΔE is negative, the system has a lower energy and the MC step is accepted. If ΔE is positive, the Boltzmann factor is given by,

$$p = \exp(-\Delta E/k_{\rm B}T) \tag{10}$$

which is calculated and compared with a random number z between 0 and 1. $k_{\rm B}$ represents the Boltzmann constant (1.38 \times 10⁻²³ J K⁻¹) and T the temperature (298 K). If the probability p is higher than z, the MC step is accepted, if not the step is refused and the previous state is considered as a new state. The possible protonation and deprotonation processes and the associated energy changes are detailed in Table 1.

Surface titrating site distribution

Heterogeneous/homogeneous and patches with heterogeneous or homogeneous distribution are considered. The homogeneous distribution corresponds to a perfect crystal arrangement. The heterogeneous distribution results from a defect or a chemical impurity on a crystal plan, material coexistence or by a passivation of the surface.³⁷ The patch occurs when different materials coexist or when crystal planes are not large enough to neglect boundary interactions.^{38,39}

Four different spatial site distributions are studied: (i) homogeneous site distribution (Fig. 1a), (ii) heterogeneous random distribution (Fig. 1b), and (iii) homogeneous (Fig. 1c)

Table 1 Chemical reactions at the NP surface and the associated energy changes

Initial charge	Possible charge	Acid/base chemical reaction	Change in energy $\Delta E (k_{\rm B}T)$
0	+1	Site $-H + H^+ \stackrel{1/K_{a1}^0}{\Longleftrightarrow}$ Site $-H_2^+$	$\Delta E = \Delta E_{\text{electrostatic}} + (\text{pH} - \text{pK}_{\text{a1}}^{0}) \ln(10)$
	-1	Site $-H \stackrel{K_{a2}^0}{\Longleftrightarrow} Site^- + H^+$	$\Delta E = \Delta E_{\text{electrostatic}} - (pH - pK_{\text{a2}}^0)\ln(10)$
+1	0	Site $-H_2^+ \stackrel{K_{al}^0}{\Longleftrightarrow}$ Site $-H_2^+ + H_2^+$	$\Delta E = \Delta E_{\text{electrostatic}} - (pH - pK_{\text{a1}}^{0})ln(10)$
	-1	$Site - H_2^+ \stackrel{K_{al}^0 \cdot K_{a2}^0}{\rightleftharpoons} Site^- + 2H^-$	$\Delta E = \Delta E_{\text{electrostatic}} - (2pH - pK_{a1}^{0} - pK_{a2}^{0})\ln(10)$
-1	0	$\operatorname{Site}^- + \operatorname{H}^+ \stackrel{1/K_{a2}^0}{\Longleftrightarrow} \operatorname{Site} - \operatorname{H}$	$\Delta E = \Delta E_{\text{electrostatic}} + (\text{pH} - \text{p}K_{\text{a2}}^{0})\ln(10)$
	+1	$Site^{-} + 2H^{+} \stackrel{1/(K_{a1}^{0} \cdot K_{a2}^{0})}{\rightleftharpoons} Site - H_{2}^{+}$	$\Delta E = \Delta E_{\text{electrostatic}} + (2pH - pK_{a1}^{0} - pK_{a2}^{0})\ln(10)$

Paper **PCCP**

and (iv) heterogeneous random sites confined in patches (Fig. 1d). The two patches exhibit a face to face configuration and have a radius of 3 nm (polar coordinates of the patch centers $\theta_1 = \pi$; $\varphi_1 = 0$, $\theta_2 = 0$; $\varphi_2 = 0$). In most cases, 50 titrating sites are considered, corresponding to a mean surface charge density equal to 25 mC m⁻² and 128 mC m⁻² in the patches. Such surface site densities are representative of experimental situations regarding the surface properties of metal oxide nanoparticles.⁴⁰

To generate the homogeneous distribution, the following procedure is used. First, all sites are charged. Then, their positions are adjusted with the Metropolis criterion to obtain an ideal arrangement. This problem is similar to the Thomson atomic model.41 For a heterogeneous distribution, sites are distributed randomly at the surface taking into account an excluded volume between sites. Patch distributions are built using similar processes but sites are confined in a spherical cap. Different pK_a^0 values are used here to study their effects on the titration curves.

Results and discussion

The 1-p K_a^0 model with a single deprotonation step, characterized by eqn (8), is studied first. Then, the model is extended to amphoteric groups with two equilibrium constants corresponding to the two deprotonation steps given by eqn (7) and (8). This model is called the 2-p K_a^0 model.

$1-pK_a^0$ model

To investigate the influence of site distribution, surface charge density and dielectric constant on the deprotonation process, simulations are carried out with 20 000 Monte-Carlo steps for each pH - p K_a^0 value. A "soft" NP is considered first with a dielectric constant equal to that of water ($\varepsilon_c = \varepsilon_w$). Titration curves are systematically compared to the isolated monomer case (i.e. in the absence of electrostatic interactions) to better isolate the effects of the repulsive interactions between the different sites.

Influence of NP site distribution. As shown in Fig. 2, the deprotonation process of NPs is more effective for homogeneous and heterogeneous site distributions. This is due to the larger distances between the nearest neighbors and the lower electrostatic repulsions between negatively charged sites. The homogeneous surface is the most efficient configuration for efficient site deprotonation (or surface charging process). Nevertheless, there is a significant difference compared to the isolated monomers. At a given pH - p K_a^0 value, the ionization is less important due to electrostatic repulsions. For patch distributions, distances between sites are smaller and the charging process is less efficient. Furthermore, in the case of heterogeneous patches, distances between some sites are so close that deprotonation is not completely achieved even for high pH - p K_a^0 values.

As shown in Fig. 3a when the pH - p K_a^0 value is adjusted for different surface site distributions, there are important differences in the total energy depending on the site distribution. Plateau values are obtained in all cases when the degree of dissociation is

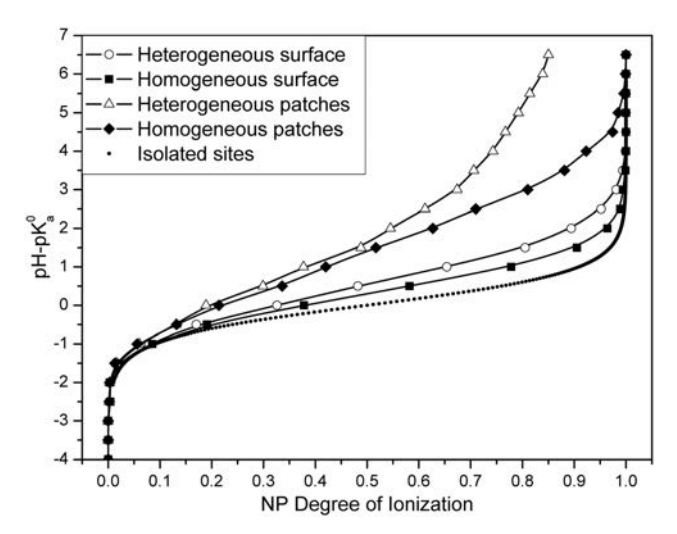


Fig. 2 Monte-Carlo titration curves of a NP with 50 sites and with different surface distributions (1-p K_a^0 model). The site distribution at the surface of the NP is found to strongly influence the degree of ionization of NPs. In particular, NP deprotonation is strongly limited for heterogeneous patches distribution. For the sake of clarity, titration curves are compared with the corresponding ideal (isolated) case, i.e. in the absence of electrostatic interactions between sites. When pH = pK_a^0 , only 20% of the sites are deprotonated (50% in the case of isolated sites experiencing no electrostatic interactions). A nonlinear relationship is shown between the degree of ionization and pH - p K_a^0

equal to one with the exception of the heterogeneous patch distribution. When representing the total energy variation as a function of the degree of ionization (Fig. 3b), a significant difference in total energy is observed between the heterogeneous/homogeneous and patch distributions due to lesser distances and more important surface site density in patches. The comparison of these two figures shows, on the one hand, the total energy as a function of the pH - p K_a^0 value and, on the other hand, the total energy as a function of the ionization degree, which clearly indicates that there is no linear relationship between the ionization degree and the pH - p K_a^0 value when different site distributions are considered.

Influence of the surface charge density and dielectric constant of NPs. To get an insight into the influence of the surface charge density, simulations are now carried out by considering heterogeneous distributions and by adjusting the number of titrating sites to 10/50/100/200/300 sites corresponding to 5/25/50/100/150 mC m⁻² respectively. In addition simulations are performed to study the influence of the dielectric constant of NPs. Three different dielectric constants are considered: one to mimic soft NPs with the same dielectric constant as water (ε_c = 78), a second one corresponding to that of titanium dioxide NPs (ε_c = 130) and the last one corresponding to NPs having low dielectric constant such as hematite NPs ($\varepsilon_c = 12$).

As shown in Fig. 4, the decrease of the surface charge density also plays an important role in the deprotonation process with differences in several pH - p K_a^0 units at high ionization degrees. With the decrease of the surface site density, deprotonation processes become easier and curves are shifted to the isolated monomer situation.

PCCP Paper

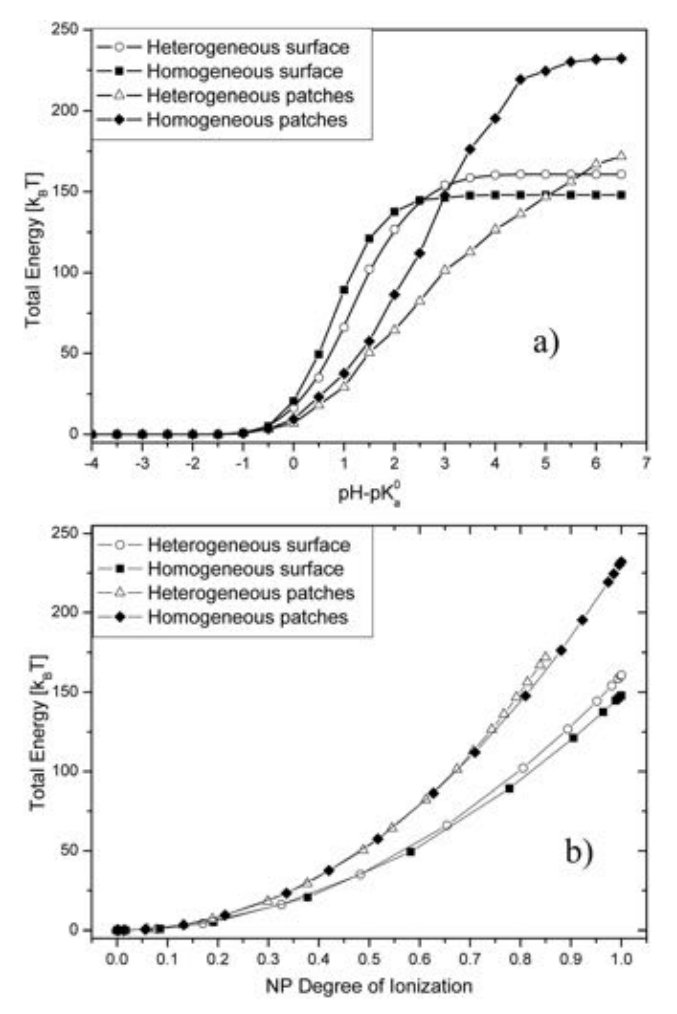


Fig. 3 (a) Variation of the total electrostatic energy as a function of pH - $p{\cal K}^0_a$ and (b) as a function of the degree of ionization for a NP with 50 sites and with different surface distributions, (1- $p{\cal K}^0_a$ model). Differences in the total energy values between the surface and patch distributions are explained by the inter-site distance values.

As observed in Fig. 5, the dielectric constant variation is also found to play an important role. The dielectric constant of "soft" NPs constitutes an intermediate case. For low dielectric constant values (hematite), since sites are less electrostatically screened, the repulsion between them are stronger and the deprotonation is more difficult. In contrast, site interactions are much more attenuated for larger values of the dielectric constant (titanium dioxide) and the deprotonation process with an increased pH $-pK_a^0$ value is more efficient.

$2-pK_a^0$ model

Influence of $\Delta p K_a^0$ and dielectric constant variation. A similar approach is presented here by taking into account two $p K_a^0$ values corresponding to two successive deprotonation steps $(p K_{a1}^0 \text{ (eqn (7))} \text{ and } p K_{a2}^0 \text{ (eqn (8))})$. The titration of a NP with a heterogeneous surface is carried out for different $\Delta p K_a^0$ values from 0.5 to 4 to get an insight into the effect of the acid/base properties of the sites on the charging behavior of NPs and to

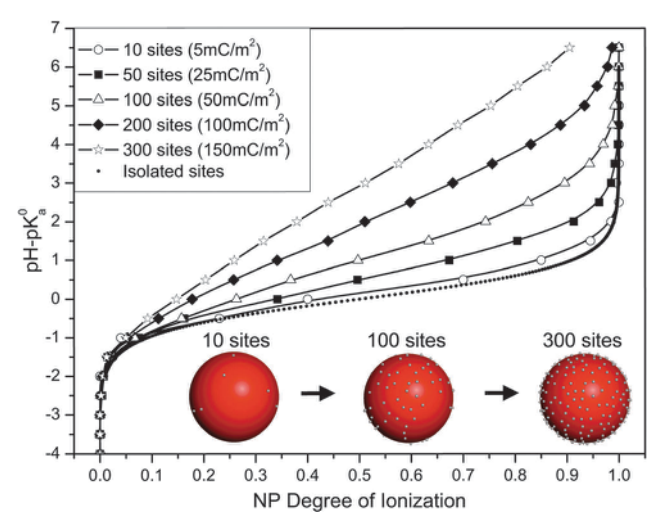


Fig. 4 Monte-Carlo titration curves for a heterogeneous surface with different charge densities (10, 50, 100, 200 and 300 sites). The increase of the surface density is found to limit the NP charging process. The corresponding charge densities in mC m $^{-2}$ are given in the inset.

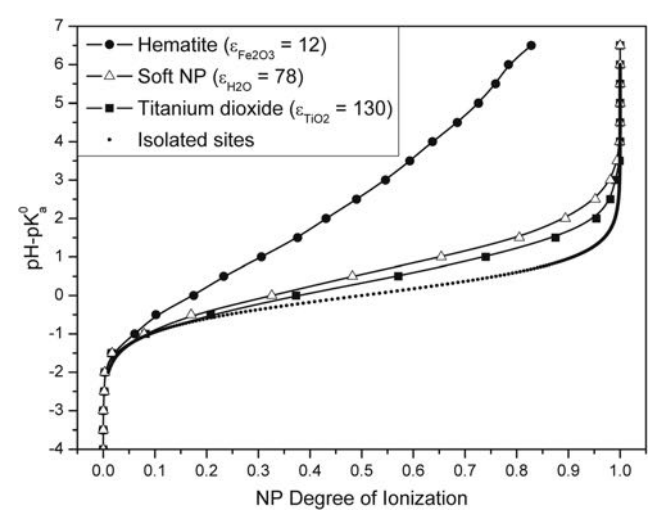


Fig. 5 Monte-Carlo titration curves for a heterogeneous surface with 50 sites (25 mC m⁻²) and with various dielectric constants. The dielectric constant is found to play an important role in the NP charging behavior by controlling the electrostatic repulsions between the different sites. Low dielectric constant NPs exhibit poor charging behavior.

help in the distinction between zero charge and isoelectric points.

As shown in Fig. 6a the $\Delta p K_a^0$ value has an important effect on the charging behavior of NPs. We start with a fully positively charged NP which is gradually deprotonated by increasing the pH $-pK_a^0$ value. It is important to note that the total surface charge is, in all cases, equal to zero when pH $-pK_a^0 = 0$ with $pK_a^0 = (pK_{a1}^0 + pK_{a2}^0)/2$. Then a second deprotonation step is induced towards the formation of negative charges by increasing further the pH $-pK_a^0$ value and, consequently, the degree of ionization of NPs increases again. At low $\Delta p K_a^0$ values ($\Delta p K_a^0 < 2$), in agreement with the acid/base properties of the sites, and when pH $-pK_a^0$ is equal to zero, the degree of ionization of NPs

Paper **PCCP**

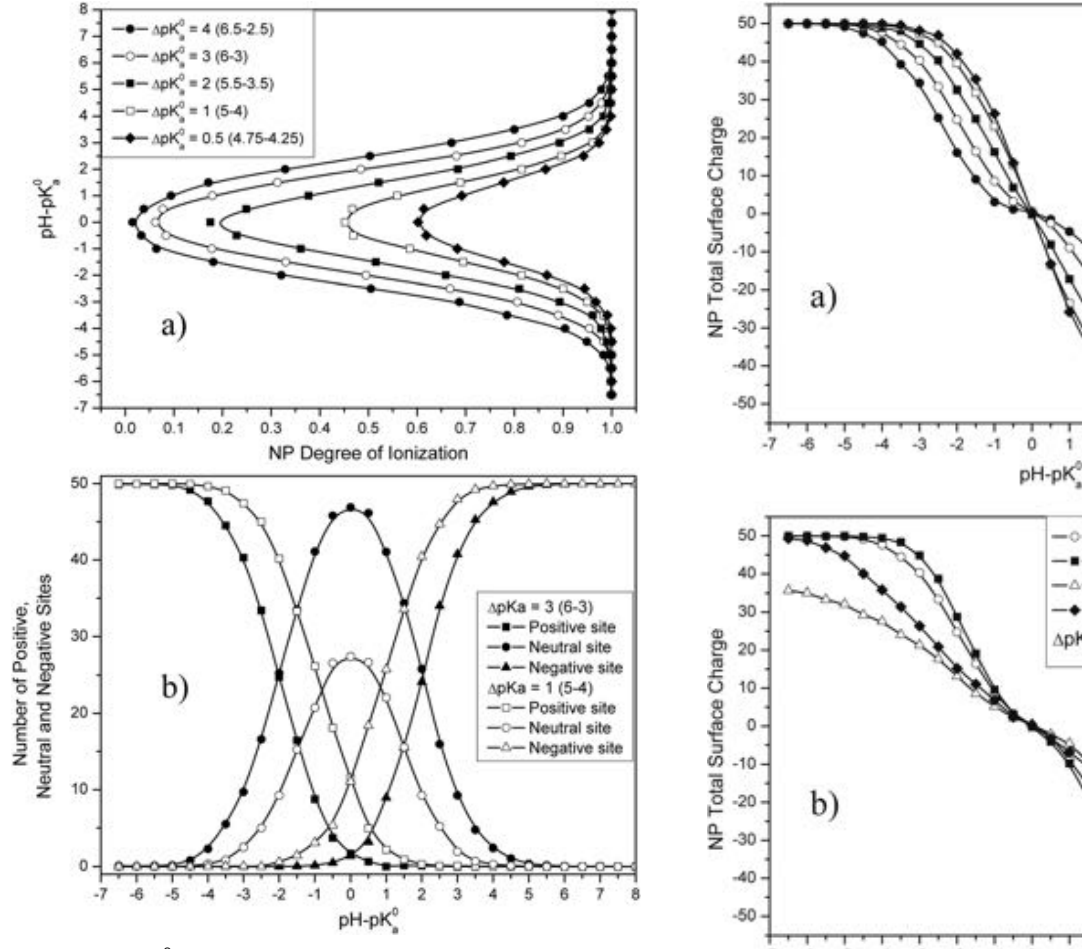


Fig. 6 (a) pH - p K_a^0 as a function of degree of ionization of NPs and (b) the number of charge type as a function of pH - p K_a^0 for a heterogeneous surface NP with variable $\Delta p K_a^0$ values (2-p K_a^0 model). At high $\Delta p K_a^0$, a step by step deprotonation process is clearly observed (hence resulting in a point of zero charge) while at low $\Delta p K_a^0$, the deprotonation process results in the coexistence of opposite and neutral charges (hence resulting in an isoelectric point). In (a) the total number of opposite charges is found to depend on the $\Delta p K_a^0$ value. The values of $p K_{a1}^0$ and $p K_{a2}^0$ are given in the brackets.

is still important due to the presence of both positive and negative charges, which are predominant regarding the neutral sites. As a result an isoelectric point is obtained here and an equivalent number of positive and negative charges is obtained at the NP surface as indicated in Fig. 6b. In that situation, the second deprotonation step, towards the formation of negative charges, begins when the first one is not completely achieved. Here the positive sites are not fully switched off. Small $\Delta p K_a^0$ values result in the dynamic coexistence of the three possible charge transition states (1 to 0, 0 to -1 and 1 to -1) as well as the concomitant presence of positive and negative sites (opposite charges). As shown in Fig. 6b, the number of opposite charges, in particular when pH - p $K_a^0 = 0$, is a function of $\Delta p K_a^0$ and increases with the decrease of $\Delta p K_a^0$. At high $\Delta p K_a^0$ ($\Delta p K_a^0 \geq 2$), the corresponding situation when pH $- pK_a^0 = 0$ is now representative of a point of zero charge, since the number of positive and negative charges are close to 0. Under such conditions, the

Fig. 7 (a) Variation of the total surface charge for different $\Delta p K_a^0$ considering a heterogeneous surface and (b) for different site distributions with $\Delta p K_a^0 = 3$ (2-p K_a^0 model). It should be noted that the shape of the titrating curves is found to depend both on the surface site distribution and $\Delta p K_a^0$ values. The presence of an isoelectric point results in sharp transitions between the positively and negatively charged domains. The values of pK_{a1}^0 and pK_{a2}^0 are given in the brackets.

pH-pK°

 $ApK_{a}^{0} = 4 (6.5-2.5)$

= 2 (5.5-3.5)

 $\Delta pK_a^0 = 0.5 (4.75-4.25)$ Heterogeneous surface

 $ApK^0 = 3 (8-3)$

 $\Delta pK^0 = 1 (5-4)$

- Heterogeneous surface

- Homogeneous patches

-■— Homogeneous surface

 $\Delta pK_{-}^{0} = 3 (6-3)$

–△— Heterogeneous patches

deprotonation process is a step by step mechanism (as observed in both Fig. 6a and b): the positive charges are first switched off before the emergence of negative charges.

In Fig. 7a are presented the effective surface charge variations of NPs as a function of the pH $- pK_a^0$ values and for different $\Delta p K_a^0$ values. The general shape is quite similar to the experimental titration curves, which are obtained via potentiometric titrations, 29,30 electrophoretic mobility or zeta potential measurements.11 It should be noted that (i) when the total charge of NPs is zero all the curves cross each other at the same point i.e. when pH - $pK_a^0 = 0$ and (ii) a sharp transition is observed in the presence of an isoelectric point from positive to negatively charged NPs. When $\Delta p K_a^0 = 3$ (Fig. 7b) it is found that the shape of the curves is also controlled by the surface site distribution. This constitutes an important outcome in the interpretation of experimental data. Heterogeneous and homogeneous distributions exhibit plateau values at the beginning PCCP Paper

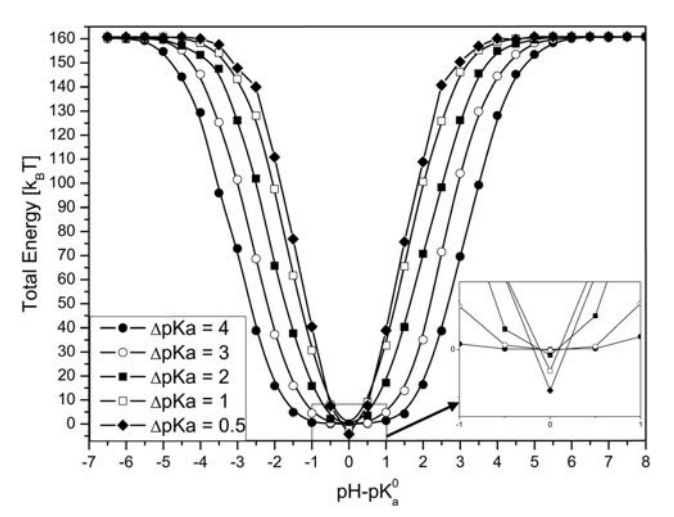


Fig. 8 Total energy variation at different $\Delta p K_a^0$ (2- $p K_a^0$ model) with N=50. At low $\Delta p K_a^0$ values, due to the concomitant presence of positive and negative sites, negative values of the total energy are obtained.

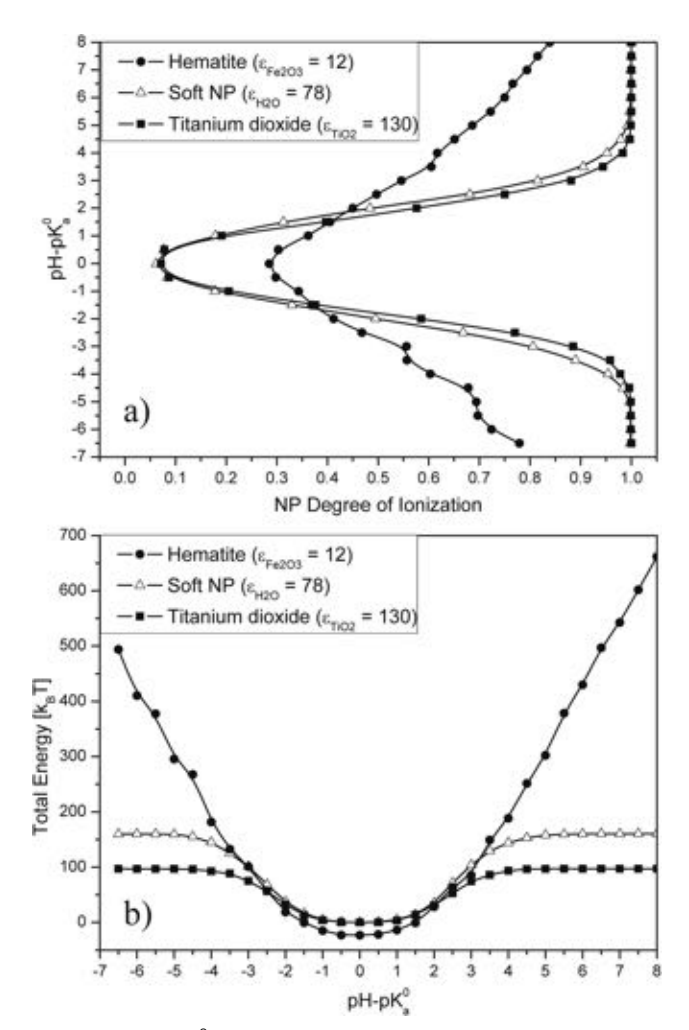


Fig. 9 (a) $pH - pK_0^0$ as a function of degree of ionization of NPs and (b) total energy as a function of $pH - pK_0^0$. The effect of the dielectric constant is investigated here for a heterogeneous surface (2- pK_0^0 model) with N = 50. A low dielectric constant promotes the presence of opposite charges when $pH - pK_0^0$ is close to zero.

and at the end of the titration processes whereas patch distributions show more linear charge variations. Total energy variations for different $\Delta p K_a^0$ values are also presented in Fig. 8. The lowest energies are found when the effective charge on the NPs is equal to zero at pH $-pK_a^0=0$. Moreover, the presence of a mixture of opposite charges for low $\Delta p K_a^0$ results in negative energies.

Complementary calculations are then carried out to understand the influence of the dielectric constant. We are considering the case with $\Delta p K_a^0 = 3$ with heterogeneous surface distribution. As shown in Fig. 9a, two different behaviors are observed by adjusting the dielectric constant. On the one hand, for titanium dioxide and "soft" NPs, having relatively high dielectric constants, most of the charges are switched-off when pH - p $K_a^0 = 0$ and a point of zero charge is obtained. The ionization degree of NPs at low and high pH values is equal to one, hence indicating fully charged surfaces. The variation of the total energy (Fig. 9b) also exhibits specific profiles with values equal to zero at the PZC. On the other hand, at low dielectric constant, sites are electrostatically less screened and a partial protonation or deprotonation process is achieved. In addition when pH - p $K_a^0 = 0$, NPs exhibit a mixture of positive, negative and neutral sites on their surface, which is much more representative of an isoelectric point model. Total energies in Fig. 9b support the observed differences and that such a system is less stable from an electrostatic point of view when low or high pH $- pK_a^0 = 0$ is considered.

Conclusions

In this work we have demonstrated that Monte Carlo simulations constitute a powerful approach to (i) get an insight into the charging behavior of metal oxide type NPs, (ii) isolate the influence of several important parameters such as acid base properties of surface sites, charge density, surface site distribution and dielectric constant and (iii) elucidate the possible transformation and properties of NPs in a changing environment. In particular, it is shown that the site distribution is playing a key role and that the homogeneous distribution is the most efficient one to obtain high ionization degrees when the $1-pK_a^0$ model is considered. Acid/ base properties are also found to play a key role, in particular, for the 2-p K_a^0 model. Indeed when $\Delta p K_a^0 \geq 2$, a point of zero charge is obtained whereas an isoelectric point occurs when smaller values are considered, in good agreement with experimental and analytical predictions. To establish a link with experimental data we presented total surface charge variations of NPs as a function of $pH - pK_a^0$ and demonstrated that they were not only controlled by the acid-base properties of the NP sites but also by the site distribution and dielectric constant. It was also found that the presence of an isoelectric point or point of zero charge resulted from two different charging processes. Finally, it should be noted that this model can be adjusted to different situations since the size, site density, dielectric constant, site distribution and acid/ base properties are input parameters. Our model could also be extended to the charging behavior of NPs in concentrated solutions including complex organic macromolecules and the

effect of the surrounding electrolytic solutions *via* the presence of explicit ions.

Acknowledgements

The authors acknowledge the financial support received from the Swiss National Foundation (project 200021_135240). The work leading to these results also received funding from the European Union Seventh Framework Programme (FP7/2007-2013) under agreement no NMP4-LA-2013-310451.

References

- 1 S. J. Klaine, P. J. J. Alvarez, G. E. Batley, T. F. Fernandes, R. D. Handy, D. Y. Lyon, S. Mahendra, M. J. McLaughlin and J. R. Lead, Environ. Toxicol. Chem., 2008, 27, 1825-1851.
- 2 G. V. Lowry, K. B. Gregory, S. C. Apte and J. R. Lead, Environ. Sci. Technol., 2012, 46, 6893-6899.
- 3 B. Nowack and T. D. Bucheli, *Environ. Pollut.*, 2007, **150**, 5–22.
- 4 F. Gottschalk, T. Sonderer, R. W. Scholz and B. Nowack, Environ. Sci. Technol., 2009, 43, 9216-9222.
- 5 Y. Ju-Nam and J. R. Lead, Sci. Total Environ., 2008, 400, 396-414.
- 6 M. Auffan, J. Rose, J.-Y. Bottero, G. V. Lowry, J.-P. Jolivet and M. R. Wiesner, Nat. Nanotechnol., 2009, 4, 634-641.
- 7 V. L. Colvin, Nat. Biotechnol., 2003, 21, 1166-1170.
- 8 A. Weir, P. Westerhoff, L. Fabricius, K. Hristovski and N. von Goetz, Environ. Sci. Technol., 2012, 46, 2242-2250.
- 9 N. von Moos and V. I. Slaveykova, Nanotoxicology, 2013, 8, 605-630.
- 10 N. von Moos, P. Bowen and V. I. Slaveykova, Environ. Sci.: Nano, 2014, 1, 214.
- 11 F. F. Loosli, P. Le Coustumer and S. Stoll, Water Res., 2013, 47, 6052-6063.
- 12 F. Mohd Omar, H. Abdul Aziz and S. Stoll, Sci. Total Environ., 2014, 468-469, 195-201.
- 13 S. Ulrich, M. Seijo, A. Laguecir and S. Stoll, J. Phys. Chem. B, 2006, 110, 20954-20964.
- 14 A. Martín-Molina, C. Rodríguez-Beas, R. Hidalgo-Ávarez and M. Quesada- Pérez, J. Phys. Chem. B, 2009, 113, 6834-6839.
- 15 S. Madurga, A. Martín-Molina, E. Vilaseca, F. Mas and M. Quesada-Pérez, J. Chem. Phys., 2007, 126, 234703.

- 16 F. L. B. da Silva and B. Jönsson, Soft Matter, 2009, 5, 2862.
- 17 H. Ohshima, J. Colloid Interface Sci., 1994, 163, 474-483.
- 18 J.-P. Jolivet, M. Henry and J. Livage, Metal oxide chemistry and synthesis: from solution to solid state, Wiley-Blackwell, 2000.
- 19 J. A. Davis, R. O. James and J. O. Leckie, J. Colloid Interface Sci., 1978, 63, 480-499.
- 20 R. A. French, A. R. Jacobson, B. Kim, S. L. Isley, R. L. Penn and P. C. Baveye, Environ. Sci. Technol., 2009, 43, 1354-1359.
- 21 A. M. E. Badawy, T. P. Luxton, R. G. Silva, K. G. Scheckel, M. T. Suidan and T. M. Tolaymat, Environ. Sci. Technol., 2010, 44, 1260-1266.
- 22 H. Ohshima, Colloid Polym. Sci., 2014, 292, 749-756.
- 23 H. Ohshima, Colloid Polym. Sci., 2014, 292, 757-761.
- 24 Z. Zhang and S. C. Glotzer, Nano Lett., 2004, 4, 1407-1413.
- 25 F. Carnal and S. Stoll, J. Phys. Chem. B, 2011, 115, 12007-12018.
- 26 G. F. Newell and E. W. Montroll, Rev. Mod. Phys., 1953, 25,
- 27 D. Frenkel and B. Smit, Understanding Molecular Simulation: From Algorithms to Applications, Academic Press, 2001.
- 28 M. Fixman, J. Chem. Phys., 1979, 70, 4995-5005.
- 29 M. Szekeres and E. Tombácz, Colloids Surf., A, 2012, 414, 302-313.
- 30 E. Tombácz, M. Szekeres and E. Klumpp, Langmuir, 2001, 17, 1420-1425.
- 31 M. Seijo, S. Ulrich, M. Filella, J. Buffle and S. Stoll, Phys. Chem. Chem. Phys., 2006, 8, 5679-5688.
- 32 B. Honig and A. Nicholls, Science, 1995, 268, 1144-1149.
- 33 N. Metropolis, A. Rosenbluth, M. Rosenbluth, A. Teller and E. Teller, J. Chem. Phys., 1953, 21, 1087-1092.
- 34 D. W. Rankin, Crystallogr. Rev., 2009, 15, 223-224.
- 35 L. J. Henderson, Am. J. Physiol., 1908, 21, 173-179.
- 36 K. A. Hasselbalch, Biochem. Z., 1916, 78, 112-114.
- 37 K. Nagashima and F. D. Blum, J. Colloid Interface Sci., 1999, 217, 28-36.
- 38 S. Ross and J. P. Olivier, On physical absorption, Wiley Interscience, New York, 1954.
- 39 J. M. Cases and B. Mutaftschiev, Surf. Sci., 1968, 9, 57-72.
- 40 K. W. Powers, S. C. Brown, V. B. Krishna, S. C. Wasdo, B. M. Moudgil and S. M. Roberts, Toxicol. Sci., 2006, 90, 296-303.
- 41 J. Thomson, Philos. Mag., 1904, 7, 237-265.

CHAPTER 4

Effect of Surface and Salt Properties on the Ion Distribution around Spherical Nanoparticles. Monte Carlo Simulations

4.1 Introduction

Surface charge properties represent key parameters to predict fate, reactivity and complexation of manufactured nanoparticles in natural, biological and industrial dispersions. In **Chapter 3**, we have shown that the nanoparticle surface properties control the surface charging process *via* electrostatic repulsions. However, the presence of charges at the NP interface induces a corresponding excess of counterions in the solution. These surface charges are not only modifying the surface properties of the nanoparticle, they also play a significant role on the structuration of the surrounding solution (see **section 2.4.5**). This chapter focuses on the influence of surface and solution properties on the condensation process. A novel approach is developed in order to better understand the surface charge electrostatic properties of spherical nanoparticles (NPs). The ion distribution around one nanoparticle is investigated using Monte Carlo simulations and by adjusting a wide range of parameters including NP properties (surface charge density and site distribution), salt concentration (ionic strength and cation concentration) and salt valency (mono-, di- and trivalent salt). A canonical Metropolis-Monte Carlo method is used to reach equilibrium states and a primitive Coulomb model is applied to describe the electrostatic interactions between explicit discrete sites, counterions and salt particles.

4.2 Main Results

4.2.1 NP charge behavior in the presence of counterions only

To get an insight into the influence of surface charge density and surface site distribution on the condensation process, Monte Carlo simulations are carried out with $5x10^6$ MC steps for each set of simulation. NP effective charge and fraction of reduced NP charge are systematically calculated to better understand the effects of ion condensation.

Influence of surface charge density

As shown in **Figure 4.1**, in which the effective charge is represented as a function of surface site number for heterogeneous distribution, two different behaviors at low and high density are observed resulting in two different slopes. Due to lower electrostatic interactions at low density, resultiong from larger distances between sites, counterions are less attracted by the nanoparticle and the effective surface charge is then less reduced. Surface titrating sites are acting as isolated charges and the effective charge follows the ideal curve in absence of condensation. On the other hand, at high density, the NP effective charge is found more reduced due to the increased affinity of the counterions with the surface and progressively shifted compared to the ideal curve without condensation.

By considering the two different slopes, a "critical site density" can be defined as a limit between the two regimes in the effective NP charge variation and corresponding to a limit of sites necessary to consider a condensation state. However, the decrease of Z_{eff} with the increase of the NP surface charge densities, as shown in **Figure 4.1**, is limited by steric effects between counterions and electrostatic interactions between them. For instance, the charge of a nanoparticle with 400 titrating sites is only 61 % reduced.

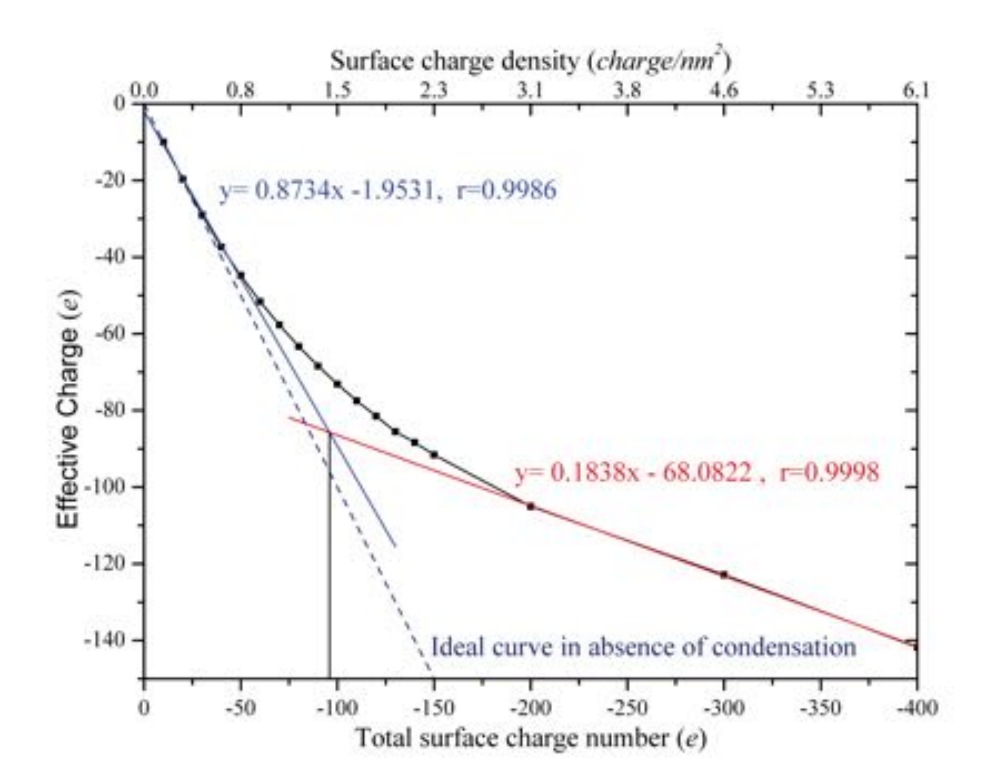


Figure 4.1: NP effective charge as a function of total surface charge number and surface charge density for a heterogeneous surface distribution without salt ions. Two different behaviors are observed at low and high surface charge density. The two regimes can be separated by a critical surface charge number which is equal here to 96 sites.

Influence of site distribution

As presented in **Figure 4.2**, when different site distributions are considered such as heterogeneous, homogeneous distributions and central charge, no significant differences in the NP effective charge variations are observed. This is an important output indicating that the surface site distribution has little effect on ion distribution. On the other hand, by considering a constant surface charge number N and by adjusting the NP size, the surface charge density is found to have a strong impact on the NP condensation behavior. Indeed, the effective surface charge is more reduced by decreasing the NP radius and consequently increasing the surface charge density which constitutes also an important result.

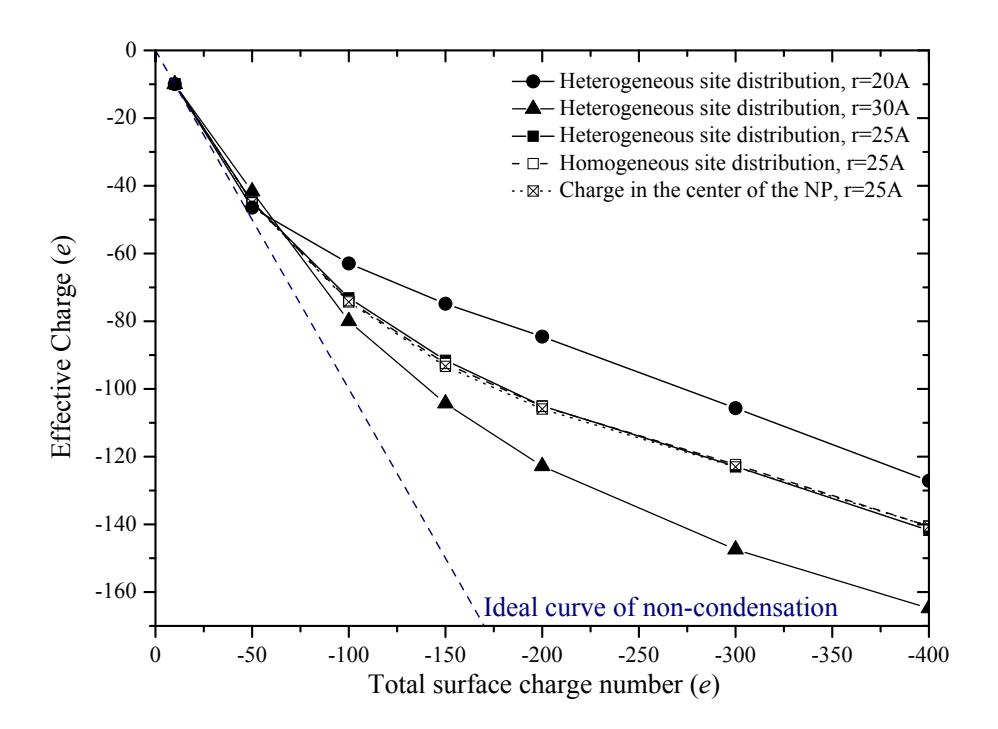


Figure 4.2: NP effective charge for different surface site distributions as a function of total surface charge number and surface charge density. Three different distributions are studied: Heterogeneous (radii of 20, 25 and 30 Å), homogeneous (25Å) distribution and equivalent charge in the center without discrete sites on the surface (25Å).

4.2.2 NP surface charge behavior in presence of salt

A complementary study is presented now by taking into account the presence of salt particles in the simulation box to investigate the influence of salt properties (valency and concentration) on the condensation process.

Influence of salt concentration

One NP with 100 sites is considered with different salt concentrations $(1x10^{-3} \text{ to } 1x10^{-2} \text{ M})$ and valencies (mono-, di- and trivalent) of cations. The number of anions is adjusted depending on the number of cations present in solution to keep the electroneutrality. As shown in **Figure 4.3**, the presence of monovalent cation has no impact on the effective charge (which is reduced by 28% similarly to the free salt reference), cations can be assimilated as counterions

Chapter 4: Ion Distribution around Spherical Nanoparticles

with the same charge. Conversely, for divalent and trivalent salt, the effective charge rapidly decreases and reach a plateau values with the increase of cation concentration(4.3. Trivalent cations are more efficient to reduce the NP charge due to stronger interactions with the surface. The NP effective charge is reduced by 91% in the trivalent case, while considering divalent salt only 55% of the NP charge is neutralized within the condensation layer. Similar behaviors are observed experimentaly *via* zeta potential experiments [1–3]. Indeed divalent and trivalent cations are found to have important effect on the overall charges of latex and titanium dioxide nanoparticles.

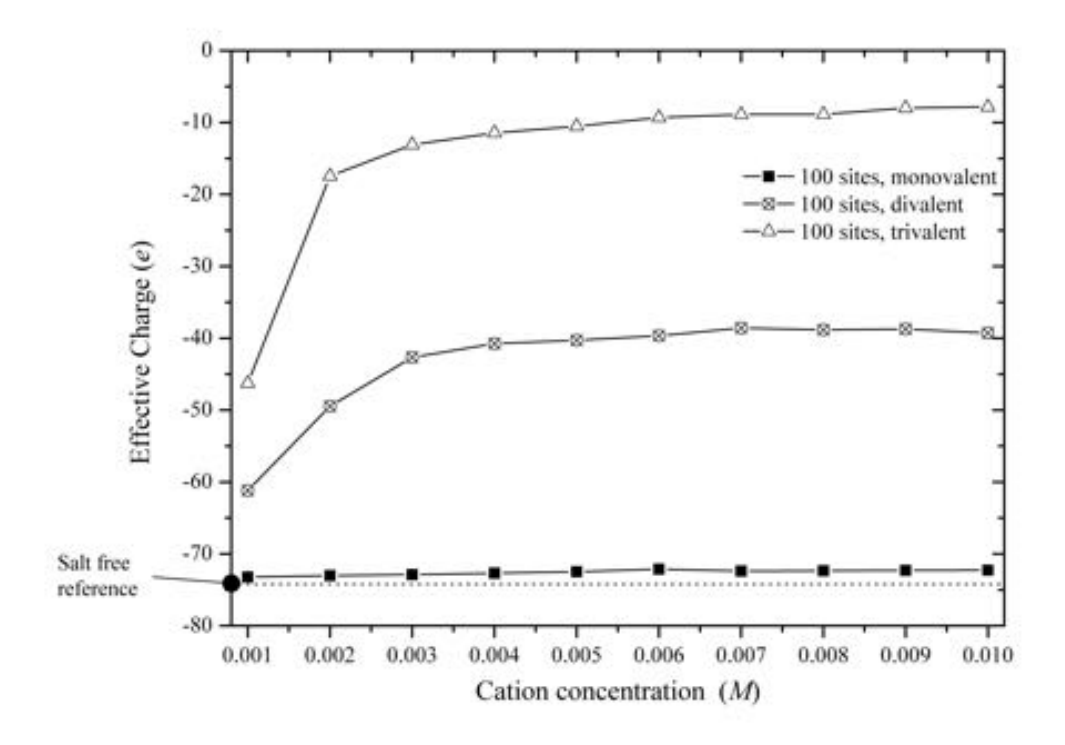


Figure 4.3: NP effective charge in presence of mono-, di- and trivalent cations as a function of different cation concentrations. The nanoparticle (25 Å radius) has 100 sites heterogeneously situated on the NP surface. The salt free effective charge is indicated as reference.

Influence of salt valency

To isolate the influence of cation valency, complementary studies are then carried out by considering a heterogeneous NP with a variable site number (10 to 400 sites) on the surface at

two constant ionic strengths equal to $5x10^{-3}$ and $1x10^{-2}$ M hence allowing the same charge concentration. For example, at $5x10^{-3}$ M, 81, 27 or 14 cations are present in the simulation box for mono-, di- or trivalent salts, respectively. For the monovalent case, similar behavior is observed for the fraction of reduced NP charge (**Figure 4.4**) compared to the case with counterions only. A continuous increase of the fraction of reduced charge is observed by increasing the surface site density. On the contrary, the presence of divalent or trivalent cations significantly modifies the effective charge of the nanoparticle. At low density and in the trivalent case, the NP charge is strongly reduced compared to divalent cations. This difference is explained by stronger interactions of trivalent cations with sites on the surface. On the other hand, at high surface charge number, the difference between di- and trivalent cations rapidly decreases with the increase of the surface charge density to finally disappear. For both ionic strengths, the fraction of reduced surface charge reaches a similar value at high surface charge number. This behavior can be explained by the restriction of the number of positive charges in the condensation layer and salt concentration value.

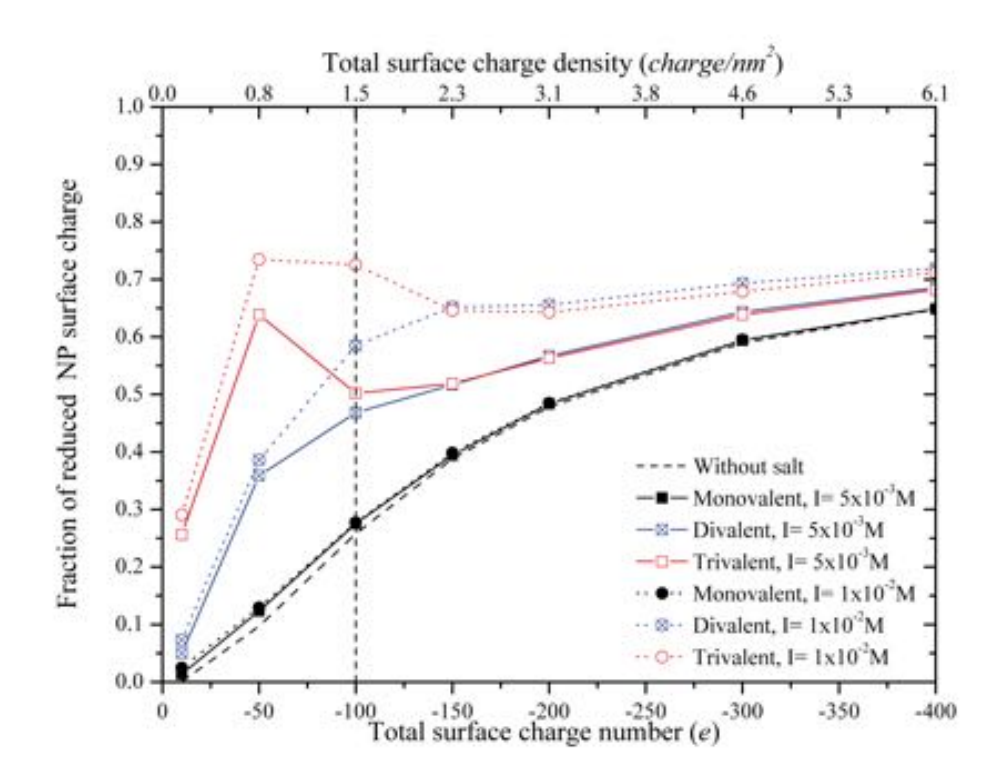


Figure 4.4: Fraction of reduced NP charge as a function of the total surface charge number and of surface charge density and at different ionic strengths $(5x10^{-3} \text{ and } 1x10^{-2})$. Mono, di- and trivalent cations are considered and compared to the case without salt.

Finally, effective charge curves for each valency with two different concentrations $(1x10^{-3} \text{ and } 5x10^{-3} \text{ M})$ are presented in **Figure 4.5** and compared to the case without salt. At low salt concentration, the effective charge is slightly reduced with the increase of the valency while keeping the shape of the "ideal" curve without salt. For low trivalent cation concentration, the shape of the effective charge curve is significantly modified due to the importance of the electrostatic interactions and condensation of cations on the negatively charged NP. By increasing the concentration to 5.10^{-3} M, di- and trivalent cations strongly alter the effective charge indicating that cation number and valency have both significant impacts on the nanoparticle surface charge. In very specific case (200 sites, 5.10^{-3} M), the nanoparticle charge is completely neutralized Indeed, after such a surface charge compensation, the effective charge continuously decreases. However, the reduction or neutralization of the nanoparticle charge is a complex process which depends on the balance between (i) electrostatic attractions between cations and nanoparticle surface, (ii) electrostatic repulsions between NP sites depending on the surface charge density

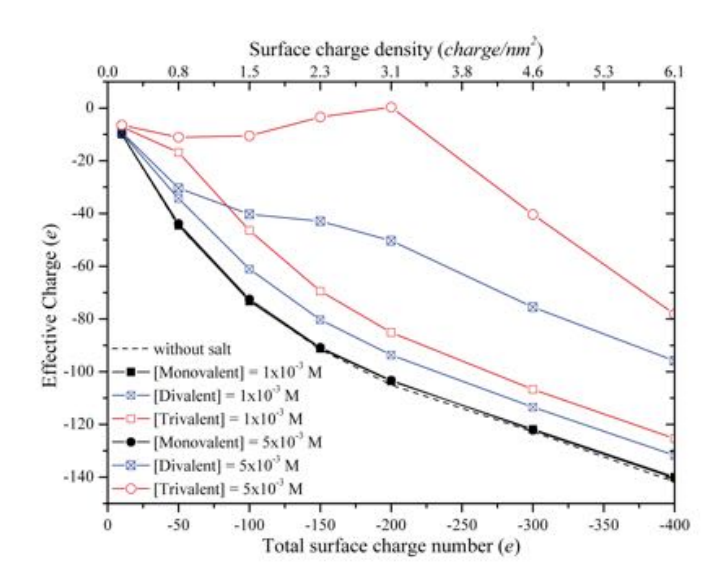


Figure 4.5: NP effective charge as a function of total surface charge number and surface charge density at two different cation salt concentrations $(1x10^{-3} \text{ and } 5x10^{-3} \text{ M})$.

and sizes, (iii) electrostatic repulsions between cations (most important contribution) and (iv) total number of cations present in the solution. The two last points can be a limit for the neutralization of the NP surface charge. In this case, the steric effect has no significant influence on the condensation process. At high salt concentration, the impact of counterions on the NP surface properties is almost negligible; the main contribution in condensation process being provided by salt cations. Interestingly enough, for high trivalent cation concentrations, radial distribution functions of anions around the NP and around cations put in evidence the presence of a double layer around the nanoparticle composed by an electrostatic positive layer (induced by cations) and an anionic layer.

4.3 Conclusions

In conclusion, ion distributions are the result of a subtle balance between the nanoparticle surface properties (mainly surface charge density) and NP surrounding environment (salt concentration and cation properties). Our results, in this chapter, indicates that the presence of explicit surface charges on the NP and in solution has a strong influence on the local ion distribution and on the effective surface charge of the nanoparticles. The reduction of the NP charge is strongly related to (i) the surface charge density (formation of a condensation layer limited by steric effect), (ii) the salt composition (di- and trivalent cations more efficient in the reduction of surface charge), (iii) the resulting electrostatic interactions (balance between cation-NP surface attractions and NP surface-NP surface and cation-cation repulsions) and (iv) the cation concentration. In very specific case (high concentration of trivalent cations and high surface charge density), a neutralization of the nanoparticle surface charge can be observed and the local environment around the nanoparticle becomes more structured with the formation of a multi-layer structure composed by anions and cations. However, in most cases, the ion distribution and consequently the NP effective charges are limited by steric effects and electrostatic repulsions.

Bibliography

- [1] Frédéric Loosli, Philippe Le Coustumer, and Serge Stoll. TiO2 nanoparticles aggregation and disaggregation in presence of alginate and Suwannee River humic acids. pH and concentration effects on nanoparticle stability. *Water Research*, 47(16):6052–6063, October 2013.
- [2] Márta Szekeres and Etelka Tombácz. Surface charge characterization of metal oxides by potentiometric acid–base titration, revisited theory and experiment. *Colloids and Surfaces A: Physicochemical and Engineering Aspects*, 414:302–313, November 2012.
- [3] Etelka Tombácz and Márta Szekeres. Interfacial AcidBase Reactions of Aluminum Oxide Dispersed in Aqueous Electrolyte Solutions. 1. Potentiometric Study on the Effect of Impurity and Dissolution of Solid Phase. *Langmuir*, 17(5):1411–1419, March 2001.

Chapter 4: Ion Distribution around Spherical Nanoparticles

Paper II

Reprinted from A. Clavier, F. Carnal, S. Stoll *J. Phys. Chem. B*, **2016** vol. 120, no.32, 7988 Copyright (2016), with permission of the *American Chemical Society*





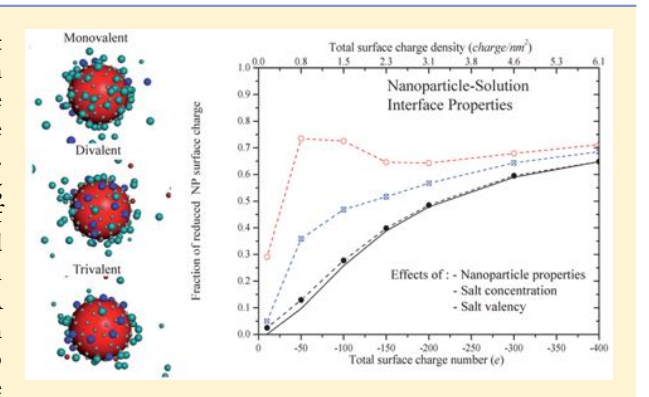
Effect of Surface and Salt Properties on the Ion Distribution around **Spherical Nanoparticles: Monte Carlo Simulations**

Arnaud Clavier, Fabrice Carnal, and Serge Stoll*

Environmental Physical Chemistry, Uni Carl Vogt, Faculty of Sciences, University of Geneva, 66, Boulevard Carl-Vogt, CH-1211 Geneva 4, Switzerland

Supporting Information

ABSTRACT: Nanoparticle surface charge properties represent key parameters to predict their fate, reactivity, and complexation in natural, biological, and industrial dispersions. In this context, we present here an original approach to better understand the surface charge electrostatic properties of spherical nanoparticles (NPs). The ion distribution around one nanoparticle is investigated using Monte Carlo simulations and by adjusting a wide range of parameters including NP properties (surface charge density and site distribution), salt concentration (ionic strength and cation concentration), and salt valency (mono-, di-, and trivalent salt). A canonical Metropolis Monte Carlo method is used to reach equilibrium states and a primitive Coulomb model is applied to describe the electrostatic interactions between explicit discrete



sites, counterions, and salt particles. Our results show that the presence of explicit surface charges on the NP and in solution has a strong influence on the local ion distribution and on the effective surface charge of the nanoparticles. The increase of surface charge density reduces the NP effective charge by the formation of a condensation layer around the nanoparticle. However, a limit of condensation is achieved due to steric effects and electrostatic repulsions. The presence of di- and trivalent cations is also found to strongly modify the effective charge and improve condensation state as long as electrostatic repulsion between the cations close to the surface are not so strong. At high trivalent cation concentration, the NP effective charge is greatly reduced and the local environment around the nanoparticle becomes more structured with the formation of a multi layer structure composed by anions and cations.

1. INTRODUCTION

Manufactured nanoparticles (NPs) are more and more present in our daily environment owing to the development and application of nanotechnologies in many important research areas, such as medicine, industry, and energy, which are expecting to revolutionize our everyday life. 1-5 Because of their very specific and unique properties in many various domains, such as optic, electronic, physics, chemistry, and so forth, 6-NPs synthesis and production is continuously increasing.9 Along with this huge development, the risk of (accidental) release in environmental compartments (soil, air, water) is also expected to increase 10,11 and so far the interactions with ecosystems, environmental or biological molecules, 8,12-14 and with human health 15,16 remain unknown. This risk is usually associated with the large specific surface of NPs that gives them a high reactivity. The potential of diffusion, penetration, and interfacial nature, strongly related to the NP sizes, also raises concern about unforeseen consequences on contaminant transport. 17,18

Unfortunately, the impact of nanoparticles at short and long terms is nowadays not clearly defined in particular in aquatic ecosystems, and the current NP concentration and distribution in the environment is not really well-known. Their interactions

with other particles and also with their environment are highly dependent on the particle properties such as size, shape, chemical composition, and especially surface charge (distribution and charge) 19-21 as well as the solution properties (pH, ion composition, ionic strength). 22-24

The presence of surface charges is one of the most important parameters for controlling the stability of nanoparticles. 25,26 These charges can originate from different processes including chemical reactions at the surface due to the presence of ionizable groups, defects in crystal lattice or adsorption of macroions or polymers at the NP surfaces.²⁷⁻³⁰ In addition. subtle modifications of the dispersion media can change the NP properties, in particular the acid/base properties of surface sites and surface charge densities. 31,32 Some physical properties such as aggregation are also controlled by NP surface charge characteristics. Nanoparticles can form aggregate via homo- or heteroaggregation processes^{21,33,34} and as a result they are eliminated from the water column via sedimentation processes. On the other hand, if stabilized with electrostatic repulsions

Received: May 20, 2016 Revised: July 22, 2016



nanoparticles are more mobile and become more bioavailable for environmental compartments resulting in an increase of their potential toxicity. ^{10,12}

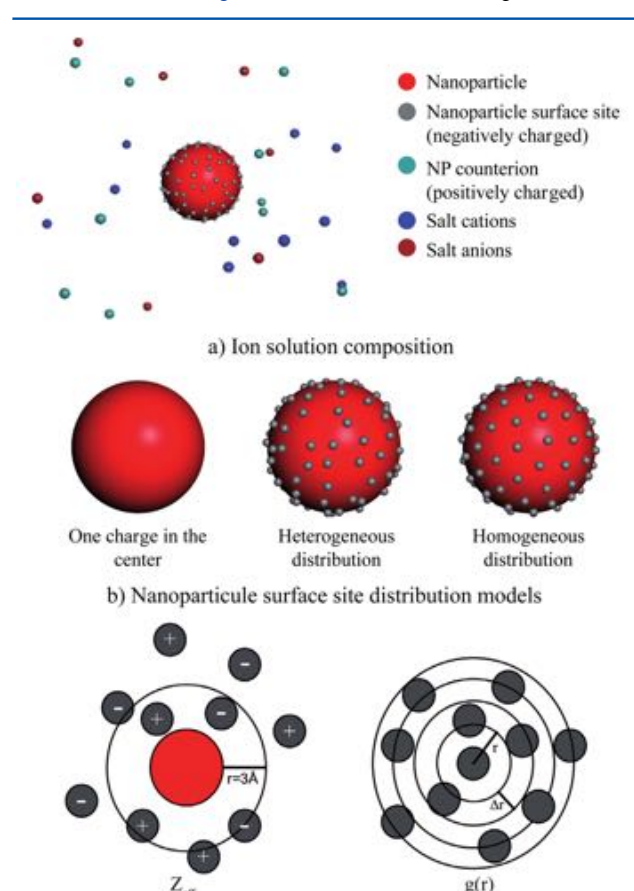
The processes of aggregation and "complex" formation of NPs with polyelectrolytes have been widely studied using experimental methods, ^{20,21,29,35–38} theoretical, ^{39–42} and numerical models⁴³⁻⁵¹ by considering physicochemical properties of solution and nanoparticles. The surface charge is one of the most important parameter in these processes and can be modeled using Monte Carlo simulations, 51,52 the Poisson-Boltzmann approximation,⁵³ or an Ising model.⁵⁴ From an experimental point of view, the NP surface charge can be characterized by ζ -potential methods,⁵¹ potentiometric acid/base titrations,³¹ and electrophoresis measurements.³⁵ On the other hand, the properties of the NP dispersion solution can have also a strong influence on the local nanoparticle environment with the possibility of aggregation, 45,52,50 incidental coatings, and subsequent reactions with ions present in solution ^{19,20,23} or biomolecules (proteins, polysaccharides). ^{29,38,57–59} Ion distribution and surface charge properties of spherical, planar, helical, or rodlike objects have been largely studied using the classical approach 42,60-64 and also quantum models.^{65,66} In the classical approach, the counterion condensation can be described using Manning 42,61,62 or Poisson-Boltzmann theory, 60,67 depending on the properties of the object (shape, charge, density). With the quantum approach, Poisson-Boltzmann and Schrödinger equations are solved to obtain the surface charge properties of NPs^{65,66} considering medium features (pH, salinity). Then, the surface charge density can be calculated as a function of the nanoparticle parameters (size, shape, band gap, effective mass, and so forth) as well as a function of the medium properties (ionic strength, applied fields, temperature, ionic species in suspension in the bulk solution, and so forth).

In this work, the effect of NP surface properties (density, site distribution, and size) and salt properties (concentration and cation valency) on the ion distribution in the vicinity of a NP, by considering discrete surface charges, is investigated regarding the presence of counterions (free salt system) and ions (salt system). By adjusting different parameters such as surface site distribution, surface charge number, cation concentration, and ionic strength, the NPs—solution interface properties are investigated in details and in a systematic way to get an insight into the role of each parameter in an independent manner. The original approach of this work consists in studying the ion distribution around spherical NPs, not only as a function of solution properties (salt concentration and valency) but also as a function of specific nanoparticle properties such as surface site distribution, surface charge density or NP size.

Metropolis Monte Carlo (MC) simulations $^{68-70}$ and a primitive Coulomb model are used here to determine the influence of NPs and solution properties. Simulations are carried out in a canonical ensemble (temperature T and volume V fixed) to obtain an equilibrium state at a fixed pH. A primitive Coulomb model 52 is used to calculate the electrostatic interactions between all the objects of the solution. Spherical charged NPs are modeled by considering a centered charge system as well as heterogeneous and homogeneous surface site distributions. In the first part of this paper, the theoretical model is presented. Then, the NP surface charge behavior is discussed for free salt and salt models by adjusting different parameters such as surface site distribution, density, cation concentration, and ionic strength.

2. THEORETICAL MODEL

2.1. Model Description. The nanoparticles and the different ions (counterions, cations, and anions) are described by a coarse grained model using spherical objects. ⁶⁹ The solvent is treated implicitly as an infinitely diluted aqueous medium having the dielectric constant of water ⁷¹ ($\varepsilon_{\rm w}=78.54$) with a fixed temperature of 298 K. All the objects are impenetrable to the solvent. A cubic simulation box is used with a size of 300 Å per side and the nanoparticle is fixed at the center of the box (Figure 1a). The minimum image convention



c) Effective charge and radial distribution function (RDF) calculation

Figure 1. (a) Snapshot of a simulation box and description of the different objects present in the solution (nanoparticle, cations, anions, NP surface sites, counterions). (b) NPs surface charge distribution: One charge in the center, heterogeneous and homogeneous surfaces. Each NP has a total charge equal to -100e on the surface and a radius of 25 Å. For better visualization, the sites on the surface are represented by spheres, smaller than ions, on the NP surface. (c) Calculation of effective charge $Z_{\rm eff}$ and radial distribution function (g(r)). The condensation layer is defined at r=3 Å. In our model, the ion concentration can be adjusted as well as the NP surface charge number and NP size.

is considered to keep the periodicity of the system⁶⁸ and the minimum distance between two NP replicates is taking into account to avoid any interaction between each image.

Concerning the NPs, as shown in Figure 1b, three different configurations are studied: Heterogeneous/homogeneous surface distributions with discrete sites on the surface and a homogeneously charged surface with an equivalent charge placed at the center of the nanoparticle. Discrete sites are

Table 1. Computer Simulation Parameters for Each Type of Simulation, Number of Sites, Counterions, and Cations as well as Salt Concentrations or Ionic Strengths^a

			cation number		
type of simulation	number of sites and counterions	salt concentration or ionic strength $(M)^{\it a}$	mono-	di-	trivalent
without salt	10 to 400	_	_	_	_
cation concentration variation	100	$C = 1 \times 10^{-3}$	16	16	16
		$C = 2 \times 10^{-3}$	32	32	32
		:	÷	:	:
		$C = 1 \times 10^{-2}$	162	162	162
constant ionic strength	10 to 400	$I = 5 \times 10^{-3}$	81	27	14
		$I = 1 \times 10^{-2}$	162	54	27
constant cation concentration	10 to 400	$C = 1 \times 10^{-3}$	16	16	16
		$C = 5 \times 10^{-3}$	81	81	81

^aMonovalent anions are added in the solution to keep the electroneutrality. C and I represent the salt concentration and ionic strength, respectively.

represented by fixed points placed on the NP surface carrying a negative elementary charge with an excluded volume of 2 Å. Each nanoparticle has a variable number of sites N at the surface (N is between 10 and 400). Manufactured or natural NP surfaces can be represented by these configurations. Homogeneous distributions correspond to a perfect crystal. If the crystal has a chemical impurity, a material coexistence, or a defect or is subject to passivation of the surface, it can be assimilated to a heterogeneous surface.^{72–74} In most cases here, heterogeneous distributions are considered with 100 sites on the surface corresponding to a density of 1.5 charge/nm². Such a surface charge density is comparable, for example, to the experimental values obtained by considering TiO₂ NPs. To generate a heterogeneous distribution, sites are randomly generated on the surface by taking into account a minimum distance between them. For a homogeneous distribution, a heterogeneous configuration is first used. Then, all sites are charged with the same charge, and finally their positions are adjusted using the Metropolis criterion to obtain a perfect configuration.

The primitive model used here has a lot of advantages on more classical schemes by allowing an explicit description of site distribution and geometries, a clear distinction of ions, a clear investigation of local effects, the possibility to account for the acid—base properties of surface sites, and the prediction of nonmonotonic behaviors in particular in the presence of di and trivalent cations.

2.2. Solution Properties. Nanoparticles have a radius of 25 Å and are surrounded by three different types of ions (counterions, salt cations, and salt anions) with a fixed radius of 2 Å and with one charge at their center. The number of counterions, represented by monovalent ions in solution, depends on the NP surface charge density. Considering cations and anions, their charge and number is related to the valency (mono-, di-, or trivalent) and concentration of cations, as well as on the ionic strength. The parameters of each simulation set are summarized in Table 1. In our simulations, the long-range electrostatic potential between all objects i and j is calculated using a primitive Coulomb model

$$U_{ij}^{\text{elec}}(r_{ij}) = \frac{z_i z_j e^2}{4\pi \varepsilon_0 \varepsilon_r r_{ij}} \tag{1}$$

where ε_0 is the vacuum permittivity (8.85 × 10⁻¹² C V⁻¹ m⁻¹), e is the elementary charge (1.60 × 10⁻¹⁹ C), $z_{i,j}$ is the charge carried by the sites and ions, and $r_{i,j}$ is the distance between

them (center-to-center). The total energy of the system (k_BT unit) is obtained by the sum of all the interactions $U_i^{\rm elec}$.

2.3. Monte Carlo Metropolis Procedure. To achieve an equilibrium state with low energies, Monte Carlo simulations are performed according to the Metropolis algorithm. 68-70 For each simulation step, counterions and salt ions are randomly translated through the box. After each movement, a new energy state $E_{\rm f}$ is calculated and compared to the initial energy state $E_{\rm i}$ and $\Delta E = E_f - E_t$ is calculated. Then, the step is accepted or not according to the Metropolis criterion. If the change in ΔE is negative, the energy is lower and the MC step is accepted. Otherwise, the Boltzmann factor, given by $p = \exp\left(-\frac{\Delta E}{k_{\rm B}T}\right)$ is calculated and compared to a random number z between 0 and 1. If the probability p is higher than z, the MC step is accepted; if not, the step is refused and the previous state is considered. Finally, at every 5×10^2 Monte Carlo steps all the positions of the particles in the box are stored so as to calculate mean values.

2.4. Mean Values. One of the important mean values which is presented in this work is the effective NP charge $Z_{\rm eff}$ calculated by considering a condensation layer equal to 3 Å around the nanoparticle. The effective charge (Figure 1c) is a function of the site number on the nanoparticle ($N_{\rm sites}$) of the number of each ion type ($N_{\rm ion} = N_{\rm C} + N_{\rm A} + N_{\rm CI}$) and of their respective charges ($z_{\rm site}$, $z_{\rm C}$, $z_{\rm A}$, and $z_{\rm CI}$) and is given by

$$Z_{\text{eff}} = N_{\text{sites}} z_{\text{site}} - \sum_{i}^{N_{\text{CI}} + N_{\text{C}} + N_{\text{A}}} N_{\text{ion}} z_{\text{ion}}$$
(2)

With this effective charge, we can determine also the fraction of reduced NP charge that represents the reduction of the net NP charge by the ions present in the condensation layer

$$f = 1 - \left| \frac{Z_{\text{eff}}}{N_{\text{sites}} z_{\text{site}}} \right| \tag{3}$$

Other statistical observables are used in this study such as the nearest neighbor distance distribution function $n_i(r, \Delta r)$, which represents the number of ions present in an elementary volume of radius r and of thickness Δr , as well as the radial distribution function $g(r)^{68}$ (Figure 1c)

$$g(r) = \frac{\rho_{\text{local}}}{\rho_{\text{total}}} = \frac{1}{\pi} \frac{V}{N} \sum_{i=1}^{N} \frac{n_i(r, \Delta r)}{4\pi r^2 \Delta r}$$
(4)

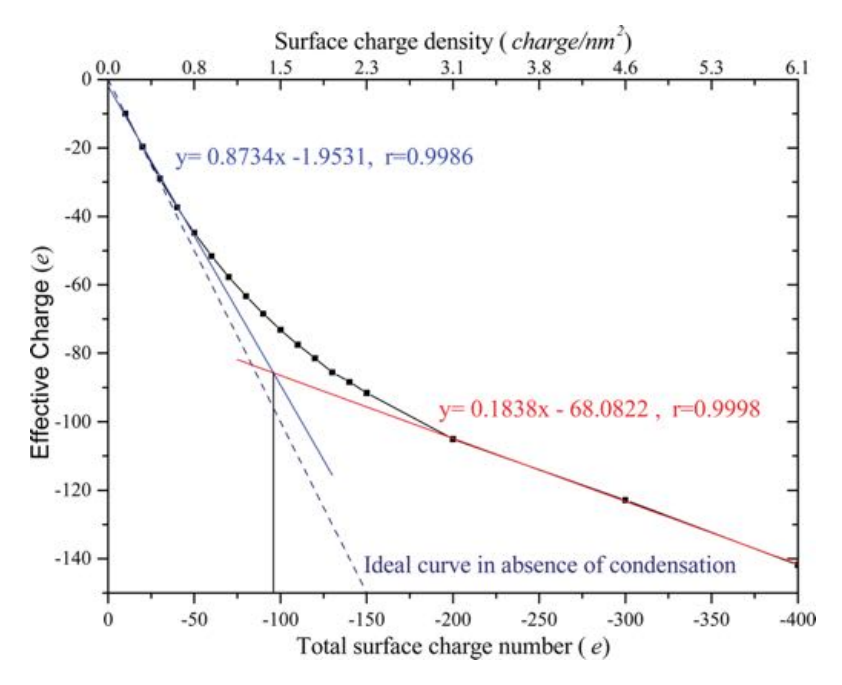


Figure 2. NP effective charge as a function of total surface charge number and surface charge density for a heterogeneous surface distribution without salt ions. The surface charge number is found to strongly influence the condensation process around the NP (radius 25 Å). With the increase of the density, the curve is shifted compared to the ideal curve (dash line) in the absence of condensation. Two different behaviors are observed at low and high surface charge density. The two regimes can be separated by a critical surface charge number that is equal here to 96 sites.

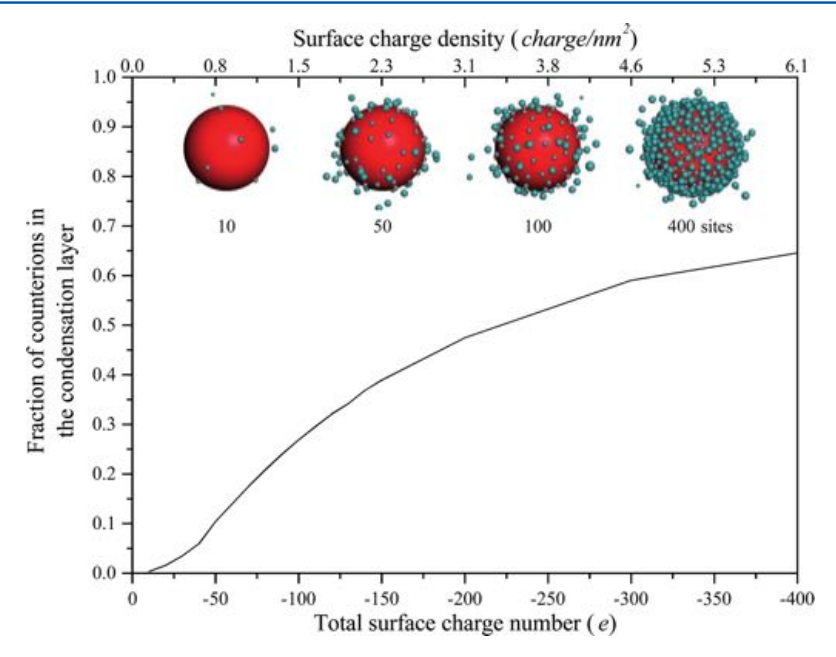


Figure 3. Fraction of counterions in the condensation layer as a function of total surface charge number and of surface charge density. Snapshots of the condensation process evolution for four different total surface charge numbers (10, 50, 100, and 400 sites) considering a heterogeneous distribution (25 Å radius). The condensation around the NP increases progressively with the total surface charge number until reaching a maximum of 65%. The counterion fraction is limited by two differents parameters: electrostatic repulsions and steric effect between counterions.

where V is the corresponding box volume, N is the number of particles, and τ is the number of MC steps to consider. g(r) is expected to give useful information on the evolution of the particle densities around the NP.

3. RESULTS AND DISCUSSION

Two complementary studies are presented. First, the monovalent counterion distribution around the nanoparticle

is investigated as a function of NP surface charge density and site distribution. Then, the model is extended to a more complex situation with the presence of salt and by considering the effect of salt concentration and ion valency.

3.1. NP Charge Behavior in the Presence of Counterions. To get an insight into the influence of surface charge density and surface site distribution on the condensation process, Monte Carlo simulations are carried out with 5×10^6

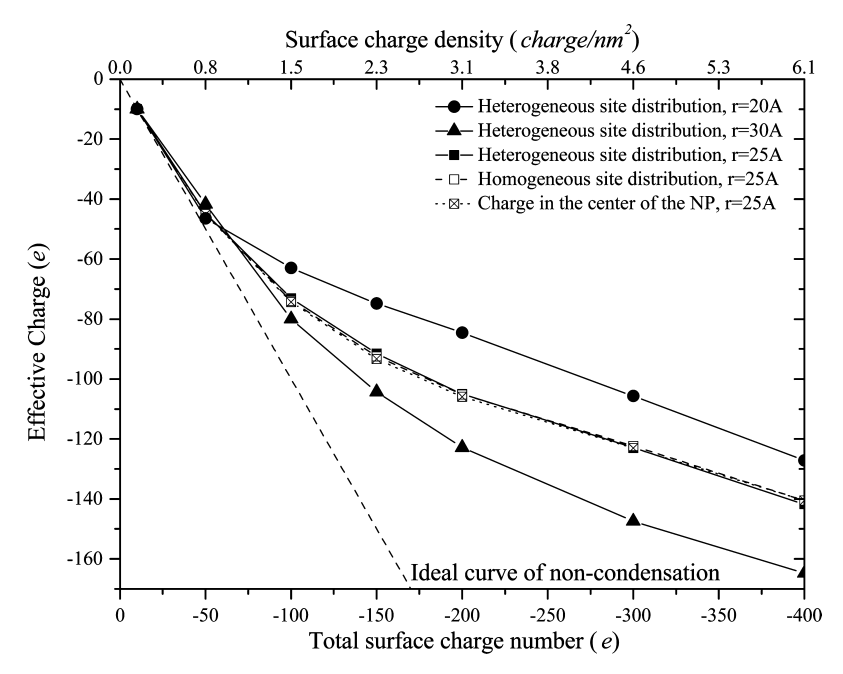


Figure 4. NP effective charge for different surface site distributions as a function of total surface charge number and surface charge density. Three different distributions are studied: Heterogeneous (radii of 20, 25, and 30 Å), homogeneous (25 Å) distribution, and equivalent charge in the center without discrete sites on the surface (25 Å). The site distribution has no significant influence in the condensation process contrary to the surface charge density.

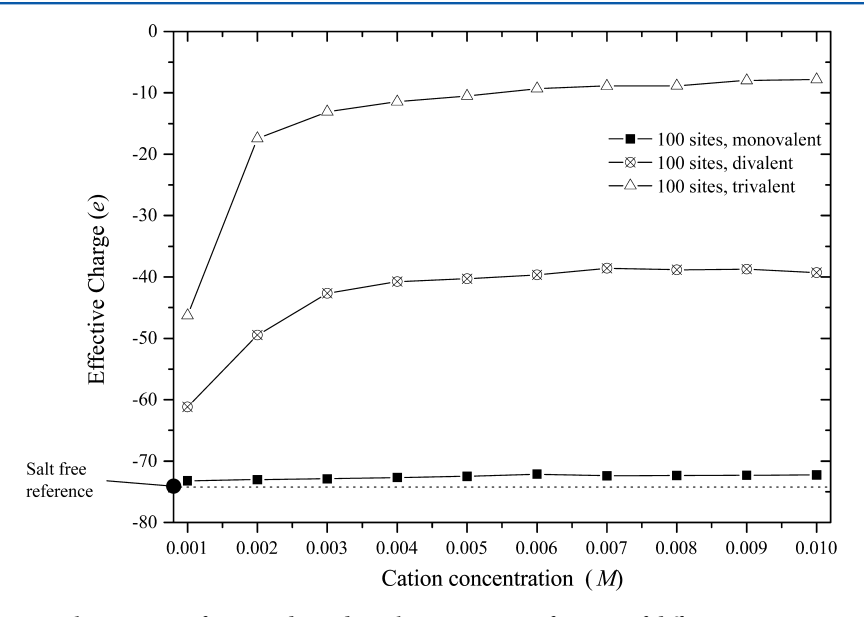


Figure 5. NP effective charge in the presence of mono-, di-, and trivalent cations as a function of different cation concentrations. The nanoparticle (25 Å radius) has 100 sites heterogeneously distributed on the NP surface. The salt-free effective charge is indicated as reference. For monovalent cations, the case is comparable to the salt free reference. For di- and trivalent cases, $Z_{\rm eff}$ rapidly increases with the concentration until reaching plateau values of -45 and -9e, respectively, corresponding to a reduction of 55% and 91% of NP surface charge.

MC steps for each set of simulation. NP effective charge and fraction of reduced NP charge are systematically calculated to better understand the effects of ion condensation.

3.1.1. Influence of Surface Charge Density. As shown in Figure 2, in which the effective charge is represented as a function of surface site number for heterogeneous distribution, two different behaviors at low and high density are observed resulting in two different slopes. At low density, the electrostatic repulsions between the surface sites are lower due to larger distances between them. Consequently, the ion

condensation is weaker leading to less reduced effective charges. On the other hand, at high density, the NP effective charge is found more reduced due to the increased affinity of the counterions with the surface. By considering the two different slopes, a "critical site density" can be defined as a limit between the two regimes in the effective NP charge variation. The decrease of $Z_{\rm eff}$ with the increase of the NP surface charge densities, as shown in Figure 2, is also limited by steric effects between counterions and electrostatic interactions between them. As shown in Figure 3, at high charge density, the fraction

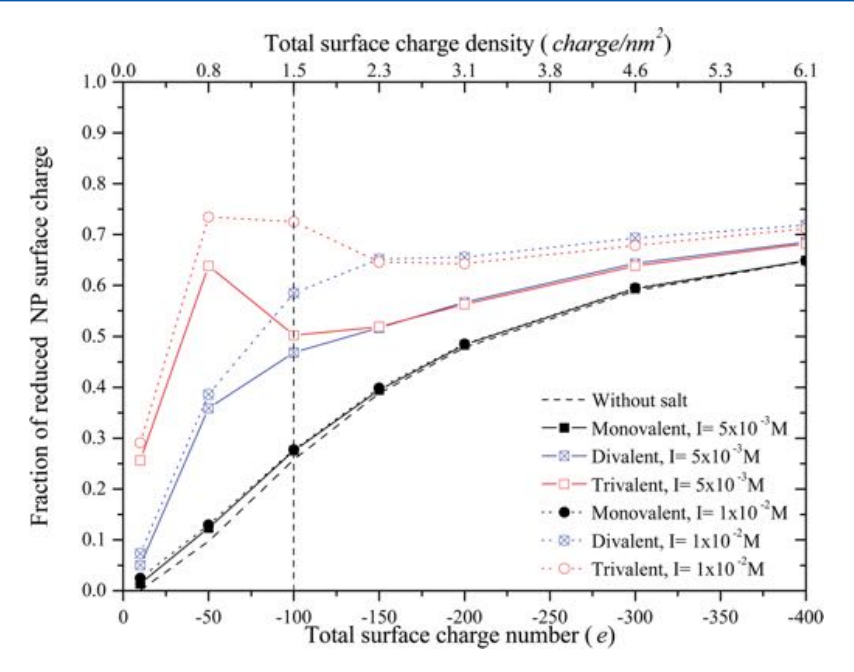


Figure 6. Fraction of reduced NP charge as a function of the total surface charge number and of surface charge density and at different ionic strengths. Mono-, di-, and trivalent cations are considered and compared to the case without salt. A significant difference is observed with the increase of the valency. At low density, the effective charge is strongly reduced by the presence of trivalent cations.

of counterions in the condensation layer reaches a limit of condensation corresponding to a counterion concentration fraction equal to 0.65 and thus a charge neutralization equal to 65%.

3.1.2. Influence of Site Distribution. As represented in Figure 4, when different site distributions are considered such as heterogeneous, homogeneous distributions, and central charge, no important differences in the NP effective charge variations are observed. This is an important output indicating that the surface site distribution has little effect on ion distribution. On the other hand, by considering a constant surface charge number N and by adjusting the NP size, the surface charge density is found to have a strong influence on the NP charging behavior. Indeed, the effective surface charge is found more reduced by decreasing the NP radius and consequently increasing the surface charge density.

3.2. NP Surface Charge Behavior in the Presence of Salt. A complementary study is presented now by taking into account the presence of salt particles in the simulation box to investigate the influence of salt properties (valency and concentration) on the condensation process. The same model is used, that is, a negatively charged NP with N sites on a heterogeneous surface with the presence of explicit counterions, cations, and anions in the solution.

3.2.1. Influence of Salt Concentration. A NP with 100 sites is considered with different salt concentrations (1×10^{-3} to 1×10^{-2} M) and valencies (mono-, di-, and trivalent) of cations. The number of anions is adjusted depending on the number of cations present in solution to keep the electroneutrality. For monovalent salt, cations can be assimilated as counterions with the same charge and are found to have no effect on the NP effective charge as shown in Figure 5 if comparison is made with the salt free reference. On the other hand, for divalent and trivalent salt, $Z_{\rm eff}$ decreases with the increase of the concentration and plateau values are rapidly obtained. Trivalent cations are more efficient to reduce the NP charge due to stronger interactions with the surface. The NP effective charge

is reduced by 91% in the trivalent case, while considering divalent salt only 55% of the NP charge is neutralized within the condensation layer. Similar behaviors are observed experimentaly via ζ -potential experiments. Indeed divalent and trivalent cations are found to have important effect on the overall charges of latex and titanium dioxide nanoparticles. 55,76

3.2.2. Influence of Cation Valency. To isolate the influence of cation valency, complementary studies are then carried out by considering a heterogeneous NP with a variable site number (10-400 sites) on the surface at two constant ionic strengths equal to 5×10^{-3} and 1×10^{-2} M hence allowing the same charge concentration (the set of parameters are defined in the Table. 1). For example, at 5×10^{-3} M 81, 27, or 14 cations are present in the simulation box for mono-, di-, or trivalent salts, respectively. For the monovalent case, similar behavior is observed for the fraction of reduced NP charge (Figure 6) compared to the case with counterions only (Figure 3). A continuous increase of the fraction of reduced charge is observed by increasing the surface site density. On the contrary, the presence of divalent or trivalent cations significantly modifies the effective charge of the nanoparticle. Two different regimes are observed at low and high density. At low density and in the trivalent case, the NP charge is strongly reduced compared to divalent cations. This difference is explained by stronger interactions of trivalent cations with sites on the surface. On the other hand, at high surface charge number the difference between di- and trivalent cations rapidly decreases with the increase of the surface charge density to finally disappear. In all cases, the fraction of reduced surface charge reaches a similar value at high surface charge density. This behavior can be explained by the restriction of the number of positive charges in the condensation layer and salt concentration value. Indeed, at constant ionic strength the number of cations in the solution decreases with the increase of valency and, as shown in Figure SI1, counterions are progressively replaced by di- and trivalent cations around the nanoparticle.

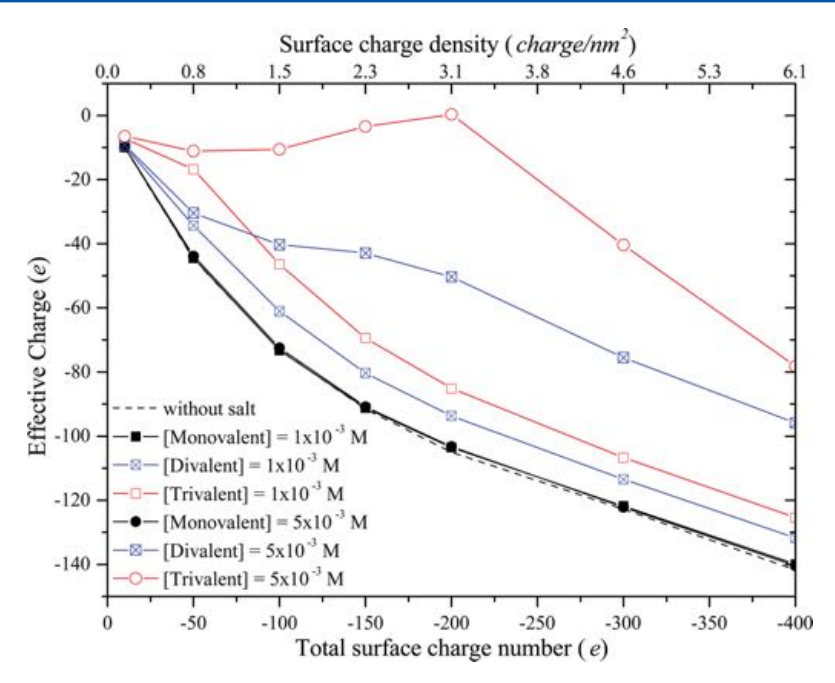


Figure 7. NP effective charge as a function of total surface charge number and surface charge density at two different cation salt concentrations (1×10^{-3} and 5×10^{-3} M). With the increase of salt concentration and valency, the influence of cations on the condensation process becomes more important. At high trivalent cation concentration, neutralization of the NP charge is observed (200 sites).

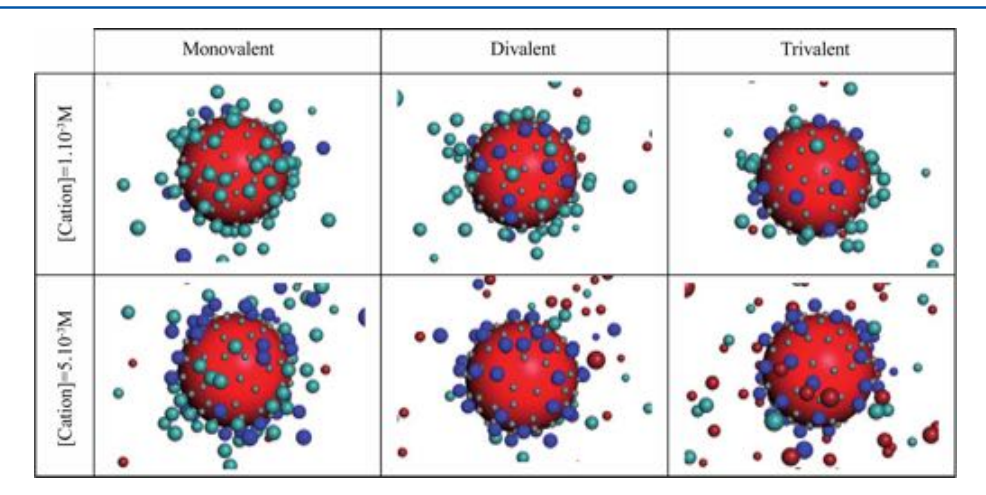


Figure 8. Evolution of the NP solution interface in the presence of salt for different valencies and cation concentrations (simulation snapshots). The NP is in red, surface sites in gray, counterions in cyan, cations in dark blue, and anions in dark red.

Complementary simulations are then performed at variable salt concentrations and thus at different ionic strengths for different salts. The effective charge of a NP with heterogeneous surface is carried out for two different salt concentrations, 1 × 10^{-3} and 5×10^{-3} M, considering mono-, di-, and trivalent salt particles. Effective charge variations for each valency and concentration are presented in Figure 7 and compared to the case without salt. At low salt concentration, the effective charge is slightly reduced with the increase of the valency while keeping the shape of the "ideal" curve without salt. For low trivalent cation concentration, the shape of the effective charge curve is significantly modified due to the importance of the electrostatic interactions and condensation of cations on the negatively charged NP. By increasing the concentration to 5 × 10⁻³ M for di- and trivalent cations, the effective charge is significantly modified by the presence of salt indicating that cation number and valency have both strong impacts on the nanoparticle surface charge. The effective charge is strongly reduced and close to zero when trivalent cations are considered and up to a surface site number charge density equal to 200 sites corresponding to the possible charge salt compensation. Indeed, after such a surface charge compensation, the effective charge continuously decreases. This nonmonotonic behavior is due to the electrostatic balance between (i) surface repulsions between NP sites that depends on the surface charge density, (ii) strong attractions between sites and trivalent cations, and (iii) strong repulsions between cations that are present around the nanoparticle (most important contribution) and to the total number of cations present in the simulation box, which can be a limit for the neutralization of the NP surface charge. In this case, the steric effect does not have a significant influence in the condensation process. It should be noted that counterions are progressively replaced by cations around the NP with the increase of salt valency. This is confirmed by the radial

distribution function given in Figure SI2. Also by observing the g(r) function, it is found that the correlation between the NP and cations becomes more important for di- and trivalent salt particles. At high salt concentration, the impact of counterions on the NP surface properties is almost negligible; the main contribution in condensation process is being provided by salt cations. Snapshots of the simulation box (Figure 8) in which the presence of cations (dark blue spheres) becomes more and more important around the NP support our conclusions.

Interestingly enough, an electrostatic positive layer is induced by cations and an anion layer is emerging around the NP for high trivalent cation concentrations. This layer structure is also put in evidence by the radial distribution function of anions around the NP and around cations given in Figure SI3. Indeed, a peak around 6 Å from the surface is observed for NP—anion systems in Figure SI3a, corresponding to the sum of cations and anions radii. The number of anions increases with cation valency as shown in Figure SI3b and as observed in the snapshots of Figure 8 (dark red spheres).

4. CONCLUSIONS

In this study, the effect of surface properties (site distribution and charge density) and solution properties (salt concentration and valency) on ion distribution around spherical nanoparticles has been investigated using Metropolis Monte Carlo simulations. We clearly observe that a nanoparticle can have a strong influence on an aqueous solution and reciprocally, this aqueous solution may have a real impact on the nanoparticle properties. In particular, the surface charge density plays a key role in the ion distribution and the condensation state around NP increases with the total surface charge number until being limited by steric effect and by electrostatic repulsions. It is important to note that this condensation process is not dependent here of the site distribution. Salt valency and concentration are also found to strongly influence the ion distribution around nanoparticles. The presence of divalent and trivalent cations strongly modifies the NP properties by decreasing the NP effective charge and improving the condensation state around the nanoparticle. At high trivalent cation concentration, $Z_{\rm eff}$ can be close to zero depending on the balance between electrostatic repulsions (site-site and cationcation), electrostatic attractions (site-cation) and number of cationic charges present in solution. Finally, our model can be adjusted for different situations because the size, site density, and distribution of nanoparticles, as well as salt valency or concentration, are input parameters. Moreover, other geometries, 61,62 such as rodlike or planar system, patch distributions,⁵² and Janus nanosphere,⁵¹ could be studied. In addition, it could be extended to titration studies of NPs in the presence of explicit ions as a function of pH, to biological molecules adsorption and coating by considering proteins, polymers, or polyelectrolytes, and to NPs aggregation by increasing the number of NPs in our simulation box.

ASSOCIATED CONTENT

S Supporting Information

The Supporting Information is available free of charge on the ACS Publications website at DOI: 10.1021/acs.jpcb.6b05104.

Radial distribution functions at different ionic strengths, cation concentrations or valencies: NP-all particles, NP-counterions, NP-cations, NP-anions, cations-anions (PDF)

AUTHOR INFORMATION

Corresponding Author

*E-mail: Serge.stoll@unige.ch. Phone + 41 22 379 0333. Fax: + 41 22 379 0329.

Notes

The authors declare no competing financial interest.

ACKNOWLEDGMENTS

This work was partially supported by the European Commission and the Swiss Secrétariat d'Etat à la Formation, à la Recherche et à l'Innovation SEFRI within the Horizon 2020 Program (NanoFASE 15.0183-2, 646002).

REFERENCES

- (1) Carl Englert, B. Nanomaterials and the Environment: Uses, Methods and Measurement. J. Environ. Monit. 2007, 9 (11), 1154.
- (2) Klaine, S. J.; Alvarez, P. J. J.; Batley, G. E.; Fernandes, T. F.; Handy, R. D.; Lyon, D. Y.; Mahendra, S.; McLaughlin, M. J.; Lead, J. R. Nanomaterials in the Environment: Behavior, Fate, Bioavailability, and Effects. *Environ. Toxicol. Chem.* **2008**, 27 (9), 1825–1851.
- (3) Praetorius, A.; Arvidsson, R.; Molander, S.; Scheringer, M. Facing Complexity through Informed Simplifications: A Research Agenda for Aquatic Exposure Assessment of Nanoparticles. *Environ. Sci. Process. Impacts* **2013**, *15* (1), 161–168.
- (4) Nowack, B.; Bucheli, T. D. Occurrence, Behavior and Effects of Nanoparticles in the Environment. *Environ. Pollut.* **2007**, *150* (1), 5–22.
- (5) Dale, A. L.; Casman, E. A.; Lowry, G. V.; Lead, J. R.; Viparelli, E.; Baalousha, M. Modeling Nanomaterial Environmental Fate in Aquatic Systems. *Environ. Sci. Technol.* **2015**, 49 (5), 2587–2593.
- (6) Rao, C. N. R.; Müller, A.; Cheetham, A. K. The Chemistry of Nanomaterials: Synthesis, Properties, and Applications; John Wiley & Sons: New York, 2006.
- (7) Cao, G.; Wang, Y. Nanostructures and Nanomaterials: Synthesis, Properties, and Applications; World Scientific: New York, 2011.
- (8) Ju-Nam, Y.; Lead, J. R. Manufactured Nanoparticles: An Overview of Their Chemistry, Interactions and Potential Environmental Implications. *Sci. Total Environ.* **2008**, 400 (1–3), 396–414.
- (9) Lövestam, G.; Rauscher, H.; Roevven, G.; Sokull Klüttgen, B.; Gibson, N.; Putaud, J.-P.; Stamm, H. Considerations on a Definition of Nanomaterial for Regulatory Purposes; Luxembourg: Publications Office of the European Union: 2010.
- (10) Auffan, M.; Rose, J.; Bottero, J.-Y.; Lowry, G. V.; Jolivet, J.-P.; Wiesner, M. R. Towards a Definition of Inorganic Nanoparticles from an Environmental, Health and Safety Perspective. *Nat. Nanotechnol.* **2009**, *4* (10), 634–641.
- (11) Nowack, B.; Ranville, J. F.; Diamond, S.; Gallego-Urrea, J. A.; Metcalfe, C.; Rose, J.; Horne, N.; Koelmans, A. A.; Klaine, S. J. Potential Scenarios for Nanomaterial Release and Subsequent Alteration in the Environment. *Environ. Toxicol. Chem.* **2012**, *31* (1), 50–59.
- (12) Colvin, V. L. The Potential Environmental Impact of Engineered Nanomaterials. *Nat. Biotechnol.* **2003**, 21 (10), 1166–1170.
- (13) Moore, M. N. Do Nanoparticles Present Ecotoxicological Risks for the Health of the Aquatic Environment? *Environ. Int.* **2006**, 32 (8), 967–976.
- (14) Li, M.; Pokhrel, S.; Jin, X.; Mädler, L.; Damoiseaux, R.; Hoek, E. M. V. Stability, Bioavailability, and Bacterial Toxicity of ZnO and Iron-Doped ZnO Nanoparticles in Aquatic Media. *Environ. Sci. Technol.* **2011**, 45 (2), 755–761.
- (15) Lead, J. R.; Smith, E. Environmental and Human Health Impacts of Nanotechnology; John Wiley & Sons: New York, 2009.
- (16) Weir, A.; Westerhoff, P.; Fabricius, L.; Hristovski, K.; von Goetz, N. Titanium Dioxide Nanoparticles in Food and Personal Care Products. *Environ. Sci. Technol.* **2012**, *46* (4), 2242–2250.

- (17) Petosa, A. R.; Jaisi, D. P.; Quevedo, I. R.; Elimelech, M.; Tufenkji, N. Aggregation and Deposition of Engineered Nanomaterials in Aquatic Environments: Role of Physicochemical Interactions. *Environ. Sci. Technol.* **2010**, 44 (17), 6532–6549.
- (18) Von Moos, N.; Bowen, P.; Slaveykova, V. I. Bioavailability of Inorganic Nanoparticles to Planktonic Bacteria and Aquatic Microalgae in Freshwater. *Environ. Sci.: Nano* **2014**, *1* (3), 214.
- (19) Besteman, K.; Zevenbergen, M. A. G.; Lemay, S. G. Charge Inversion by Multivalent Ions: Dependence on Dielectric Constant and Surface-Charge Density. *Phys. Rev. E* **2005**, 72 (6), 061501.
- (20) Nguyen, T. T.; Grosberg, A. Y.; Shklovskii, B. I. Macroions in Salty Water with Multivalent Ions: Giant Inversion of Charge. *Phys. Rev. Lett.* **2000**, 85 (7), 1568–1571.
- (21) Mukherjee, B.; Weaver, J. W. Aggregation and Charge Behavior of Metallic and Nonmetallic Nanoparticles in the Presence of Competing Similarly-Charged Inorganic Ions. *Environ. Sci. Technol.* **2010**, 44 (9), 3332–3338.
- (22) Badawy, A. M. E.; Luxton, T. P.; Silva, R. G.; Scheckel, K. G.; Suidan, M. T.; Tolaymat, T. M. Impact of Environmental Conditions (pH, Ionic Strength, and Electrolyte Type) on the Surface Charge and Aggregation of Silver Nanoparticles Suspensions. *Environ. Sci. Technol.* **2010**, 44 (4), 1260–1266.
- (23) Pigga, J. M.; Kistler, M. L.; Shew, C.-Y.; Antonio, M. R.; Liu, T. Counterion Distribution around Hydrophilic Molecular Macroanions: The Source of the Attractive Force in Self-Assembly13. *Angew. Chem., Int. Ed.* **2009**, 48 (35), 6538–6542.
- (24) Shklovskii, B. I. Screening of a Macroion by Multivalent Ions: Correlation-Induced Inversion of Charge. *Phys. Rev. E: Stat. Phys., Plasmas, Fluids, Relat. Interdiscip. Top.* **1999**, *60* (5), 5802–5811.
- (25) Albanese, A.; Tang, P. S.; Chan, W. C. W. The Effect of Nanoparticle Size, Shape, and Surface Chemistry on Biological Systems. *Annu. Rev. Biomed. Eng.* **2012**, *14* (1), 1–16.
- (26) Jiang, J.; Oberdörster, G.; Biswas, P. Characterization of Size, Surface Charge, and Agglomeration State of Nanoparticle Dispersions for Toxicological Studies. *J. Nanopart. Res.* **2009**, *11* (1), 77–89.
- (27) Lowry, G. V.; Gregory, K. B.; Apte, S. C.; Lead, J. R. Transformations of Nanomaterials in the Environment. *Environ. Sci. Technol.* **2012**, 46 (13), 6893–6899.
- (28) Ginn, T. R.; Wood, B. D.; Nelson, K. E.; Scheibe, T. D.; Murphy, E. M.; Clement, T. P. Processes in Microbial Transport in the Natural Subsurface. *Adv. Water Resour.* **2002**, *25* (8–12), 1017–1042.
- (29) Mateescu, E. M.; Jeppesen, C.; Pincus, P. Overcharging of a Spherical Macroion by an Oppositely Charged Polyelectrolyte. *Europhys. Lett. EPL* **1999**, *46* (4), 493–498.
- (30) Da Silva, F. L. B.; Jönsson, B. Polyelectrolyte-protein Complexation Driven by Charge Regulation. *Soft Matter* **2009**, *S* (15) 2862
- (31) Szekeres, M.; Tombácz, E. Surface Charge Characterization of Metal Oxides by Potentiometric Acid-base Titration, Revisited Theory and Experiment. *Colloids Surf., A* **2012**, *414*, 302–313.
- (32) Davis, J. A.; James, R. O.; Leckie, J. O. Surface Ionization and Complexation at the Oxide/water Interface: I. Computation of Electrical Double Layer Properties in Simple Electrolytes. *J. Colloid Interface Sci.* 1978, 63 (3), 480–499.
- (33) Petosa, A. R.; Jaisi, D. P.; Quevedo, I. R.; Elimelech, M.; Tufenkji, N. Aggregation and Deposition of Engineered Nanomaterials in Aquatic Environments: Role of Physicochemical Interactions. *Environ. Sci. Technol.* **2010**, 44 (17), 6532–6549.
- (34) Fabrega, J.; Luoma, S. N.; Tyler, C. R.; Galloway, T. S.; Lead, J. R. Silver Nanoparticles: Behaviour and Effects in the Aquatic Environment. *Environ. Int.* **2011**, *37* (2), 517–531.
- (35) Keller, A. A.; Wang, H.; Zhou, D.; Lenihan, H. S.; Cherr, G.; Cardinale, B. J.; Miller, R.; Ji, Z. Stability and Aggregation of Metal Oxide Nanoparticles in Natural Aqueous Matrices. *Environ. Sci. Technol.* **2010**, 44 (6), 1962–1967.
- (36) Nur, Y.; Lead, J. R.; Baalousha, M. Evaluation of Charge and Agglomeration Behavior of TiO2 Nanoparticles in Ecotoxicological Media. *Sci. Total Environ.* **2015**, *535*, 45–53.

- (37) Godymchuk, A.; Karepina, E.; Yunda, E.; Bozhko, I.; Lyamina, G.; Kuznetsov, D.; Gusev, A.; Kosova, N. Aggregation of Manufactured Nanoparticles in Aqueous Solutions of Mono- and Bivalent Electrolytes. *J. Nanopart. Res.* **2015**, *17* (5), 1–8.
- (38) Burak, Y.; Ariel, G.; Andelman, D. Competition between Condensation of Monovalent and Multivalent Ions in DNA Aggregation. *Curr. Opin. Colloid Interface Sci.* **2004**, 9 (1–2), 53–58.
- (39) De Vries, R.; Cohen Stuart, M. Theory and Simulations of Macroion Complexation. *Curr. Opin. Colloid Interface Sci.* **2006**, *11* (5), 295–301.
- (40) Groot, R. D. Ion Condensation on Solid Particles: Theory and Simulations. *J. Chem. Phys.* **1991**, 95 (12), 9191–9203.
- (41) Attard, P. Ion Condensation in the Electric Double Layer and the Corresponding Poisson-Boltzmann Effective Surface Charge. *J. Phys. Chem.* **1995**, 99 (38), 14174–14181.
- (42) O'Shaughnessy, B.; Yang, Q. Manning-Oosawa Counterion Condensation. *Phys. Rev. Lett.* **2005**, *94* (4), 048302.
- (43) Markus, A. A.; Parsons, J. R.; Roex, E. W. M.; de Voogt, P.; Laane, R. W. P. M. Modeling Aggregation and Sedimentation of Nanoparticles in the Aquatic Environment. *Sci. Total Environ.* **2015**, 506–507, 323–329.
- (44) Ravindran, S.; Wu, J. Overcharging of Nanoparticles in Electrolyte Solutions. *Langmuir* **2004**, 20 (17), 7333–7338.
- (45) Grønbech-Jensen, N.; Beardmore, K. M.; Pincus, P. Interactions between Charged Spheres in Divalent Counterion Solution. *Phys. A* **1998**, 261 (1–2), 74–81.
- (46) Ulrich, S.; Seijo, M.; Laguecir, A.; Stoll, S. Nanoparticle Adsorption on a Weak Polyelectrolyte. Stiffness, pH, Charge Mobility, and Ionic Concentration Effects Investigated by Monte Carlo Simulations. *J. Phys. Chem. B* **2006**, *110* (42), 20954–20964.
- (47) Carnal, F.; Stoll, S. Adsorption of Weak Polyelectrolytes on Charged Nanoparticles. Impact of Salt Valency, pH, and Nanoparticle Charge Density. Monte Carlo Simulations. *J. Phys. Chem. B* **2011**, *115* (42), 12007–12018.
- (48) Kuldová, J.; Uhlík, F.; Košovan, P. The Drag of the Tails: Diffusion of Sticky Nanoparticles in Dilute Polymer Solutions. *J. Chem. Phys.* **2015**, *143* (24), 243129.
- (49) Das, A. K.; Hsiao, P.-Y. Charged Dendrimers in Trivalent Salt Solutions under the Action of DC Electric Fields. *J. Phys. Chem. B* **2014**, *118* (23), 6265–6276.
- (50) Belloni, L. Colloid-Counterion Mixtures: An Advanced Integral Equation. *J. Phys.: Condens. Matter* **2002**, *14* (40), 9323–9337.
- (51) De Carvalho, S. J.; Metzler, R.; Cherstvy, A. G. Critical Adsorption of Polyelectrolytes onto Charged Janus Nanospheres. *Phys. Chem. Chem. Phys.* **2014**, *16* (29), 15539.
- (52) Seijo, M.; Ulrich, S.; Filella, M.; Buffle, J.; Stoll, S. Effects of Surface Site Distribution and Dielectric Discontinuity on the Charging Behavior of Nanoparticles. A Grand Canonical Monte Carlo Study. *Phys. Chem. Chem. Phys.* **2006**, 8 (48), 5679.
- (53) Fixman, M. The Poisson-Boltzmann Equation and Its Application to Polyelectrolytes. *J. Chem. Phys.* **1979**, 70 (11), 4995–5005.
- (54) Newell, G. F.; Montroll, E. W. On the Theory of the Ising Model of Ferromagnetism. *Rev. Mod. Phys.* **1953**, 25 (2), 353–389.
- (55) Loosli, F.; Le Coustumer, P.; Stoll, S. Effect of Electrolyte Valency, Alginate Concentration and pH on Engineered TiO2 Nanoparticle Stability in Aqueous Solution. *Sci. Total Environ.* **2015**, 535, 28–34.
- (56) Chen, K. L.; Elimelech, M. Aggregation and Deposition Kinetics of Fullerene (C60) Nanoparticles. *Langmuir* **2006**, 22 (26), 10994–11001
- (57) Carnal, F.; Clavier, A.; Stoll, S. Modelling the Interaction Processes between Nanoparticles and Biomacromolecules of Variable Hydrophobicity: Monte Carlo Simulations. *Environ. Sci.: Nano* **2015**, 2 (4), 327–339.
- (58) De Carvalho, S. J.; Caetano, D. L. Z. Adsorption of Polyelectrolytes onto Oppositely Charged Cylindrical Macroions. *J. Chem. Phys.* **2013**, *138* (24), 244909.

- (59) Berret, J.-F.; Yokota, K.; Morvan, M.; Schweins, R. Polymer—Nanoparticle Complexes: From Dilute Solution to Solid State. *J. Phys. Chem. B* **2006**, *110* (39), 19140–19146.
- (60) Lamm, G.; Pack, G. R. Counterion Condensation and Shape within Poisson–Boltzmann Theory. *Biopolymers* **2010**, 93 (7), 619–639.
- (61) Manning, G. S. Counterion Condensation on Charged Spheres, Cylinders, and Planes. J. Phys. Chem. B 2007, 111 (29), 8554–8559.
- (62) Manning, G. S. Counterion Condensation on a Helical Charge Lattice. *Macromolecules* **2001**, *34* (13), 4650–4655.
- (63) Manning, G. S. Electrostatic Free Energy of the DNA Double Helix in Counterion Condensation Theory. *Biophys. Chem.* **2002**, 101–102, 461–473.
- (64) Burak, Y.; Ariel, G.; Andelman, D. Competition between Condensation of Monovalent and Multivalent Ions in DNA Aggregation. *Curr. Opin. Colloid Interface Sci.* **2004**, 9 (1–2), 53–58.
- (65) Fanyao, Q.; Morais, P. C. Nanoparticle Surface Charge Density in Ionic Magnetic Fluids: The Effect of Particle—particle Interaction. *J. Appl. Phys.* **2003**, *93* (10), 7385–7387.
- (66) Qu, F.; Morais, P. C. An Oxide Semiconductor Nanoparticle in an Aqueous Medium: A Surface Charge Density Investigation. *J. Phys. Chem. B* **2000**, 104 (22), 5232–5236.
- (67) Denton, A. R. Coarse-Grained Modeling of Charged Colloidal Suspensions: From Poisson-Boltzmann Theory to Effective Interactions. 2012, ArXiv12121758 Cond-Mat.
- (68) Frenkel, D.; Smit, B. Understanding Molecular Simulation: From Algorithms to Applications; Academic Press: New York, 2001.
- (69) Landau, D. P.; Binder, K. A Guide to Monte Carlo Simulations in Statistical Physics, 3rd ed.; Cambridge University Press: Cambridge, 2009
- (70) Metropolis, N.; Rosenbluth, A. W.; Rosenbluth, M. N.; Teller, A. H.; Teller, E. Equation-of-State Calculations by Fast Computing Machines. *J. Chem. Phys.* **1953**, *21*, 1087–1092.
- (71) Rankin, D. W. H. CRC Handbook of Chemistry and Physics, 89 ed.; Lide, D. R., Ed.; Crystallogr. Rev. **2009**, 15 (3), 223–224.10.1080/08893110902764125
- (72) Nagashima, K.; Blum, F. D. Proton Adsorption onto Alumina: Extension of Multisite Complexation (MUSIC) Theory. *J. Colloid Interface Sci.* **1999**, 217 (1), 28–36.
- (73) Ross, S.; Olivier, J. P. On physical absorption; http://cds.cern.ch/record/109362 (accessed May 21, 2014).
- (74) Powers, K. W.; Brown, S. C.; Krishna, V. B.; Wasdo, S. C.; Moudgil, B. M.; Roberts, S. M. Research Strategies for Safety Evaluation of Nanomaterials. Part VI. Characterization of Nanoscale Particles for Toxicological Evaluation. *Toxicol. Sci.* **2005**, *90* (2), 296–303
- (75) Giammar, D. E.; Maus, C. J.; Xie, L. Effects of Particle Size and Crystalline Phase on Lead Adsorption to Titanium Dioxide Nanoparticles. *Environ. Eng. Sci.* **2007**, 24 (1), 85–95.
- (76) Oriekhova, O.; Stoll, S. Investigation of FeCl3 Induced Coagulation Processes Using Electrophoretic Measurement, Nanoparticle Tracking Analysis and Dynamic Light Scattering: Importance of pH and Colloid Surface Charge. *Colloids Surf., A* **2014**, *461*, 212–219.

CHAPTER 5

Determination of Nanoparticle Attachment
Efficiencies and Heteroaggregation Rates in
Presence of Natural Organic Matter for
Contrasting Conditions using Monte Carlo
Modelling

Chapter 5: Heteroaggregation of Nanoparticles in Presence of NOM

1 In the previous chapters, the impact of NP properties (acid-base, dielectric constant, surface charge density and distribution) as well as solution properties (presence of mono, di and trivalent ions, pH) on NP surface charging behavior (Chapter 3) and ion distribution (Chapter 4) have been investigated. This is an important issue to get an insight into the role of NP properties on the interaction forces between NPs and between NPs and aquagenic compounds. Indeed, once released in aquatic systems, NPs will interact with natural compounds such as suspended particles or organic matter and heteroaggregation will control their ultimate fate. Unfortunately, systematic experimental methods to study heteroaggregation are not straightforward and still scarce. In addition, the description of heteroaggregation rate constants and heteroaggregation attachment efficiencies is still a matter of debate since no clear definition exists. In this chapter, an original cluster-cluster Monte Carlo model is developed to get an insight into heteroaggregation process description. A two component system composed of NPs and NOM fulvic acid monomers is investigated by considering several water models to cover contrasting conditions from fresh to marine waters. For that purpose, homo- and hetero- elementary attachment efficiencies between NPs and NOM units are adjusted (NP-NP, NOM-NOM and NP-NOM). The influence of NP/NOM ratio, NOM-NOM homoaggregation versus heteroaggregation, and surface coating effects is systematically studied. From a quantitative point of view, aggregation rate constants as well as attachment efficiencies are calculated as a function of physical time so as to characterize the individual influence of each parameter and to allow future comparison with experimental data. Heteroaggregation processes and global attachment efficiencies corresponding to several mechanisms and depending on the evolution of heteroaggregates structures all along the simulation are defined.

5.1 Introduction

With the progress of nanomaterials and nanotechnologies [1–4], the production of manufactured nanoparticles (NPs) and consequently their potential impacts in our daily life are continuously increasing [5–9]. The main interest for nanotechnologies comes from the very large specific surface area and surface properties of NPs, which provide them high chemical reactivity at the nanoscale level. Due to these very specific properties, NPs are used in many different domains such as cosmetic, (nano)medicine, energy, textiles, and (nano)pesticides [10–13]. Unfortunately, many open questions remain with respect to NP release, fate and effects on ecosystems and human health [5, 14–19].

In the environment, determining the fate, transport and NP transformation processes remains challenging and strongly dependent on a wide range of intrinsic and extrinsic parameters [18, 20–23]. In the aquatic environments, the chemical reactivity and transport properties of NPs are expected to be strongly controlled by water properties such as pH, water hardness, ionic composition, temperatur [24–29], presence of living organisms [14, 25, 30–32] and also suspended particle matter (SPM) [33–38]. Subtle changes in water chemistry can profoundly modify NP surface properties, interactions with the surrounding compounds as well as key processes such as NP aggregation and dissolution [25, 39, 40]. In particular, the presence of natural organic matter (NOM) at a concentration of few mg/L is expected to have an important impact on the NP surface properties (coating, surface charge modification) and heteroaggregation behavior [37, 38, 41].

Heteroaggregation, which describes the aggregation of dissimilar particles, is a key process having significant consequences on the NP fate, transport, bioavailability, uptake and ecotoxicity in environmental systems such as water, soil and atmosphere [19, 42, 43]. Consequently, quantitative information on heteroaggregation such as aggregation rate constants and attachment efficiencies is urgently needed to parameterize NP environmental transport and fate models [23, 44–47]. Attachment efficiencies (α) represent a key parameter in these processes and illustrate the probability of an efficient collision between identical or different compounds. α values are controlled by the balance between attractive and repulsive forces occurring between compounds and characterize the presence of a potential barrier. In absence of repulsive forces and barrier, all the collisions are efficient and α is equal to unity. Attachment efficiencies can be calculated by estimating the repulsive potential barrier between particles. In simple cases,

Chapter 5: Heteroaggregation of Nanoparticles in Presence of NOM

electrostatic and van der Waals interactions are usually described using the DLVO theory, then the Fuchs stability ratio [66] is determined and related to the attachment efficiency.

Aggregation processes have been largely described and studied using experimental methods [33, 37, 48–50] and numerical/theoretical models [26, 51–54] in various domains such as aerosol formation, flocculation processes for water treatment, blood coagulation and volcanic dust eruption. Most of these studies start from the description made by Marian von Smoluchowski, who developed a mathematical kernel of equations to characterize second-order rate processes of spherical particles under Brownian motion and/or in specific force fields (laminar shear, gravity, ...) [55–58]. In addition to this analytical approach, several aggregation models were also numerically developed in 2D and 3D, such as the Witten and Sander Diffusion Limited Aggregation [59,60] and the Cluster-Cluster Aggregation models [54,61,62]. Furthermore, fractal dimension concepts were introduced to provide a mathematical description of the aggregate structures and to characterize different aggregation regimes [63–65].

From an experimental point of view, various methods were developed to determine aggregation rate constants and extract attachment efficiencies [67] and aggregate fractal dimensions [68,69]. Aggregation rates and attachment efficiency values are generally determined by following the evolution of the particle size as a function of time *via* Dynamic Light Scattering (DLS) [70–72], laser diffraction (LD) [37,73] or Nanoparticle Tracking Analysis (NTA) [72], or by following the differential settling of homo/heteroaggregates in sediments *via* batch methods [48,67]. Quantification of heteroaggregation between citrate stabilized gold nanoparticles and hematite colloids was investigated using a novel approach involving time-resolved dynamic light scattering and parallel experiments designed to quantify nanoparticle attachment and heteroaggregate surface charge [80]. This study, in particular, underlined the importance of surface coverage in heteroaggregation. However, most of the methods and models were developed and parametrized to investigate aggregation of one type of particles (homoaggregation), especially in the experimental approaches.

When increasing the system heterogeneity, e.g. by considering two types of particles (NPs and NOM), the system becomes rapidly more complicated to describe, with an increase of the number of possible scenarios (**Figure 5.1**). From numerical and experimental points of views, a more extended description of particle interactions (NPs-NOM; NPs-NPs; NOM-NOM), water and system properties is required to get an insight into different heteroaggregation processes.

On the other hand, the type and quality of information obtained from experiments is dependent on the method used. Some techniques will be better designed for the description of fast aggregation rates (LD) while others will be more adapted to slow regimes (DLS, settling batch methods). In most cases, the most reliable information is obtained for early stages of aggregation, whereas a quantitative description of later stages of aggregation is generally limited. In addition, concentration effects and mixing procedures are also expected to play important roles on the heteroaggregation mechanisms, rates and heteroaggregate morphologies. Furthermore, the competition between homo- and heteroaggregation remains complex to distinguish in experiments.

In light of these experimental challenges, computer simulations represent a powerful approach to investigate in detail heteroaggregation processes between NPs and NOM and get an insight into the impact of specific parameters such as the concentration ratio between NOM and NPs or processes such as NOM coating (and evolution with time) and impact on heteroaggregation. In this study, a cluster-cluster aggregation model is developed in order to investigate heteroaggregation mechanisms of a NP and NOM mixture and by adjusting individual attachment efficiencies. Different relevant environmental scenarios such as: (i) heteroaggregation in marine waters (high ionic strength promoting homoaggregation) (ii) fresh waters (low ionic strength promoting heteroaggregation over homoaggregation) and (iii) ultrapure waters (resulting in heteroaggregation only) are considered via the adjustment of the individual attachment efficiencies. In this study, we are assuming a strong interaction between NPs and NOM in a situation representative of a system composed of positively charged NPs in presence of negatively charged NOM units. The low expected concentrations of NPs in natural systems compared to the high NOM concentrations is taken into account by adjusting the relative concentrations between both types of particles. Monte Carlo modelling provides the opportunity to get an insight into heteroaggregation mechanisms and to follow the evolution of the attachment efficiency parameter from primary heteroaggregation to global attachment values. Moreover, computer simulations allow to cover a wide range of different parameters and environmental scenarios.

In the first part of this paper, theoretical concepts and the heteroaggregation model are presented. Then, the model is validated based on homoaggregation simulations. Surface and solution properties (attachment efficiencies, NOM/NP concentrations) are then adjusted to investigate some specific environmental processes such as surface coating and saturation, and heteroaggregation in presence of NOM homoaggregation. Finally, kinetic aggregation rates are

Chapter 5: Heteroaggregation of Nanoparticles in Presence of NOM

calculated for different water models as well as the corresponding heteroaggregation attachment efficiencies.

5.2 Model theory and description

5.2.1 Aggregation theory

The individual aggregation rate between two particles of sizes i and j is usually defined by:

$$k_{ij}^{agg} = \alpha_{ij} k_{ij}^{coll} \tag{5.1}$$

where, on the one hand, k_{ij}^{col} represents the collision rate constant, which is generally dependent on particle sizes and densities as well as corresponding transport model (Brownian motion, orthokinetic or differential sedimentation [56]. On the other hand, the sticking probability or attachment efficiency α_{ij} is dependent on the sum of the interaction forces between the two particles. This attachment efficiency is comprised between zero and unity. Zero corresponds to a stable suspension without aggregation (predominance of repulsive forces) while $\alpha_{ij} = 1$ corresponds to a system where each contact between particles is efficient regarding the formation of irreversible bonds.

In the Smoluchowski theory [56], a kernel of equations is used to describe each possible reaction between particles. Then the formation rate of aggregates of size k is defined by:

$$\frac{dn_k}{d} = \frac{1}{2} \sum_{i=k-j=1}^{k-1} \alpha_{ij} k_{ij}^{coll} n_i n_j - n_k \sum_{i=1}^{\infty} \alpha_{ik} k_{ik}^{coll} n_i$$
 (5.2)

Where $n_{i,j,k}$ is the number concentration of particles of sizes i,j,k at time t. The first part of the equation represents the formation rate of aggregates k resulting from the collision of particles of size i and j, respectively, while the second part describes the removal of these aggregates resulting from collisions with particles of size i.

For small identical particles (under 1μ m), the perikinetic case with Brownian motion is the most relevant and equation 5.2 can be rewritten for the very early stage of the aggregation process as:

$$\left(\frac{dn_k}{d}\right)_{t\to 0} = -\frac{k_{homo}^{particle}}{2}n_1^2$$
(5.3)

where $k_{homo}^{particle}$ represents the aggregation rate constant for primary particles, defined as particle removal rate constant, equal to $k_{homo}^{particle} = \frac{8k_bT}{3\mu}$, k_b the Boltzmann constant, T the temperature and μ the viscosity. For aqueous dispersion, at T = 293K and $\mu = 110^{-3}$ m² s⁻¹, and the rate constant is equal to 1.09 10^{-17} m³ s⁻¹. Another parameter, which is derived from this equation, is the aggregation rate constant k_{homo}^{agg} which describes the evolution of the object concentration (total number of particles and aggregates). This parameter, also referred to heteroaggregation rate constant, is directly related to the particle removal rate constant and is equal to $k_{homo}^{particle}/2$, i.e. 5.4710^{-18} m³ s⁻¹.

5.2.2 Aggregation model

Our model is based on a Monte Carlo (MC) cluster-cluster aggregation model (CCA). MC modelling is a common approach used to simulate the Brownian motion of small scale particles [74–76]. In this study, simulations are performed to reproduce this random displacement, to consider the interaction between particles via a set of attachment efficiencies and to get an insight into the primary stage of heteroaggregation. Simulations are carried out in a canonical ensemble of volume V and temperature T fixed. NPs and NOM are described by an off-lattice three-dimensional coarse-grained model. NPs and NOM are described by an off-lattice threedimensional coarse-grained model. The particles are modelled using spherical units (nanoparticles and NOM monomers). Therefore, particles refer to isolated primary NPs and NOM. With time, particles are forming aggregates with complex morphologies. The designation "objects" refers to aggregates and particles (i.e. aggregates, isolated NPs and NOM units). NOM is modelled as fulvic acids (FA) which are one of the major component of humic substances. FA are represented at the coarse grained level with a radius of 1 nm [41] whereas NP radius is arbitrarily set to 10 nm. Of course, the model allows adjustment of different sizes of nanoparticles, as far as particles are in the Brownian motion range. An infinitely diluted aqueous solution with a continuum representation of the solvent and a fixed temperature of 298K is considered. The modelling cell is cubic and the minimum image convention is used to keep the periodicity of the system. The size of the simulation box can vary and be adjusted, depending on the particle volume occupied. To create the initial system configuration, particles are inserted randomly inside the simulation cell and an excluded volume test is made to avoid any direct contact. For each simulation step, all particles are randomly moved one by one according to their sizes (equivalent volume), based on the assumption that smaller particle will move faster, and all the resulting contacts are tested after each displacement. If the center-to-center distance between two particles is lower than the sum of the respective particle radii, then a MC attachment test is performed by comparing a random number chosen between 0 and 1 to the attachment efficiency corresponding to the type of contact. Then, the movement is accepted or not according to the initial set of attachment values.

To consider realistic displacements all the particles (NPs and NOM) and aggregates are not moving at the same velocity. All the movements as well as the physical time are based on the displacement of the NPs. This displacement is arbitrarily fixed to 1 nm (10%) of the nanoparticle radius. The displacement of the rest of the objects is based on the cubic root of the volume ratio, $r_{dis} = \sqrt[3]{\frac{V_{FreeNP}}{V_{object}}}$. This formula allows taking into account the equivalent volume of each objects. When this ratio is higher than 1, the object is translated x times where x represents the integer of r_{dis} . Otherwise, in the case of $r_{dis} < 1$, the object is moved once by the factor $r_{dis} \times 1nm$.

Finally, at each MC step of the simulation, all the positions and status are recorded and stored so as to perform post data treatment and calculation of mean values and variables such as the number of particles and objects variation with time on which calculations of kinetic rate constants are based. For each system studied, ten replicates are considered to improve data interpretation from a statistical point of view.

5.2.3 Physical time versus Monte Carlo time

All our simulations are performed using a Monte Carlo procedure [77,78] which allows the formation of aggregates as a function of the MC time (MC steps). One of the most important parameter in our model analysis is the physical time t. To establish a link between the particle displacement and physical time, we have developed and validated a procedure which calculate the correspondence between MC steps and physical time. This model is based on the mean free path calculation due to Brownian motion and on the Einstein-Stokes equation for spherical particles. In three dimensions, the mean square displacement of a Brownian particle can be written as:

$$\langle r^2 \rangle = 6Dt \tag{5.4}$$

where D is the Stokes-Einstein diffusion coefficient defined as:

$$D = \frac{k_b T}{6\pi \mu R} \tag{5.5}$$

with R is the particle radius. By combining equations 5.4 and 5.5, a link is established between the particle size, displacement, temperature, solution viscosity, and physical time. In our heteroaggregation model, displacement is based on the isolated nanoparticle displacement and on the ratio of the equivalent volumes. To further validate our procedure, one thousand NPs, with a radius R equal to 10 nm, were introduced in an infinite simulation box and randomly moved by a radius of 1 nm during 10^6 MC steps. Each 10 MC steps, the average mean free path of all the nanoparticles was calculated as a function of t. After performing a set of different simulations, the correspondence between one MC step and the physical time was determined and found equal to 7.45 ns/MC step for a temperature and a viscosity respectively equal to 293K and 1.10^{-3} m² s⁻¹.

5.2.4 Attachment efficiency

Experimentally, the attachment efficiency [79] is generally defined as the ratio between the aggregation rate and the aggregation rate when all the collisions are expected to be efficient, for example at high ionic strength. In our model, the individual and initial attachment efficiency is not computed but constitutes an input parameter which is representative of individual NP and NOM surface properties, solution chemistry, and resulting interaction forces. As shown in **Figure 5.1**, several attachment efficiencies can describe heteroaggregation at different time scales of the process. At the very early stages, during the formation of dimers and trimers, α'_{homo} or α'_{hetero} are usually considered, while at long stages a more system-specific, α_{global} must be defined. Between both extreme cases, other attachment efficiency values are defined so as to describe intermediate situations such as α''_{hetero} corresponding to secondary aggregation from the dimer and trimer collisions and α_{hetero} relevant to the two first type steps of aggregation (primary and secondary). Since the heteroaggregate sizes and morphologies will evolve

all along the heteroaggregation process, the effective attachment values are expected to change from primary to secondary heteroaggregation, and heteroaggregation to global attachment efficiencies as shown in **Figure 5.1**. This is a crucial issue with important consequences on the design of long time scale NP fate transport model. Indeed, in some cases, NP surfaces can be rapidly coated with NOM because of α_{hetero} equal to 1, resulting in surface saturation, leading to system stabilization with an α_{global} value close to zero.

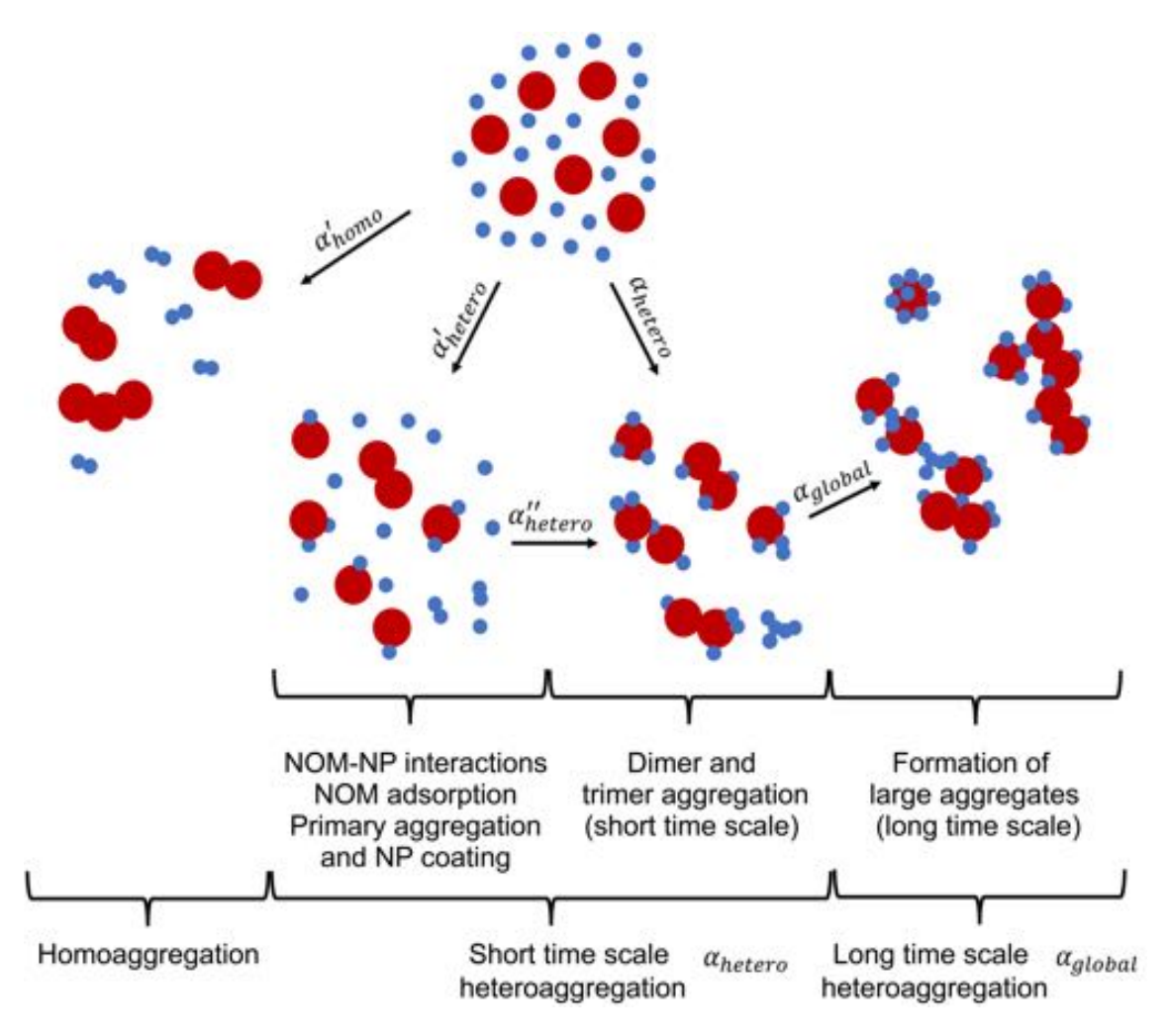


Figure 5.1: Description of homo- and heteroaggregation processes and corresponding attachment efficiencies.

To characterize NP coating process with NOM in our model, the number of NOM particles attached on the NP surface n_{att} is recorded and the fraction of surface saturation f_s is calculated as the ratio of the sum of NOM projected surfaces over the total NP surface according to:

Chapter 5: Heteroaggregation of Nanoparticles in Presence of NOM

$$f_s = \frac{\sum_{i=0}^{n_{ads}} \pi R_i}{4\pi R_{NP}} \tag{5.6}$$

where R_i represents the radius of the NOM particle adsorbed.

In this study, different attachment efficiency values for homo/heteroaggregation are given in **Table 5.1** so as to explore different and contrasting conditions, from marine to fresh waters. These individual attachment efficiency values are arbitrarily selected so as to simulate aquatic media with low (fresh water 0.01 and 0.1) and high ionic strength (marine water). All along this work, strong attractions between positive NP and negative NOM are considered modelling by an $\alpha_{NP-NOM}=1$.

Table 5.1: Individual attachment efficiencies representative of ultra-pure water, marine and fresh (0.1 and 0.01) water models.

	α_{NP-NOM}	$\alpha_{NOM-NOM}$	α_{NP-NP}
Type of contact		00	
Ultrapure	1.0	0.0	0.0
Fresh 0.01	1.0	0.01	0.0
Fresh 0.1	1.0	0.1	0.0
Marine	1.0	1.0	1.0

5.3 Results

5.3.1 Model validation

Before investigating the influence of NP and NOM concentrations as well as the effect of various individual attachment efficiencies on the relative importance of heteroaggregation, validation of the numerical model developed here is required and, more particularly, the procedure used for the calculation of the physical time. For that purpose, homoaggregation simulations were carried out with 15000 MC steps with a simulation box of 4000 nm in length containing 1000 NPs and with $\alpha_{NP-NP}=1.0$. The numbers of particles and objects were systematically calculated as a function of the physical time so as to estimate aggregation rate constants *via* the variation with time of the number of particles and objects according to equation 5.3.

As shown in **Figure 5.2.(a)**, for homoaggregation, the number of objects and particles continuously decreases with the physical time t. The loss of NPs is more efficient (faster) than the removal of objects all along the simulation time. This is due to the correlation between formation and removal of particles during the aggregation process. Indeed, when a dimer is formed, two particles disappear in the counting of particles. Furthermore, as shown in **Figure 5.2.(b)**, the concentration of objects and particles is correlated to the physical time. At the very early stages of the aggregation process, i.e., when dimers and trimers are formed, linear curves are observed and aggregation and particle removal rate constants can be extrapolated with values equal respectively to $5.81 \ 10^{-18}$ and $1.18 \ 10^{-17} \ m^3 \ s^{-1}$. These values are in good agreement if comparison is made with the values calculated from the Smoluchowski theory (section 2.1). The factor two is well observed between $k_{homo}^{particle}$ and k_{homo}^{agg} ($k_{homo}^{particle}$)/ $k_{homo}^{particle}$ = 2.03) indicating that the physical time calculated by our diffusion model fits well.

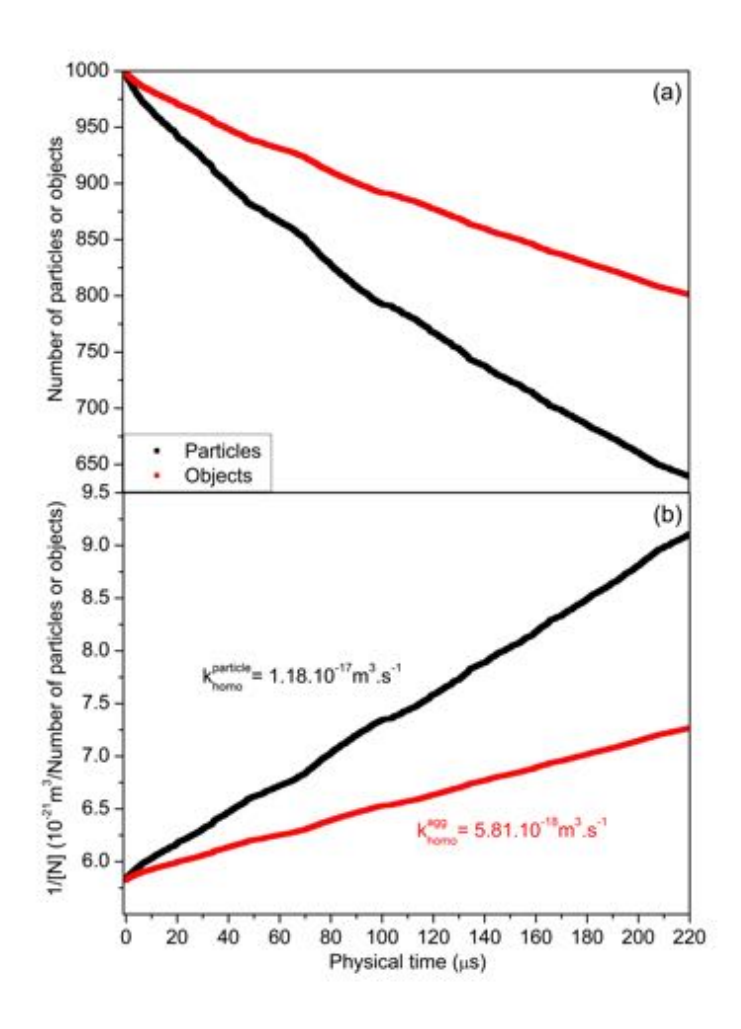


Figure 5.2: Homoaggregation process with $\alpha_{NOM-NOM}=1$. a) Variation versus physical time of the number of particles and objects (particles and aggregates). b) Variation of $\frac{1}{[N]}$ as a function of physical time where [N] represents the particle and object concentration allowing the calculation of the kinetic rate constants $k_{homo}^{particle}$ and k_{homo}^{agg} respectively.

5.3.2 Surface coating and heteroaggregation rates at constant natural organic matter concentration

To get an insight into the influence of the relative NP/NOM concentration ratio on NP surface coating process, and impact on heteroaggregation, simulations are performed over 10^6 MC steps in ultrapure water corresponding to $\alpha_{NP-NOM}=1.0$ and $\alpha_{NP-NP}=\alpha_{NOM-NOM}=0.0$ (**Table 5.1**). The NP number is adjusted from 1 to 100 which, considering the size of the simulation box, is equivalent to a variation between 1.6 and 157 10^{16} particles.L⁻¹. As shown

in Figure 5.3.(a) in which the percentage of surface saturation and the average number of adsorbed NOM per NPs are plotted as a function of the physical time, two different behaviors are observed at short and long-time scales for each NP concentration. At the early stages of the simulation, the fraction of surface saturation and the number of absorbed NOM increase rapidly until reaching a plateau value at long time. The number of efficient collisions is dominant at the beginning of the simulation due to NP surface availability for the NOM particles. Fraction of surface saturation reaches a maximum for a ratio of 1 NP and 1000 NOM and is equal to 85%, which corresponds to 340 adsorbed particles (full surface saturation would correspond to 400 NOM adsorbed). As shown by Smith et al [80], the surface coverage of a particle is limited by the geometry of the object studied and by the particles already attached on the surface, resulting in a value substantially lower than 1.0. With increasing NP concentration, saturation decreases as well as the number of NOM particles in the solution (Figure 5.3.(b)) and promotes heteroaggregation instead of saturation at high ratio (5% for 50/1000, 2% for 100/1000). This saturation effect is the result of the balance between the number of NOM in the simulation box and the accessible surface of the NP which is a function of the number of NOM already adsorbed on the NP as shown in Figure 5.4. At high NP/NOM ratio, the number of free NOM particles in the simulation box tends to zero quite quickly. On the other hand, at low NP ratio, free surface decreases rapidly with increasing the number of adsorbed NOM. It should be noted that the NP surface available is also reduced by the formation of heteroaggregates as shown in **Figure 5.4**. Indeed, NOM particles, once adsorbed at the NP surface, can act as bridging units between NPs and reduce the possibility of NOM particles to be adsorbed.

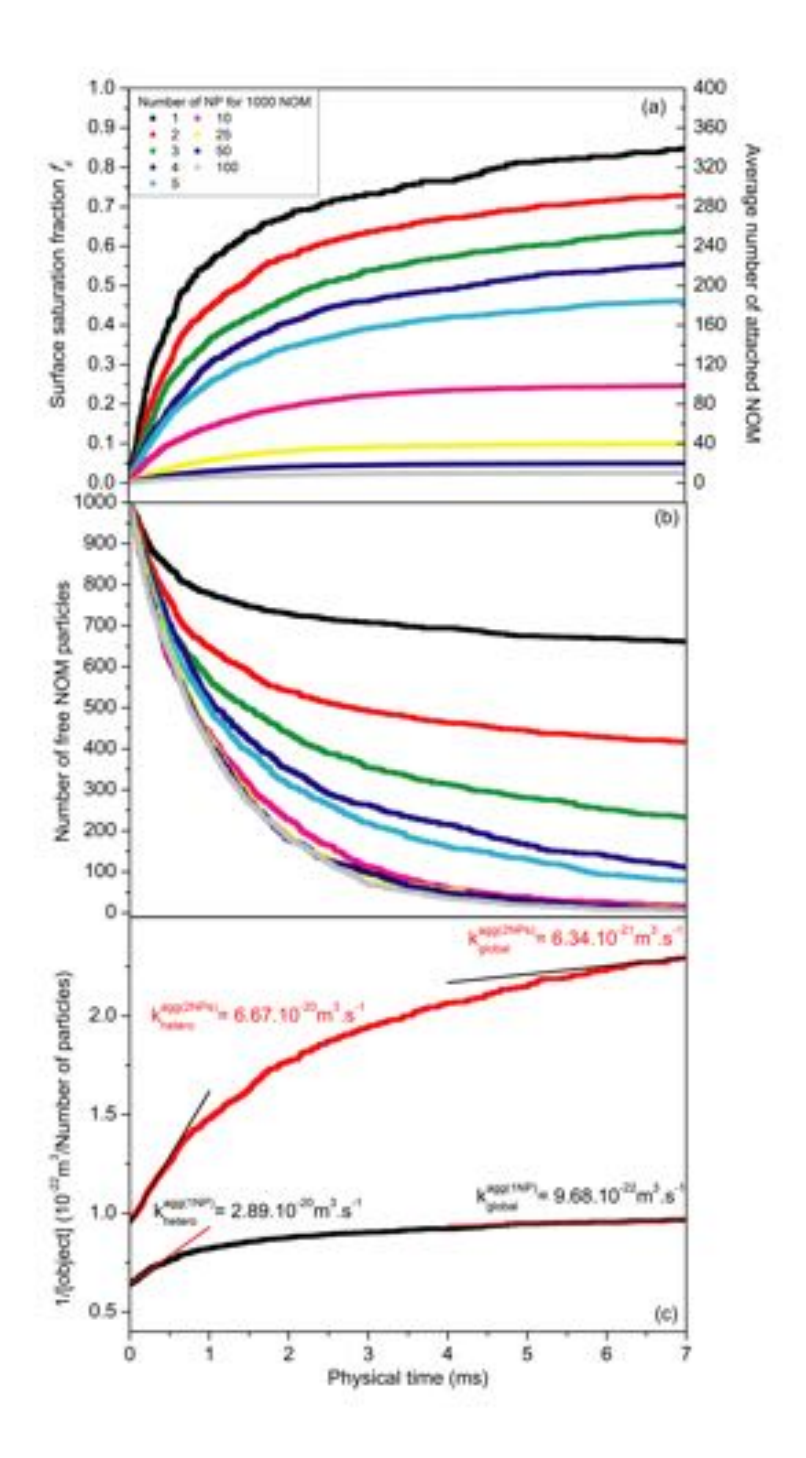


Figure 5.3: Heteroaggregation (Surface Coating) in presence of NOM and NPs. a) Surface saturation variation and average number of NOM attached to the NP surface as a function of NPs and physical time. b) Variation of the number of individual NOM particles (not attached) as a function of physical time. c) Determination of the heteroaggregation rate constant in presence of one and two NPs based on the variation of the number of objects.

Furthermore, saturation effects are playing a key role at different periods of the heteroaggregation process and in particular on the heteroaggregation rate constants. As shown in **Figure 5.3.(c)**, the heteroaggregation rate constant can be extrapolated from the temporal evolution of the object concentration and comparison can be made of the heteroaggregation rate progress at short and long time at low NP/NOM ratios. At the early stages, NP free surface is available and the heteroaggregation process takes place with a continuous decrease of the number of objects whereas, with time, the capacity of adsorbing NOM particles becomes more and more limited. As a result, the number of objects is slowly decreasing with time and, very interestingly, two distinct values of k corresponding respectively to heteroaggregation (α_{hetero}^{agg}) at short time and in presence of surface saturation effect at "long" time (α_{global}^{agg}) can be calculated. Saturation effects are therefore reducing the heteroaggregation rate constants and consequently the effective attachment efficiency.

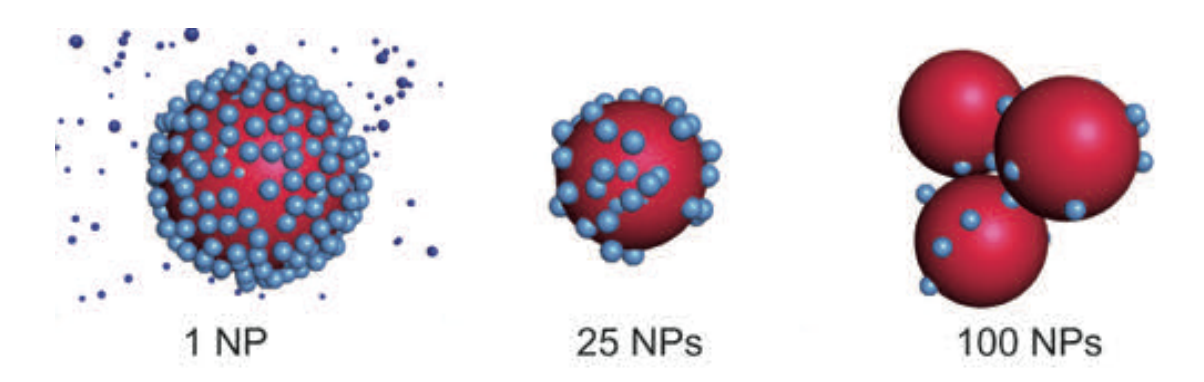


Figure 5.4: Evolution of the NP surface coating in presence of 1000 NOM units and for three different NP concentrations (a) 1, (b) 25 and (c) 100 NPs (simulation snapshots). Nanoparticles are in red (R=10nm), NOM attached and non-attached are respectively in clear blue and dark blue (R=1nm). Adsorbed NOM is represented by bigger spheres for a better visualization.

5.3.3 Heteroaggregation rates at variable NOM concentration

Heteroaggregation is now discussed by considering a fixed NP number and variable NOM concentration. Different scenarios regarding the initial attachment efficiencies are investigated and the corresponding heteroaggregation rate constants and attachment efficiencies α_{hetero} are determined. The heteroaggregation process is studied by considering different number ratios of NPs and NOM (2.10⁻³ to 2.10⁻²), corresponding to 10 NPs and 500 to 5000 NOM particles present in the simulation box at the initial time. Four different models of waters: marine, ul-

Chapter 5: Heteroaggregation of Nanoparticles in Presence of NOM

trapure, and fresh waters "0.1" and "0.01" are considered. The main difference between these different conditions is related to the importance of homoaggregation, especially between NOM particles. The case of marine water is a favorable and "reference" case where all the collisions are efficient (i.e. all individual attachment efficiencies are equal to 1). 30000 MC steps are carried out for each NPs/NOM ratio and for each water model we concentrate on the very first stages of the heteroaggregation. Our analysis is once again based on the variation with time of the total number of objects.

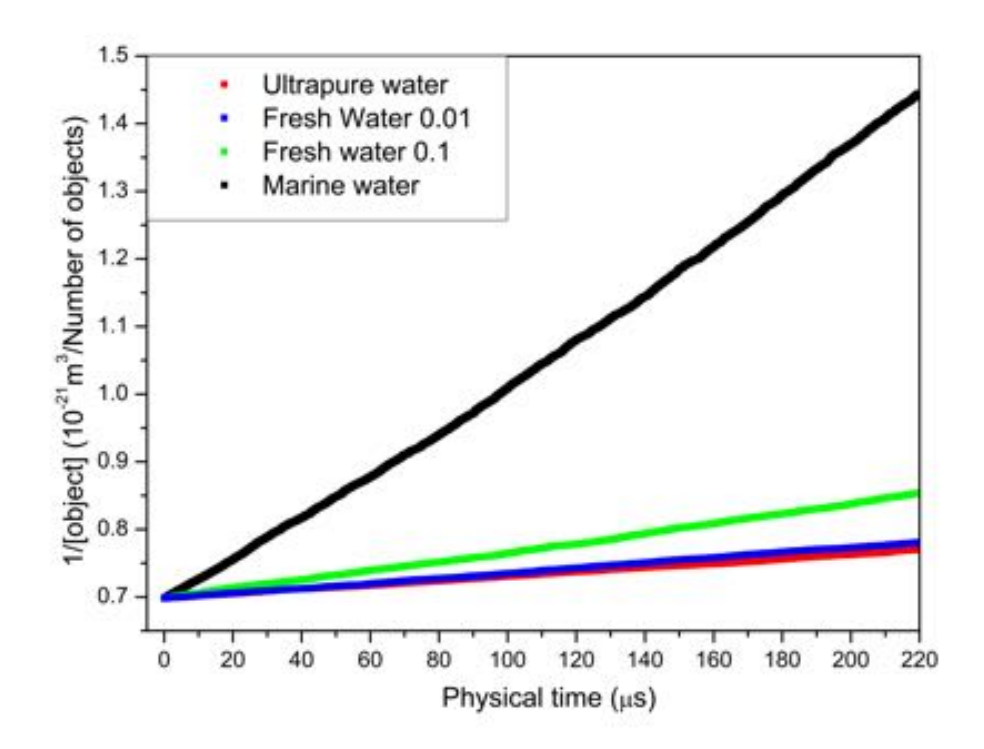


Figure 5.5: Variation of the inverse of the object concentration for the different water models with $\alpha_{NP-NOM} = 1$ and for 1000 NOM particles.

As shown in **Figure 5.5**, in which the time variation of the inverse of the object concentration is given for the different water models, at a fixed ratio (10 NPs and 1000 NOM), distinct behaviors are observed. For the marine water, homoaggregation between NOM as well as NPs plays a key role in the overall aggregation process. Indeed, the object number is rapidly decreasing as a function of time indicating a fast aggregation process. For freshwaters and ultrapure water, the object removal rate is found to be lower and progressively shifted to low values with

the decrease of $\alpha_{NOM-NOM}$. The ultrapure water condition is found to be very similar to fresh water when NOM homoaggregation is weak. To make the analysis more quantitative, aggregation rate constants have been determined by linear regression at the first stages of the simulation (30-40 μ s) at different NOM concentrations and listed in **Table 5.2**.

Table 5.2: Heteroaggregation rate constants, k_{hetero}^{agg} (10⁻¹⁸ m³ s⁻¹) for ultrapure, marine and fresh water models at different NOM concentrations. NPs = 10.

Total number of NOM units	500	1000	2000	3000	4000	5000
Ultrapure	0.65	0.30	0.16	0.10	0.08	0.06
Fresh 0.01	0.71	0.36	0.20	0.14	0.12	0.10
Fresh 0.1	1.36	0.65	0.52	0.46	0.45	0.44
Marine	3.00	3.08	3.18	3.59	3.84	4.16

In **Figure 5.6**, the heteroaggregation rate constants are explicitly represented as a function of NOM concentration. It is found that for marine water, the heteroaggregation rate constant is continuously increasing with the number of NOM. Particles rapidly disappear and form a significant number of aggregates as shown in **Figure 5.8**. On the other hand, in ultrapure and fresh water 0.1 and 0.01, heteroaggregation rate constants are slightly decreasing with the increase of the NOM concentration to reach plateau values. k_{hetero}^{agg} becomes low at high NOM concentration compared to marine waters in which homoaggregation is the dominant mechanism. Indeed, in the case of marine waters, the heteroaggregation rate constant is close to the theoretical value obtained for homoaggregation especially for high NOM concentration, as expected, because except for the slightly different size of NP and NOM, they almost behave as a homoaggregating system due to the same individual attachment efficiencies. It should be noted that the kinetic rate constant is smaller than the theoretical value owing to the fact that two processes are involved here i.e. homoaggregation but also NOM adsorption at the NP surface which reduces the heteroaggregation rates compared to homoaggregation.

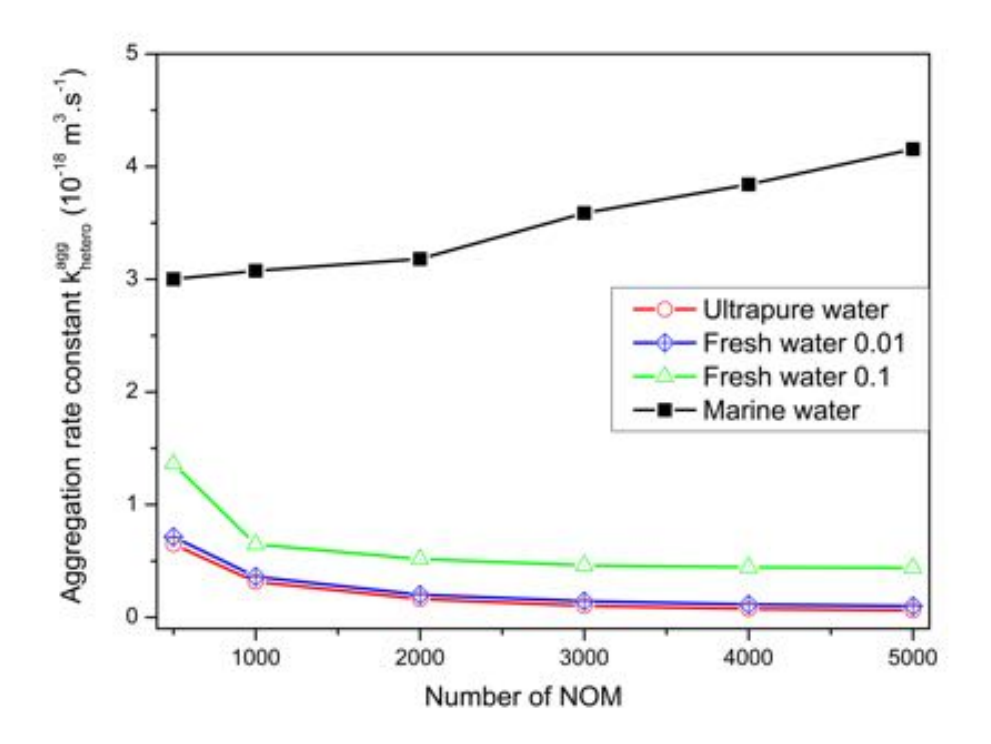


Figure 5.6: Evolution of the heteroaggregation rate constant for each water models as a function of the number of NOM.

In ultrapure and fresh waters, k_{hetero}^{agg} is found to be significantly smaller and decreases with the NOM concentration. The heteroaggregation process is controlled by the balance between the available free space at the NP surface and the probability of collision between NPs and NOM. At low concentration, surface saturation is less important hence promoting the heteroaggregation and consequently the increase of k_{hetero}^{agg} .

In **Figure 5.7**, the effective heteroaggregation attachment efficiencies of each water model and different relative concentration ratio are calculated by considering marine water aggregation as the highest possible aggregation rate. α_{hetero}^{agg} values, derived from heteroaggregation rate constant, are plotted as a function of the NP/NOM ratio and reported in **Table 5.3**.

Table 5.3: Heteroaggregation attachment efficiencies for ultrapure and fresh water at different NOM concentrations.

Number of NOM particles	Ultrapure Water (0.0)	F	resh Water (0.01)	Fr	esh Water (0.1)
500	0.216		0.238		0.454
1000	0.103		0.118		0.211
2000	0.051		0.063		0.163
3000	0.029		0.040		0.129
4000	0.020		0.030		0.116
5000	0.015		0.024		0.101
01.	< 0.02 0.0	2-0.1	0.1-0.2	>02	

 α_{het} < 0.02 0.02-0.1 0.1-0.2 > 0.2

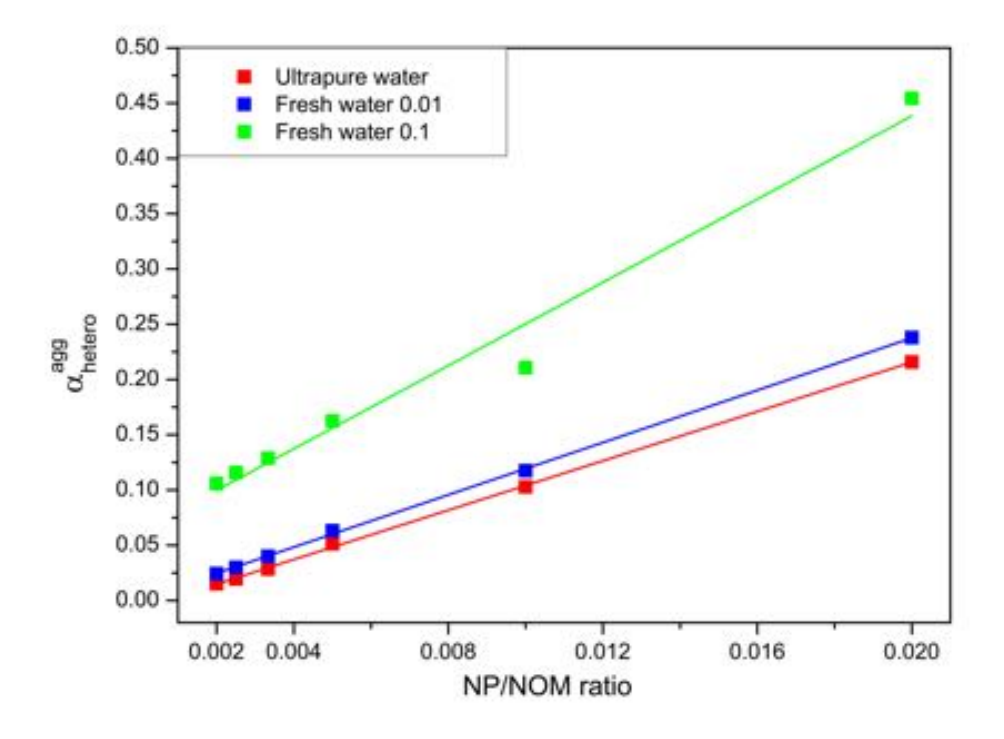


Figure 5.7: Variation of the heteroaggregation attachment efficiencies for each water model as a function of the NP/NOM ratios.

Chapter 5: Heteroaggregation of Nanoparticles in Presence of NOM

At high NOM concentration, the attachment efficiencies are close to zero due to surface saturation effects and reduced collision probability. In the case of fresh water 0.01, these values are a little bit higher due to limited homoaggregation which takes place ($\alpha_{hetero}^{agg} \approx 0.01$). At low $\alpha_{NOM-NOM}$, the attachment efficiencies of ultrapure and fresh water 0.01 have similar behavior due to the weak impact of homoaggregation on the heteroaggregation process. The more available free NP surface as well as a decrease of saturation effects contribute to a better heteroaggregation between NOM and NPs. This increase of α_{hetero}^{agg} with NOM concentration decrease is also observed in fresh water 0.1. However, in this case, the homoaggregation has a strong impact on the hetero attachment efficiencies with a more significant increase of heteroaggregation rate constant ($\alpha_{hetero}^{agg} = 0.45$).

As shown here a subtle change in the input parameters, or environmental conditions, such as the individual attachment efficiencies can have a strong impact on the heteroaggregation process and related attachment efficiency values. To help in data interpretation and observations, simulation snapshots are given in **Figure 5.8**. Saturation effects are illustrated if one considers the ultrapure water case and by increasing the NOM concentration. On the other hand, the presence of NOM homoaggregates is clearly shown for fresh water 0.1 and marine waters for which the saturation effect on the surface is respectively reduced or absent, resulting in an increase of α_{hetero}^{agg} values.

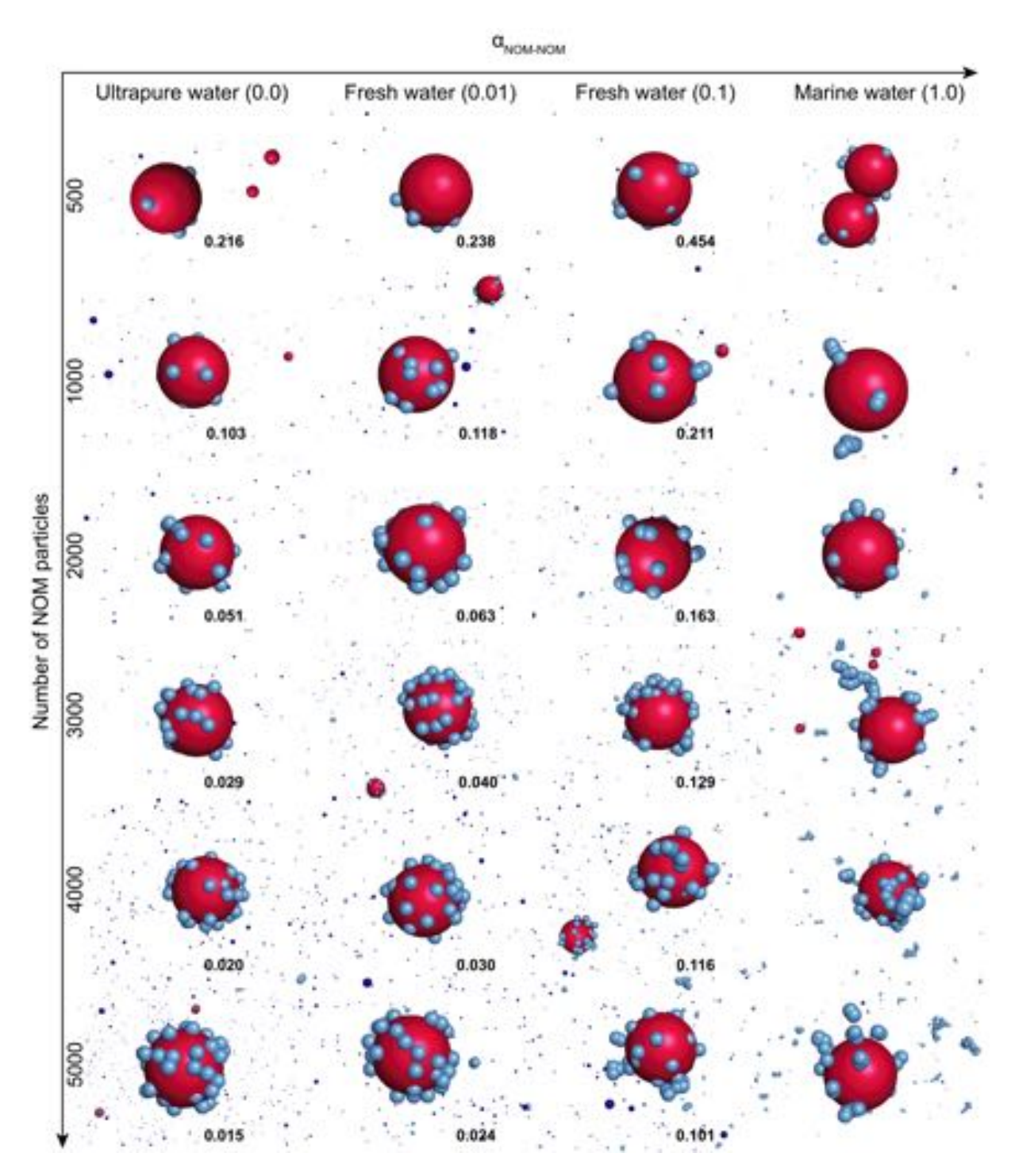


Figure 5.8: Snapshots of heteroaggregates and homoaggregates at different NOM concentrations and in different water models. α_{hetero}^{agg} values are indicated for each situation excepted for marine water case where is equal to one (most favorable conditions).

5.4 Conclusions

In this study, various environmental scenarios from fresh to marine waters as well as mechanisms such as coating process, homo- and heteroaggregation have been investigated *via* the development of an original and novel Monte Carlo cluster-cluster aggregation approach. We have shown that Monte Carlo calculations when linked with physical time can constitute a powerful approach to get an insight into heteroaggregation process between NPs and NOM units and to obtain a better description of heteroaggregation in different water models. Complex processes such as surface saturation, homoaggregation and heteroaggregation are expected to control the aggregation kinetics of NPs. Concentration ratios of NPs and NOM have been found to play a key role in the heteroaggregation processes. From a mechanistic point of view, NOM can act as bridging units or aggregates to create large heteroaggregates. Marine water represents a specific and favorable case of aggregation where all contacts are effective. On the other hand, in ultrapure and fresh waters, a competition between homo- and heteroaggregation occurs depending on the initial attachment efficiencies indicating that a subtle change in the surface properties of the particle as well as in the water chemistry will have a significant impact on the heteroaggregation process.

The simulations and results described in this paper constitute a preliminary step towards the description of more complex processes and systems, which could involve more than two components i.e. by including inorganic colloids or by considering NOM as small aggregates already present in the dispersing medium. One could also think instead of using arbitrary individual attachment values to compute them *via* calculations of Fuchs stability ratio *via* DLVO theory or to simply use experimental values.

5.5 Acknowledgements

The authors acknowledge support receive from the European Commission and the Swiss Secrétariat d'Etat à la Formation et à la Recherche et à l'Innovation SEFRI within the Horizon 2020 Program (NanoFASE 15.0183-2, 646002) and University of Geneva.

Bibliography

- [1] Joerg Lahann. Environmental nanotechnology: Nanomaterials clean up. *Nature Nanotechnology*, 3(6):320, June 2008.
- [2] Andrew D. Maynard, Robert J. Aitken, Tilman Butz, Vicki Colvin, Ken Donaldson, Günter Oberdörster, Martin A. Philbert, John Ryan, Anthony Seaton, Vicki Stone, Sally S. Tinkle, Lang Tran, Nigel J. Walker, and David B. Warheit. Safe handling of nanotechnology, November 2006.
- [3] V. Raffa, O. Vittorio, C. Riggio, and A. Cuschieri. Progress in nanotechnology for health-care. *Minimally Invasive Therapy & Allied Technologies*, 19(3):127–135, June 2010.
- [4] Konstantin Sobolev, Miguel Ferrada Gutiérrez, and The American Ceramic Society. How Nanotechnology Can Change the Concrete World. In *Progress in Nanotechnology*, pages 113–116. John Wiley & Sons, Inc., 2009.
- [5] Indu Bhatt and Bhumi Nath Tripathi. Interaction of engineered nanoparticles with various components of the environment and possible strategies for their risk assessment. *Chemosphere*, 82(3):308–317, January 2011.
- [6] Brian Carl Englert. Nanomaterials and the environment: uses, methods and measurement. *Journal of Environmental Monitoring*, 9(11):1154, 2007.
- [7] Stephen J. Klaine, Pedro J. J. Alvarez, Graeme E. Batley, Teresa F. Fernandes, Richard D. Handy, Delina Y. Lyon, Shaily Mahendra, Michael J. McLaughlin, and Jamie R. Lead. Nanomaterials in the environment: Behavior, fate, bioavailability, and effects. *Environmental Toxicology and Chemistry*, 27(9):1825–1851, September 2008.
- [8] Nicole C. Mueller and Bernd Nowack. Exposure Modeling of Engineered Nanoparticles in the Environment. *Environmental Science & Technology*, 42(12):4447–4453, June 2008.
- [9] Paul Schulte, Charles Geraci, Ralph Zumwalde, Mark Hoover, and Eileen Kuempel. Occupational Risk Management of Engineered Nanoparticles. *Journal of Occupational and Environmental Hygiene*, 5(4):239–249, April 2008.
- [10] Qianqian Cao and Michael Bachmann. Electrostatic complexation of linear polyelectrolytes with soft spherical nanoparticles. *Chemical Physics Letters*, 586:51–55, October 2013.

- [11] Alex Weir, Paul Westerhoff, Lars Fabricius, Kiril Hristovski, and Natalie von Goetz. Titanium Dioxide Nanoparticles in Food and Personal Care Products. *Environmental Science & Technology*, 46(4):2242–2250, February 2012.
- [12] Jennifer L West and Naomi J Halas. Applications of nanotechnology to biotechnology: Commentary. *Current Opinion in Biotechnology*, 11(2):215–217, April 2000.
- [13] J. M. Wilkinson. Nanotechnology applications in medicine. *Medical device technology*, 14(5):29–31, June 2003.
- [14] Mélanie Auffan, Jérôme Rose, Jean-Yves Bottero, Gregory V. Lowry, Jean-Pierre Jolivet, and Mark R. Wiesner. Towards a definition of inorganic nanoparticles from an environmental, health and safety perspective. *Nature Nanotechnology*, 4(10):634–641, October 2009.
- [15] John Gregory. *Particles in water: properties and processes*. IWA Publishing, London, 2005.
- [16] Yon Ju-Nam and Jamie R. Lead. Manufactured nanoparticles: An overview of their chemistry, interactions and potential environmental implications. *Science of The Total Environment*, 400(1–3):396–414, August 2008.
- [17] Gregory V. Lowry, Kelvin B. Gregory, Simon C. Apte, and Jamie R. Lead. Transformations of Nanomaterials in the Environment. *Environmental Science & Technology*, 46(13):6893–6899, July 2012.
- [18] M. N. Moore. Do nanoparticles present ecotoxicological risks for the health of the aquatic environment? *Environment International*, 32(8):967–976, December 2006.
- [19] Enrique Navarro, Anders Baun, Renata Behra, Nanna B. Hartmann, Juliane Filser, Ai-Jun Miao, Antonietta Quigg, Peter H. Santschi, and Laura Sigg. Environmental behavior and ecotoxicity of engineered nanoparticles to algae, plants, and fungi. *Ecotoxicology*, 17(5):372–386, July 2008.
- [20] Vicki L. Colvin. The potential environmental impact of engineered nanomaterials. *Nature Biotechnology*, 21(10):1166–1170, October 2003.
- [21] Amy L. Dale, Elizabeth A. Casman, Gregory V. Lowry, Jamie R. Lead, Enrica Viparelli, and Mohammed Baalousha. Modeling Nanomaterial Environmental Fate in Aquatic Systems. *Environmental Science & Technology*, 49(5):2587–2593, March 2015.

- [22] Julia Fabrega, Samuel N. Luoma, Charles R. Tyler, Tamara S. Galloway, and Jamie R. Lead. Silver nanoparticles: Behaviour and effects in the aquatic environment. *Environment International*, 37(2):517–531, February 2011.
- [23] Nicole Sani-Kast, Martin Scheringer, Danielle Slomberg, Jérôme Labille, Antonia Praetorius, Patrick Ollivier, and Konrad Hungerbühler. Addressing the complexity of water chemistry in environmental fate modeling for engineered nanoparticles. *Science of The Total Environment*, 535:150–159, December 2015.
- [24] James A. Davis, Robert O. James, and James O. Leckie. Surface ionization and complexation at the oxide/water interface: I. Computation of electrical double layer properties in simple electrolytes. *Journal of Colloid and Interface Science*, 63(3):480–499, March 1978.
- [25] Laura-Jayne A. Ellis, Eugenia Valsami-Jones, Jamie R. Lead, and Mohammed Baalousha. Impact of surface coating and environmental conditions on the fate and transport of silver nanoparticles in the aquatic environment. *Science of The Total Environment*, 568:95–106, October 2016.
- [26] Arturo A. Keller, Hongtao Wang, Dongxu Zhou, Hunter S. Lenihan, Gary Cherr, Bradley J. Cardinale, Robert Miller, and Zhaoxia Ji. Stability and Aggregation of Metal Oxide Nanoparticles in Natural Aqueous Matrices. *Environmental Science & Technology*, 44(6):1962–1967, March 2010.
- [27] A. A. Koelmans, N. J. Diepens, I. Velzeboer, E. Besseling, J. T. K. Quik, and D. van de Meent. Guidance for the prognostic risk assessment of nanomaterials in aquatic ecosystems. *Science of The Total Environment*, 535:141–149, December 2015.
- [28] Bernd Nowack and Thomas D. Bucheli. Occurrence, behavior and effects of nanoparticles in the environment. *Environmental Pollution*, 150(1):5–22, November 2007.
- [29] Bernd Nowack, James F. Ranville, Stephen Diamond, Julian A. Gallego-Urrea, Chris Metcalfe, Jerome Rose, Nina Horne, Albert A. Koelmans, and Stephen J. Klaine. Potential scenarios for nanomaterial release and subsequent alteration in the environment. *Environmental Toxicology and Chemistry*, 31(1):50–59, January 2012.
- [30] Anika Braun, Erwin Klumpp, Rafig Azzam, and Christoph Neukum. Transport and deposition of stabilized engineered silver nanoparticles in water saturated loamy sand and silty loam. *Science of The Total Environment*, 535:102–112, December 2015.

- [31] Fabrice Carnal, Arnaud Clavier, and Serge Stoll. Modelling the interaction processes between nanoparticles and biomacromolecules of variable hydrophobicity: Monte Carlo simulations. *Environ. Sci.: Nano*, 2(4):327–339, 2015.
- [32] Mohamed E. Labib. The origin of the surface charge on particles suspended in organic liquids. *Colloids and Surfaces*, 29(3):293–304, January 1988.
- [33] Mohammed Baalousha. Aggregation and disaggregation of iron oxide nanoparticles: Influence of particle concentration, pH and natural organic matter. *Science of The Total Environment*, 407(6):2093–2101, March 2009.
- [34] Geert Cornelis, Liping Pang, Casey Doolette, Jason K. Kirby, and Mike J. McLaughlin. Transport of silver nanoparticles in saturated columns of natural soils. *Science of The Total Environment*, 463-464:120–130, October 2013.
- [35] Jose Garcia, Jasmina Markovski, J. McKay Gifford, Onur Apul, and Kiril D. Hristovski. The effect of metal (hydr)oxide nano-enabling on intraparticle mass transport of organic contaminants in hybrid granular activated carbon. *Science of The Total Environment*, 586:1219–1227, May 2017.
- [36] Zhen Li, Endalkachew Sahle-Demessie, Ashraf Aly Hassan, Jonathan G. Pressman, George A. Sorial, and Changseok Han. Effects of source and seasonal variations of natural organic matters on the fate and transport of CeO2 nanoparticles in the environment. *Science of The Total Environment*, 609:1616–1626, December 2017.
- [37] Antonia Praetorius, Jérôme Labille, Martin Scheringer, Antoine Thill, Konrad Hungerbühler, and Jean-Yves Bottero. Heteroaggregation of Titanium Dioxide Nanoparticles with Model Natural Colloids under Environmentally Relevant Conditions. *Environmental Science & Technology*, 48(18):10690–10698, September 2014.
- [38] Beng Joo Reginald Thio, Dongxu Zhou, and Arturo A. Keller. Influence of natural organic matter on the aggregation and deposition of titanium dioxide nanoparticles. *Journal of Hazardous Materials*, 189(1–2):556–563, May 2011.
- [39] Amro M. El Badawy, Todd P. Luxton, Rendahandi G. Silva, Kirk G. Scheckel, Makram T. Suidan, and Thabet M. Tolaymat. Impact of Environmental Conditions (pH, Ionic Strength, and Electrolyte Type) on the Surface Charge and Aggregation of Silver Nanoparticles Suspensions. *Environmental Science & Technology*, 44(4):1260–1266, February 2010.

- [40] Biplab Mukherjee and James W. Weaver. Aggregation and Charge Behavior of Metallic and Nonmetallic Nanoparticles in the Presence of Competing Similarly-Charged Inorganic Ions. *Environmental Science & Technology*, 44(9):3332–3338, May 2010.
- [41] Marianne Seijo, Serge Ulrich, Montserrat Filella, Jacques Buffle, and Serge Stoll. Modeling the Adsorption and Coagulation of Fulvic Acids on Colloids by Brownian Dynamics Simulations. *Environmental Science & Technology*, 43(19):7265–7269, October 2009.
- [42] Y. Nur, J. R. Lead, and M. Baalousha. Evaluation of charge and agglomeration behavior of TiO2 nanoparticles in ecotoxicological media. *Science of The Total Environment*, 535:45–53, December 2015.
- [43] Nadia von Moos, Paul Bowen, and Vera I. Slaveykova. Bioavailability of inorganic nanoparticles to planktonic bacteria and aquatic microalgae in freshwater. *Environmental Science: Nano*, 1(3):214, 2014.
- [44] Joris T. K. Quik, Dik van De Meent, and Albert A. Koelmans. Simplifying modeling of nanoparticle aggregation—sedimentation behavior in environmental systems: A theoretical analysis. *Water Research*, 62:193–201, October 2014.
- [45] Joris T. K. Quik, Jeroen J. M. de Klein, and Albert A. Koelmans. Spatially explicit fate modelling of nanomaterials in natural waters. *Water Research*, 80:200–208, September 2015.
- [46] Antonia Praetorius, Martin Scheringer, and Konrad Hungerbühler. Development of Environmental Fate Models for Engineered Nanoparticles—A Case Study of TiO2 Nanoparticles in the Rhine River. *Environmental Science & Technology*, 46(12):6705–6713, June 2012.
- [47] Egon Dumont, Andrew C. Johnson, Virginie D. J. Keller, and Richard J. Williams. Nano silver and nano zinc-oxide in surface waters Exposure estimation for Europe at high spatial and temporal resolution. *Environmental Pollution*, 196:341–349, January 2015.
- [48] Lauren E. Barton, Mathieu Therezien, Melanie Auffan, Jean-Yves Bottero, and Mark R. Wiesner. Theory and Methodology for Determining Nanoparticle Affinity for Heteroaggregation in Environmental Matrices Using Batch Measurements. *Environmental Engineering Science*, 31(7):421–427, June 2014.
- [49] Alexandre Albanese and Warren C.W. Chan. Effect of Gold Nanoparticle Aggregation on Cell Uptake and Toxicity. *ACS Nano*, 5(7):5478–5489, July 2011.

- [50] Frédéric Loosli, Philippe Le Coustumer, and Serge Stoll. TiO2 nanoparticles aggregation and disaggregation in presence of alginate and Suwannee River humic acids. pH and concentration effects on nanoparticle stability. Water Research, 47(16):6052–6063, October 2013.
- [51] Mathieu Therezien, Antoine Thill, and Mark R. Wiesner. Importance of heterogeneous aggregation for NP fate in natural and engineered systems. *Science of The Total Environment*, 485-486:309–318, July 2014.
- [52] M E Costas, M Moreau, and L Vicente. Some analytical and numerical solutions for colloidal aggregation with fragmentation. *Journal of Physics A: Mathematical and General*, 28(11):2981–2994, June 1995.
- [53] A. A. Markus, J. R. Parsons, E. W. M. Roex, P. de Voogt, and R. W. P. M. Laane. Modeling aggregation and sedimentation of nanoparticles in the aquatic environment. *Science of The Total Environment*, 506–507:323–329, February 2015.
- [54] Paul Meakin. Diffusion-limited aggregation in three dimensions: Results from a new cluster-cluster aggregation model. *Journal of Colloid and Interface Science*, 102(2):491–504, December 1984.
- [55] D. Elderfield. Smoluchowski and beyond: a field theoretical study of coagulation/fragmentation processes. *Journal of Physics A: Mathematical and General*, 20(3):L135, 1987.
- [56] M. Elimelech, R. Williams, J. Gregory, and X. Jia. *Particle deposition and aggregation: Measurement, modelling and simulation*. Butterworth-Heinemann, 1998.
- [57] Francis Filbet and Philippe Laurençot. Numerical Simulation of the Smoluchowski Coagulation Equation. *SIAM Journal on Scientific Computing*, 25(6):2004–2028, January 2004.
- [58] D S Krivitsky. Numerical solution of the Smoluchowski kinetic equation and asymptotics of the distribution function. *Journal of Physics A: Mathematical and General*, 28(7):2025–2039, April 1995.
- [59] P. Meakin. The structure of two-dimensional Witten-Sander aggregates. *Journal of Physics A: Mathematical and General*, 18(11):L661, 1985.

- [60] T. A. Witten and L. M. Sander. Diffusion-Limited Aggregation, a Kinetic Critical Phenomenon. *Physical Review Letters*, 47(19):1400–1403, November 1981.
- [61] Yasuyuki Kusaka, Tomonori Fukasawa, and Yasuhisa Adachi. Cluster–cluster aggregation simulation in a concentrated suspension. *Journal of Colloid and Interface Science*, 363(1):34–41, November 2011.
- [62] Hailing Xiong, Hang Li, Weiping Chen, Jian Xu, and Laosheng Wu. Application of the Cluster–Cluster Aggregation model to an open system. *Journal of Colloid and Interface Science*, 344(1):37–43, April 2010.
- [63] Rajat K Chakraborti, Kevin H Gardner, Joseph F Atkinson, and John E Van Benschoten. Changes in fractal dimension during aggregation. Water Research, 37(4):873–883, February 2003.
- [64] M. Kolb and H. J. Herrmann. Surface fractals in irreversible aggregation. *Physical Review Letters*, 59(4):454–457, July 1987.
- [65] C. Kranenburg. The fractal structure of cohesive sediment aggregates. *Estuarine, Coastal and Shelf Science*, 39(6):451–460, January 1994.
- [66] G. R. Wiese and T. W. Healy. Effect of particle size on colloid stability. *Transactions of the Faraday Society*, 66(0):490–499, 1970.
- [67] Nicholas K. Geitner, Niall J. O'Brien, Amalia A. Turner, Enda J. Cummins, and Mark R. Wiesner. Measuring Nanoparticle Attachment Efficiency in Complex Systems. *Environmental Science & Technology*, 51(22):13288–13294, November 2017.
- [68] Bruce E. Logan and John R. Kilps. Fractal dimensions of aggregates formed in different fluid mechanical environments. *Water Research*, 29(2):443–453, February 1995.
- [69] A. M. Puertas, A. Fernández-Barbero, and F. J. De las Nieves. Aggregation between oppositely charged colloidal particles. In *Trends in Colloid and Interface Science XIV*, Progress in Colloid and Polymer Science, pages 55–58. Springer, Berlin, Heidelberg, 2000.
- [70] Adamo R. Petosa, Deb P. Jaisi, Ivan R. Quevedo, Menachem Elimelech, and Nathalie Tufenkji. Aggregation and Deposition of Engineered Nanomaterials in Aquatic Environments: Role of Physicochemical Interactions. *Environmental Science & Technology*, 44(17):6532–6549, September 2010.

- [71] A. R. M. Nabiul Afrooz, Saber M. Hussain, and Navid B. Saleh. Aggregate size and structure determination of nanomaterials in physiological media: importance of dynamic evolution. *Journal of Nanoparticle Research*, 16(12):2771, December 2014.
- [72] Julian A. Gallego-Urrea, Jani Tuoriniemi, and Martin Hassellöv. Applications of particle-tracking analysis to the determination of size distributions and concentrations of nanoparticles in environmental, biological and food samples. *TrAC Trends in Analytical Chemistry*, 30(3):473–483, March 2011.
- [73] Jérôme Labille, Carrie Harns, Jean-Yves Bottero, and Jonathan Brant. Heteroaggregation of Titanium Dioxide Nanoparticles with Natural Clay Colloids. *Environmental Science & Technology*, 49(11):6608–6616, June 2015.
- [74] Christophe Labbez and Bo Jönsson. A New Monte Carlo Method for the Titration of Molecules and Minerals. In *Applied Parallel Computing*. *State of the Art in Scientific Computing*, pages 66–72. 2009.
- [75] Haoyang Haven Liu, Sirikarn Surawanvijit, Robert Rallo, Gerassimos Orkoulas, and Yoram Cohen. Analysis of Nanoparticle Agglomeration in Aqueous Suspensions via Constant-Number Monte Carlo Simulation. *Environmental Science & Technology*, 45(21):9284–9292, November 2011.
- [76] Marianne Seijo, Serge Ulrich, Montserrat Filella, Jacques Buffle, and Serge Stoll. Effects of surface site distribution and dielectric discontinuity on the charging behavior of nanoparticles. A grand canonical Monte Carlo study. *Physical Chemistry Chemical Physics*, 8(48):5679, 2006.
- [77] Daan Frenkel. Introduction to Monte Carlo Methods. In *Computational Soft Matter: from Synthetic Polymers to Proteins*, volume 23, pages 29–60. NIC Series, Jülich, 2004.
- [78] Daan Frenkel and Berend Smit. *Understanding Molecular Simulation: From Algorithms to Applications*. Academic Press, October 2001.
- [79] J. Lyklema. Fundamentals of Interface and Colloid Science: Soft Colloids. Elsevier, March 2005. Google-Books-ID: roFTFahmLC4C.
- [80] Brian M. Smith, Daniel J. Pike, Michael O. Kelly, and Jeffrey A. Nason. Quantification of Heteroaggregation between Citrate-Stabilized Gold Nanoparticles and Hematite Colloids. *Environmental Science & Technology*, 49(21):12789–12797, November 2015.

CHAPTER 6

Conclusions and Perspectives

6.1 General conclusions

he main objective of the present thesis was to develop several models in order to better understand and describe NP behavior and transformations in aquatic systems. The impact of several properties such as the surface properties (density, site distributions, acid/base properties), dispersing medium ion composition (valency, concentration) and composition (NOM presence, NP concentration) were systematically investigated. Due to the large number of possible scenarios and owing to the multiple number of adjusting parameters, a computer modelling approach was chosen. For that purpose, Monte Carlo simulations (random sampling and Metropolis methods) were adopted to answer several key and fundamental questions. As far as possible, relevant environmental scenarios and specific situation were considered.

The surface charging behavior of a spherical nanoparticle was first considered (**Chapter 3**). Simple and multiple deprotonation processes $(1-pK_a^0 \text{ and } 2-pK_a^0 \text{ models})$ were investigated for three types of metal oxide nanoparticles (titanium dioxide, hematite and soft NPs) by following effect of pH variations on the nanoparticles. The influence of NP intrinsic properties was individually explored in order to investigate their impact on the possible NP transformations in environment but also in laboratory experiments regarding, for example, NP titrating processes. The analysis of quantities such as NP total surface charge and the degree of ionization demonstrated that surface charge density and site distributions play a significant role on the nanoparticle surface charging process. The distance between charges, depending on the site density and distribution, and consequently, the electrostatic repulsions occurring at the NP surface have found to strongly modify the titration curves. Moreover, different surface charging behavior and configurations were observed depending on the acid/base properties of the nanoparticles, in particular for double deprotonation processes $(2-pK_a^0)$. Point of zero charge and isoelectric point were found to result from different charging process (step-by-step process and sharp transition).

Then, in a second time, the ionic distribution issue around NPs was studied in presence of explicit ions (**Chapter 4**). Counterion, cation and anion particle were taken into account. Therefore, in addition to the surface properties (as studied in the previous model), the solution properties such as salt concentration, ionic strength and valency were investigated considering a spherical charged nanoparticle. Besides the fact that salt properties altered the NP surface, in particular the effective surface charge, our simulations clearly indicated the fact that the pres-

ence of charged NPs had a strong impact on an aqueous solution. Regarding the surface properties, the increase of the surface charge density was found to reduce the NP effective charge by forming a condensation layer. Moreover, di- and trivalent cations were found to improve the condensation state and to strongly modify the NP effective charge compared to monovalent and free salt cases. However, both mechanisms were limited by steric effects as well as strong cation-cation electrostatic repulsions, respectively, and no charge inversion was observed. In very specific cases (high trivalent concentration), a neutralization of the charge on the nanoparticle was observed with the formation of multiple layers (first layer composed by cations and second layer by anions). This particular situation was strongly related to the electrostatic interaction balance between each compounds (NP site-NP site, NP site-cation, cation-cation).

The last model developed in this thesis work, but also within the framework of the H2020 NanoFASE project, was related to NP heteroaggregation in presence of natural organic matter (Chapter 5). A novel Monte Carlo aggregation model was developed and validated using the Smoluchowski theory. The heteroaggregation processes between NPs and acid fulvic units were investigated for various relevant water models and for different NP/NOM concentration ratio. A better understanding of the attachment efficiency values was also proposed in order to characterize the different steps occurring during heteroaggregation: (i) primary attachment efficiency (α') corresponding to the formation of dimer and trimer aggregates (primary heteroaggregation, behavior at short times), secondary or heteroaggregation attachment efficieny (α'' or α_{hetero}) corresponding to the heteroaggregation of dimer and trimer aggregates and (iii) alpha global attachment efficiency (α_{qlobal}) corresponding to the heteroaggregation of large aggregates (behavior at long times). For that purpose, marine water represented a specific and favorable case corresponding to a diffusion limited situation (all contacts are effective) and allowed the calculation of attachment efficiency values for different scenario. Our results demonstrated that surface coating effects had a strong impact on aggregation and two different behavior were obtained. A rapid primary heteroaggregation at short time and a limited aggregation at long time due to a saturation effects hence decreasing NOM attachment on the NP surface. In ultrapure and fresh water, a subtle modification of the NP surface and solution properties was found to strongly alter heteroaggregation process. NOM homoaggregation represented then a key parameter in heteroaggregation, promoting the formation of large heteroaggregates via bridging mechanism.

6.2 Perspectives

The three models developed for this thesis work constitute just a first step in the development of methods for a better understanding of NP reactivity, transformation and transport in environmental compartments. Our models are not restricted to the scenarios we have investigated all along these work. Indeed, the different models presents the advantage of being flexible as a function of the desired scenario *via* the modification of the input parameters. For instance, the NP size and type as well as acid/base properties may be adapted to study the surface charging behavior and the ion distribution around cerium or silver nanoparticles. Furthermore, the attachment efficiency values in the heteroaggregation model can be modified to consider low interactions between NPs and NOM units so as to take into account changes in the surface charge properties.

The complexity of our models may also be increased and a wide range of alternatives are possible. First, simulations of a system with several NPs with explicit sites and ions would be interesting to study the interactions between nanoparticles and then to derive attachment efficiencies. Secondly, the presence of other compounds could be taken into account, for instance, by adding a third component in our heteroaggregation process (inorganic particles) or by considering the presence of polymers during the surface charging process. The complexity of NOM description could be improved, and instead of considering monomers, NOM may be described by a wide range of homoaggregates with different sizes, as found in aquatic systems. Finally, other processes occurring in water may be integrated such as sedimentation and fragmentation only above a certain size. One of the moment more straightforward perspective, currently under consideration, consists to mix the two first models and investigate the NP surface charging process in presence of explicit counterions and salt particles.

Finally, the three different studies presented in this thesis work correspond to generic coarsegrained systems. It would be interesting to extend or compare these models to realistic experimental or environmental systems by either parametrizing our models with experimental data or using MC simulation has a tool to get an insight into the nanoscopic behavior of a specific system simultaneously with macroscopic properties obtained from experiments. For that purpose, future collaboration is under consideration to study the NP heteroaggregation process with organic matter. Experimental data will be provided such as NP/NOM concentrations and individual attachment efficiencies so as to determine heteroaggregation attachment efficiencies for numerical models. However, all these improvements will require to consider and evaluate the computational limitations such as CPU times.

APPENDIX A

Supporting Informations of Paper II

Effect of Surface and Salt Properties on the Ion Distribution around Spherical Nanoparticles. Monte Carlo Simulations. Supporting Informations

Reprinted from A. Clavier, F. Carnal, S. Stoll *J. Phys. Chem. B*, **2016** vol. 120, no.32, 7988. Copyright (2016), with permission of the *American Chemical Society*



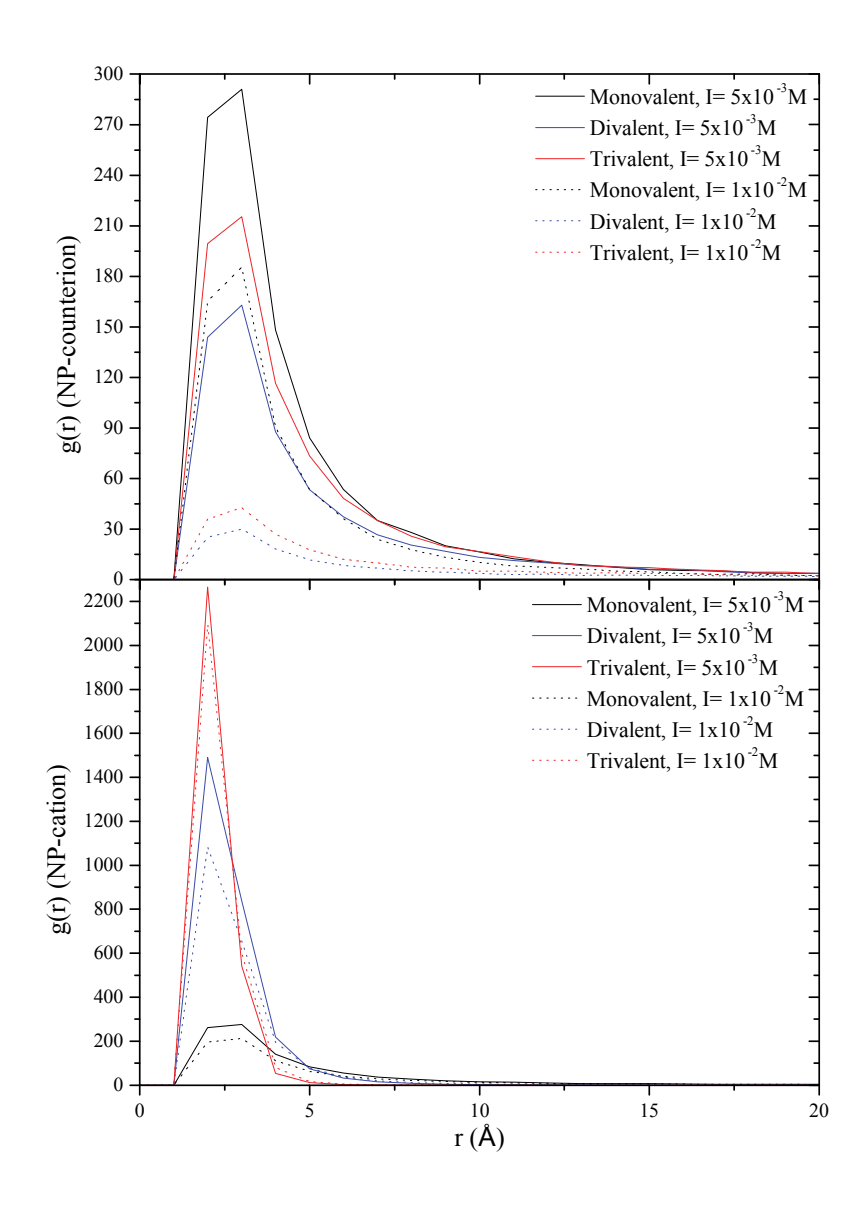


Figure S1. Radial Distribution Function g(r) for a) NP-counterion and b) NP-cation systems for different ionic strengths and valencies. A 100 sites NP with a heterogeneous distribution and a radius of 25Å is studied. g(r) starts from the surface of the NP. With the increase of the valency, counterions are progressively excluded from the interface around the nanoparticle and replaced by cations.

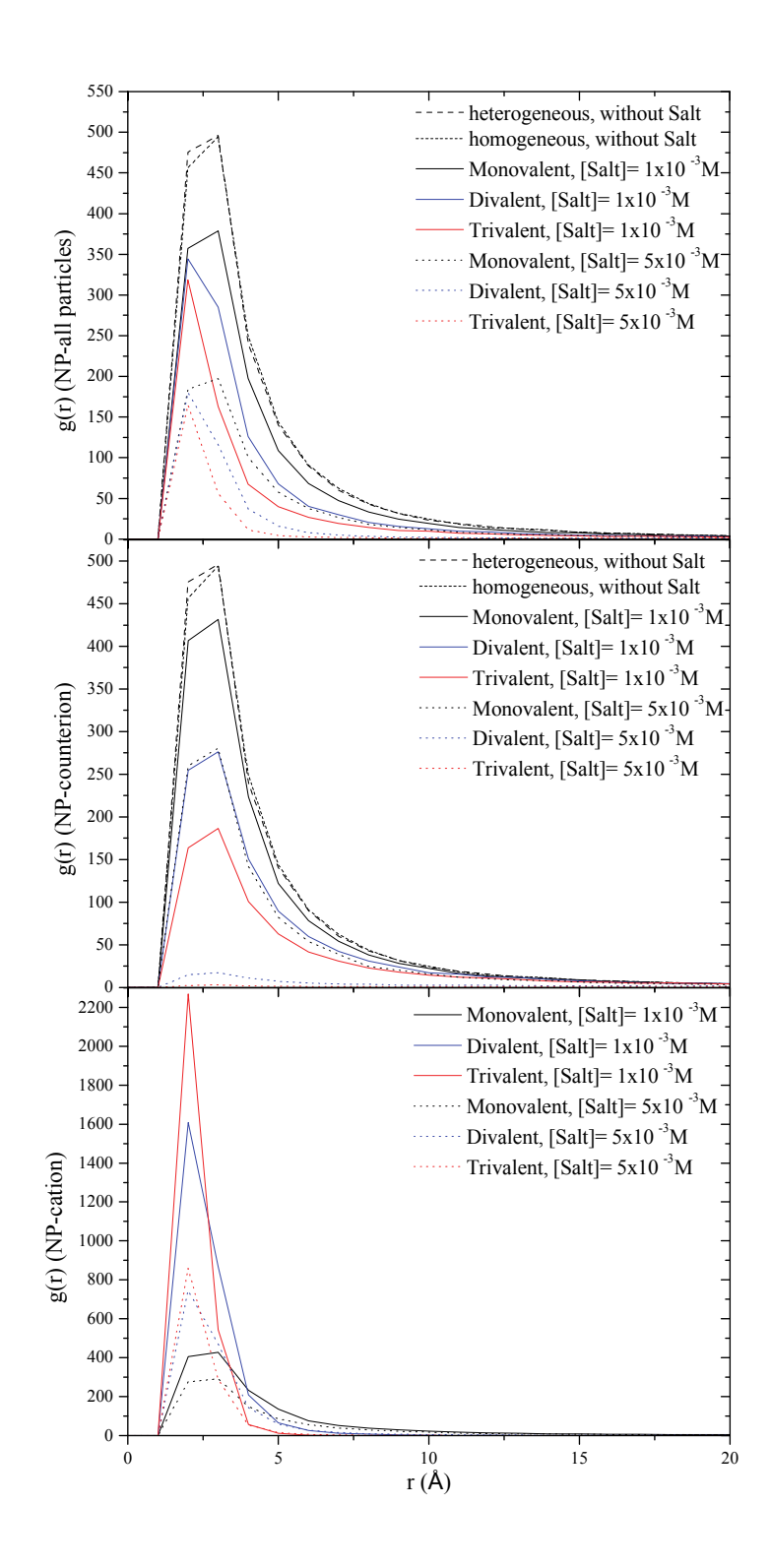


Figure S2. Radial Distribution Function g(r) for a) NP-all particles, b) NP-counterion and c) NP-cation systems for different cation concentrations and valencies. Description of the NP surrounding (100 sites).

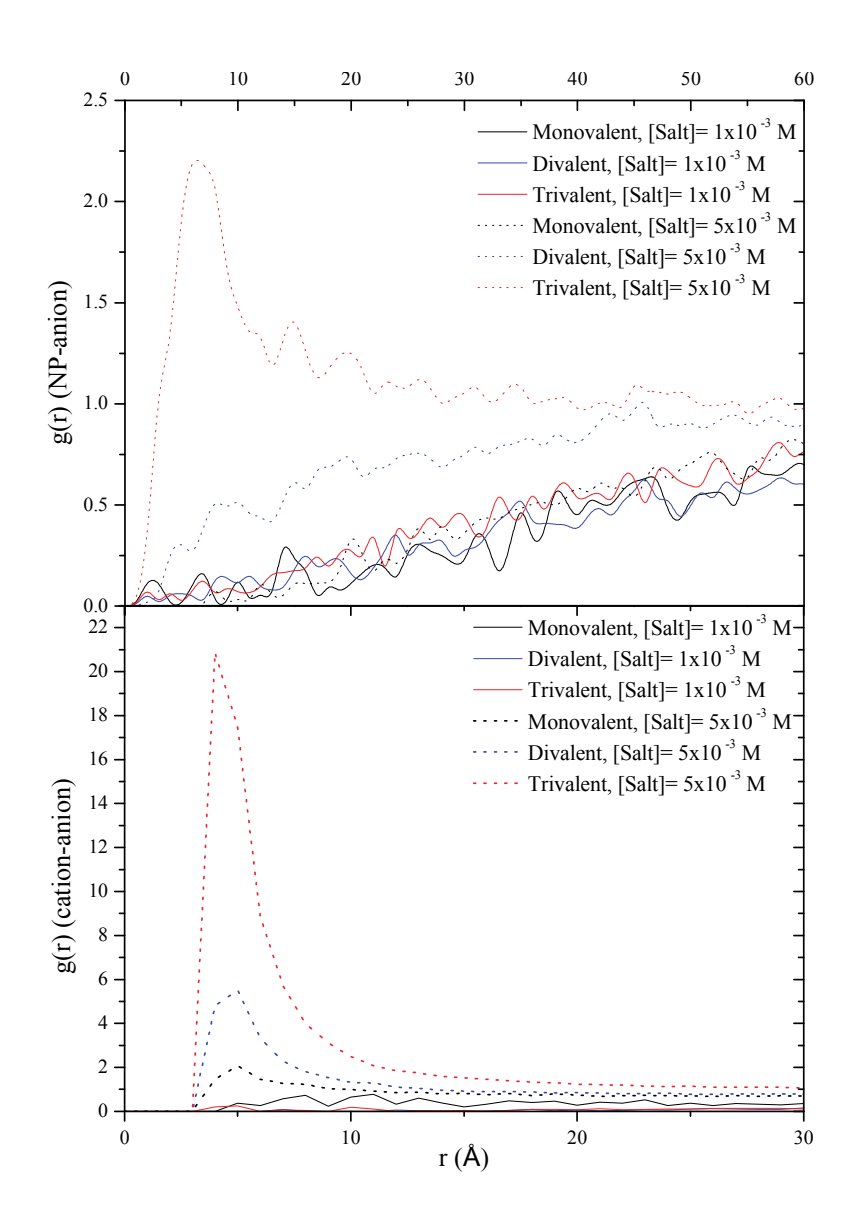


Figure S3. Radial Distribution Function g(r) for a) NP-anion and b) cation-anion systems for different cation concentrations and valencies. A second layer made up of anions is observed around the NP due to the presence of a positive layer made of cations.

APPENDIX B

Paper Published in Chimia

Manufactured Nanoparticle Behavior and Transformations in Aquatic Systems. Importance of Natural Organic Matter

Reprinted from F., F.M., Loosli, Omar, F., Carnal, O., Oriekhova, A., Clavier, Z., Chai, and S., Stoll *Chimia*, **2014** vol. 68, no.11, 783-787.



Chimia 68 (2014) 783-787 © Schweizerische Chemische Gesellschaft

Manufactured Nanoparticle Behavior and Transformations in Aquatic Systems. Importance of Natural Organic Matter

Frédéric Loosli, Fatehah Mohd Omar, Fabrice Carnal, Olena Oriekhova, Arnaud Clavier, Zhi Chai, and Serge Stoll*

Abstract: Major concerns to elucidate the fate of nanomaterials and manufactured nanoparticles in aquatic systems are related to the lack of data on nanoparticle transformations under relevant environmental conditions. The present article discusses some of the important physicochemical processes controlling the behavior of manufactured nanoparticles in aqueous systems by focusing on their interaction with natural organic matter, which is expected to play a crucial role when adsorbing at the nanoparticle surface. The precise knowledge and consequences of such adsorption processes are important not only to predict the nanoparticle stability and dispersion state but also to evaluate their chemical reactivity and ecotoxicology. Most importantly, findings indicate that the presence of natural organic matter, at typical environmental concentrations, can induce significant disagglomeration of large nanoparticle agglomerates into small fragments. Such a result constitutes an important outcome with regard to the risk associated with the possible transformation and redispersion of large assemblies containing manufactured nanoparticles.

Keywords: Aggregation · Aquatic systems · Disagglomeration · Nanoparticle coating · Natural organic matter

Introduction

Manufactured nanoparticles (NPs) are synthesized to have surface properties that have never been encountered by man and other organisms in nature. With the development of nanomaterials and nanotechnologies, NPs are produced in large amounts and their volumes are found to increase continuously in the environment due to the inefficient collection, treatment and recycling of manufactured materials containing nanoparticles.[1,2] NPs are currently used in areas such as cosmetics, electronics, pharmaceuticals, catalysis, food and material sciences and the surfaces of NPs are frequently modified or coated to improve their properties and stability for industrial applications.[3,4]

Once released into the aquatic system it is still not clear how the chemical reactivity and physical properties of NPs will change according to pH, concentration of dissolved ions, water hardness, presence of various aquagenic compounds and living organisms.^[5-8] Interactions between NPs and natural organic matter (NOM) such as biomacromolecules (exo-polysaccharides, proteins) and humic substances (humic and fulvic acids as soluble entities) will rapidly alter their dynamic properties regarding immobilization versus diffusion, [9-13] and consequently their bioavailability and ecotoxicity.[14-20] It should also be noted that depending on synthesis, storage and processing conditions NPs will also be agglomerated with the possibility to undergo disagglomeration in presence of NOM and thus be redispersed.[21-25] Disagglomeration processes add to the diversity and complexity of the evaluation of the fate, transport and transformations of NPs. The aim of this article is to review some important aspects and questions that are relevant to the NPs' behavior in aquatic systems by focusing on the importance of NPs characterization and some key physicochemical processes such as agglomeration, disagglomeration, surface charge modification and coating. These points are illustrated with examples from our research activities.

Aquatic Systems as Recipients for Manufactured NPs. Importance of Natural Aquatic Compounds

NOM is normally present in aquatic systems at the mg/L level and it is now

clearly established that the presence of natural organic compounds will largely modify NPs surfaces[11,26] and that such modifications will have a significant impact on their fate, transport, reactivity, uptake by organisms, and toxicity properties.[15,16,27] The available information on the interaction processes between NPs and natural aquatic compounds suggests complex chemical reactions and adsorption processes at the NPs surfaces which in the end result in NPs agglomeration, stabilization, disagglomeration or dissolution as shown in Fig. 1. The understanding of agglomeration or disagglomeration requires knowledge of the influence of a large number of parameters including; i) NOM concentration, molecular weight distribution and conformation, hydrophobicity, charge density; ii) NPs size distribution and concentration, crystalline phase, geometry, surface charge and chemistry, and iii) solution properties such as pH, temperature, ionic strength and composition (including the colloidal fraction). So far, a limited number of experiments have been made to study in a systematic way the interactions between NOM and NPs, adsorption and coating mechanisms (involving electrostatic interactions, hydrophobic forces, H-bonding, cation bridging, ligand exchange, etc.), then the resulting NPs stability and properties, such as ageing, of the surface coating. It should be noted that combining quantitative results from different studies is also very difficult, owing

*Correspondence: Dr. S. Stoll
Environmental Physical Chemistry
F.-A. Forel Institute, Earth and Environmental
Sciences
Faculty of Sciences, University of Geneva
10 route de Suisse
CH-1290 Versoix
Tel.: + 41 22 379 03 33
E-mail: serge.stoll@unige.ch

APPENDIX C

Paper Published in

Environmental Science: Nano

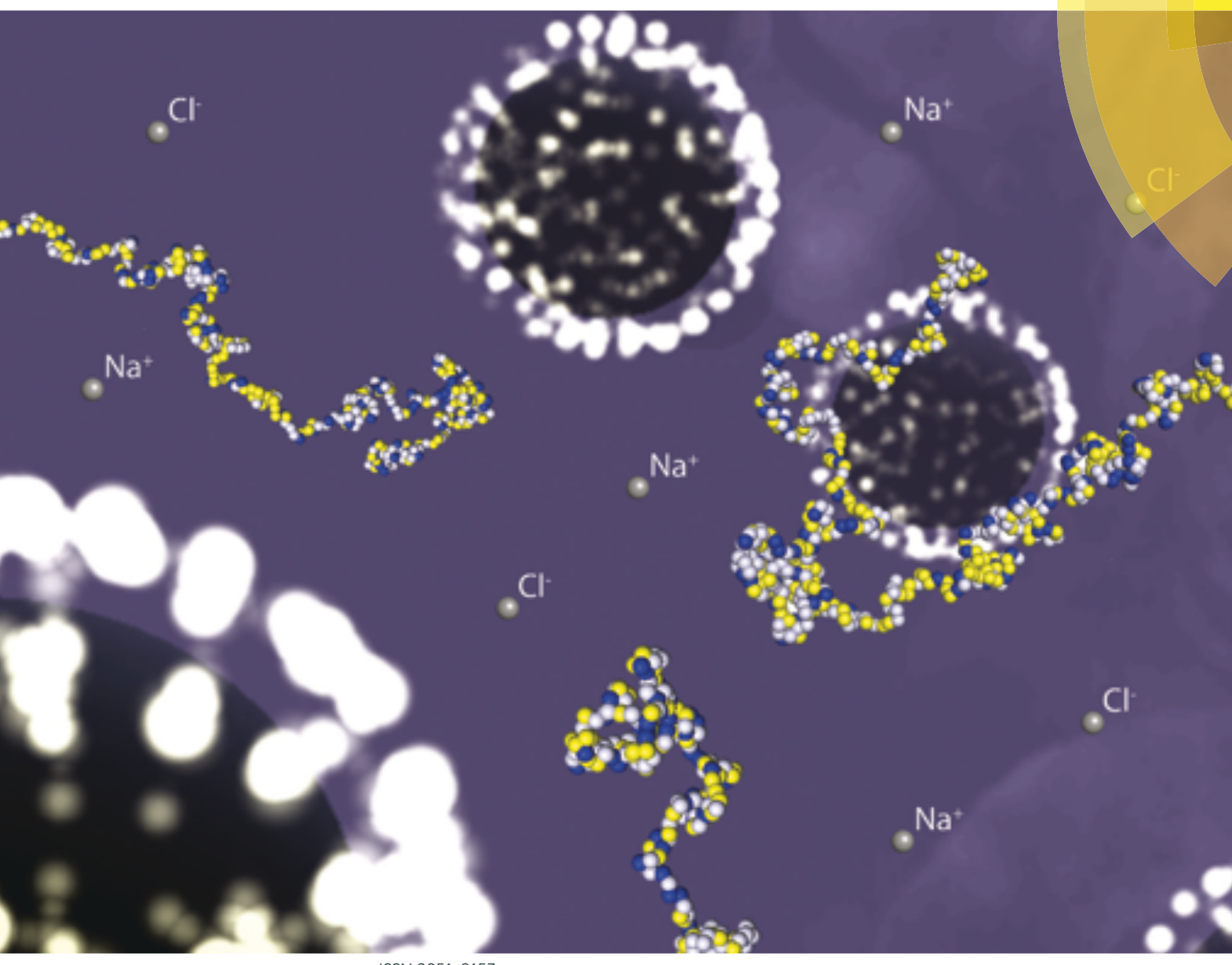
Modelling the interaction processes between nanoparticles and biomacromolecules of variable hydrophobicity: Monte Carlo simulations.

Reprinted from F., Carnal, A., Clavier, and Stoll, S. *Environmental Science: Nano*, **2015** vol. 2, no.4, 327-339.



Environmental Science Nano

rsc.li/es-nano



ISSN 2051-8153



Serge Stoll *et al.*

Modelling the interaction processes between nanoparticles and biomacromolecules of variable hydrophobicity: Monte Carlo simulations

Environmental Science Nano



PAPER



Cite this: *Environ. Sci.: Nano*, 2015, **2**, 327

Modelling the interaction processes between nanoparticles and biomacromolecules of variable hydrophobicity: Monte Carlo simulations†

Fabrice Carnal, Arnaud Clavier and Serge Stoll*

The conformational properties and formation of a complex between a weak flexible biomacromolecule chain of variable hydrophobicity and one negatively charged nanoparticle in the presence of explicit counterions are investigated here using Monte Carlo simulations. The influence of the charge distribution and hydrophobicity, monomer distribution of the chain as well as the pH of the solution are systematically investigated. It is shown that the isolated chain conformations, built with random and block distribution of carboxylic, amino and hydrophobic groups, are the result of the subtle competition between intrachain attractive and repulsive electrostatic interactions as well as intrachain attractive short-range interactions due to hydrophobic properties. Extended conformations are found at low and high pH and folded conformations at physiological pH when hydrophilic and block polymer chains are considered. On the other hand, hydrophobic chain conformations do not show pH dependency and remain folded. The intrachain attractive electrostatic interactions clearly promote the deprotonation of carboxylic groups at low pH and the protonation of amino groups at high pH with higher efficiency for hydrophilic chains. The additional set of electrostatic interactions due to the presence of one negatively charged nanoparticle limits the deprotonation of carboxylic groups at low pH. Moreover, the attractive interactions between the biomacromolecule and the nanoparticle allow to observe the formation of a complex considering intermediate and hydrophilic chains even close to the chain isoelectric point due to the charge inhomogeneity distribution. Hydrophobic chain segments are not affected by the presence of the nanoparticle and remain desorbed. In all cases, the presence of one nanoparticle influences the biomacromolecule structures and acid/base properties, leading to more stretched conformations.

Received 25th March 2015, Accepted 24th June 2015

DOI: 10.1039/c5en00054h

rsc.li/es-nano

Nano impact

Nowadays, research is still needed to develop conceptual models to understand the physico-chemical parameters governing the fate, interactions and transformations of nanoparticles in environmental systems and living organisms, and to optimize predictive and mechanistic appreciation in the generated nanoparticle activity. In such context, Monte Carlo simulations are used here to elucidate in detail the possible transformation and properties of nanoparticles and biomacromolecules (denaturation) in changing environments. This study constitutes a novel and original approach to predict key parameters influencing the nanoparticle reactivity and their possible interactions with biological and environmental molecules of variable hydrophobicity.

1. Introduction

Nanoparticles are widely involved in our daily life and industrial processes today.¹⁻⁴ They can achieve at the nanoscale level very useful and reactive structures such as spheres, tubes, platelets, needle-like structures, *etc.* Due to their large specific surface area, nanoparticle reactivity is high which allows specific physico-chemical properties such as adsorption, catalysis, changes in mechanical and optical properties

Environmental Physical Chemistry, F.-A. Forel Institute, University of Geneva, 10 Route de Suisse, 1290 Versoix, Switzerland. E-mail: serge.stoll@unige.ch † Electronic supplementary information (ESI) available. See DOI: 10.1039/c5en00054h

of materials, *etc.* to be achieved. Their surrounding environment in natural or biological systems is also of main importance since nanoparticles have the tendency to form aggregates of larger dimensions.⁵ Nanoparticles with soft cores, such as dendrimers, are known to successfully encapsulate ligands and metal ions^{6,7} and multivalent salt concentration is known to play a key role since collapsed dendrimer conformations as well as effective charge inversion can be observed, opening the way to new applications in the area of gene delivery.^{8,9}

Research in predicting nanoparticle fate, transport and transformations in environmental aquatic and biological systems, reactivity and its link to toxicity remains challenging

APPENDIX D

Paper Published in *Polymers*

Polypeptide-Nanoparticle Interactions and Corona Formation Investigated by Monte Carlo Simulations.

Reprinted from F., Carnal, A., Clavier, and Stoll, S. *Polymers*, **2016** vol. 8, no.6, 203.







Article

Polypeptide-Nanoparticle Interactions and Corona Formation Investigated by Monte Carlo Simulations

Fabrice Carnal *, Arnaud Clavier and Serge Stoll

University of Geneva, F.-A. Forel Institute, Environmental Physical Chemistry, 66 Boulevard Carl-Vogt, 1205 Geneva, Switzerland; arnaud.clavier@unige.ch (A.C.); serge.stoll@unige.ch (S.S.)

* Correspondence: fabrice@carnal.name; Tel.: +41-22-379-03-28

Academic Editors: Christine Wandrey, Carlo Cavallotti and Paul Dubin Received: 19 February 2016; Accepted: 12 May 2016; Published: 25 May 2016

Abstract: Biomacromolecule activity is usually related to its ability to keep a specific structure. However, in solution, many parameters (pH, ionic strength) and external compounds (polyelectrolytes, nanoparticles) can modify biomacromolecule structure as well as acid/base properties, thus resulting in a loss of activity and denaturation. In this paper, the impact of neutral and charged nanoparticles (NPs) is investigated by Monte Carlo simulations on polypeptide (PP) chains with primary structure based on bovine serum albumin. The influence of pH, salt valency, and NP surface charge density is systematically studied. It is found that the PP is extended at extreme pH, when no complex formation is observed, and folded at physiological pH. PP adsorption around oppositely-charged NPs strongly limits chain structural changes and modifies its acid/base properties. At physiological pH, the complex formation occurs only with positively-charged NPs. The presence of salts, in particular those with trivalent cations, introduces additional electrostatic interactions, resulting in a mitigation of the impact of negative NPs. Thus, the corona structure is less dense with locally-desorbed segments. On the contrary, very limited impact of salt cation valency is observed when NPs are positive, due to the absence of competitive effects between multivalent cations and NP.

Keywords: Nanoparticle complexation; polypeptide adsorption; polypeptide corona; acid/base properties; Monte Carlo simulations

1. Introduction

Serum albumins, the most abundant plasma proteins in the mammalian circulatory system synthesized in the liver, have been a subject of interest for many years. As a result, they are now well characterized and largely involved in fundamental research, biomedical, and industrial applications. Typically, these proteins are involved in binding and transport of a large range of compounds, such as fatty acids, amino acids (AAs), metals, drugs, or inorganic ions [1–4]. Human and bovine serum albumin (HSA and BSA) display about 76% of sequence homologies with native structures known to be heart-shaped and composed of three homologous domains [5,6]. However, the activity of serum albumin proteins is strongly dependent on target-specific binding and thus on conformational properties. Various physicochemical factors can affect the protein stability, inducing structure changes that lead to denaturation and loss of biological activity.

Depending on solution pH and ionic strength, serum albumin proteins can adopt different conformations, described as extended, fast, native (N), basic, and aged, from acidic to basic pH [7–10]. The three homologous domains of BSA/HSA have different stabilities in acidic/basic environments and are involved in the protein denaturation process. Moreover, structural transitions have the ability to be reversible with pH variations [11]. The ionic environment effect is an important parameter, since repulsive electrostatic interactions are decreased with salt, thus affecting stability and diffusivity of